Energy Research and Development Division
FINAL PROJECT REPORT

ASSESSMENT OF LARVAL ENTRAINMENT BY COOLING WATER INTAKE SYSTEMS:

Models of Larval Dispersal and Recruitment Incorporating Coastal Boundary Layer Flow

Prepared for: California Energy Commission
Prepared by: University of California, Davis, Bodega Bay Marine Laboratory

SEPTEMBER 2007
CEC-500-2013-049

PREPARED BY:

Primary Author(s):
John L. Largier
J. Wilson White
Linden Clarke
Kerry J. Nickols

University of California, Davis
Bodega Bay Marine Laboratory
Bodega Bay, CA 94923

Contract Number: 500-04-025

Prepared for:

California Energy Commission

Joe O'Hagan
Contract Manager

Linda Spiegel
Office Manager
Energy Generation Research Office

Laurie ten Hope
Deputy Director
ENERGY RESEARCH AND DEVELOPMENT DIVISION

Robert P. Oglesby
Executive Director

DISCLAIMER

This report was prepared as the result of work sponsored by the California Energy Commission. It does not necessarily represent the views of the Energy Commission, its employees or the State of California. The Energy Commission, the State of California, its employees, contractors and subcontractors make no warranty, express or implied, and assume no legal liability for the information in this report; nor does any party represent that the uses of this information will not infringe upon privately owned rights. This report has not been approved or disapproved by the California Energy Commission nor has the California Energy Commission passed upon the accuracy or adequacy of the information in this report.

PREFACE

The California Energy Commission Energy Research and Development Division supports public interest energy research and development that will help improve the quality of life in California by bringing environmentally safe, affordable, and reliable energy services and products to the marketplace.

The Energy Research and Development Division conducts public interest research, development, and demonstration (RD&D) projects to benefit California.

The Energy Research and Development Division strives to conduct the most promising public interest energy research by partnering with RD&D entities, including individuals, businesses, utilities, and public or private research institutions.

Energy Research and Development Division funding efforts are focused on the following RD&D program areas:

- Buildings End-Use Energy Efficiency
- Energy Innovations Small Grants
- Energy-Related Environmental Research
- Energy Systems Integration
- Environmentally Preferred Advanced Generation
- Industrial/Agricultural/Water End-Use Energy Efficiency
- Renewable Energy Technologies
- Transportation

Assessment of Larval Entrainment by Cooling Water Intake Systems: Models of Larval Dispersal and Recruitment Incorporating Coastal Boundary Layer Flow is the final report for the Environmental Effects of Cooling Water Intake Structures Project (Contract Number 500-04-025) conducted by University of California, Davis, Bodega Bay Marine Laboratory. The information from this project contributes to Energy Research and Development Division's Energy-Related Environmental Research Program.

For more information about the Energy Research and Development Division, please visit the Energy Commission's website at www.energy.ca.gov/research/ or contact the Energy Commission at 916-327-1551.

ABSTRACT

A major source of uncertainty in assessing the effects on fish and invertebrate species from withdrawing large amounts of water for cooling by coastal power plants is the inability of accurately quantifying the number of planktonic larvae lost to such facilities and to accurately predict the consequences of these losses at the population level. At present several methods are in widespread use that attempt to quantify such impacts on fish and invertebrate populations, but all rely on several simplifying assumptions about circulation and population dynamics that are unlikely to yield accurate results for coastal populations with complex patterns of larval movement and demography. This study used recent oceanographic observations to develop idealized models of nearshore circulation and population dynamics that reflect the key features of larval transport and post-settlement demography affecting population persistence. These models were used for demonstrating the importance of these features, obtaining better estimates of fish entrainment from cooling water withdrawal (which occurs when organisms are trapped against water intake screens or carried into the power plant's cooling system), developing recommendations for cooling water intake structure placement, and exploring alternative metrics for quantifying the effects of cooling water intakes.

Keywords: cooling water intake, larval entrainment, planktonic, coastal boundary layer, Lagrangian particle-tracking model

Please use the following citation for this report:

Largier, John L., White, Wilson, Clarke, Linden, Nickols, Kerry J. (University of California, Davis, Bodega Bay Marine Laboratory). 2007. ***Assessment of Larval Entrainment by Cooling Water Intake Systems: Models of Larval Dispersal and Recruitment Incorporating Coastal Boundary Layer Flow.*** California Energy Commission. Publication number: CEC-500-2013-049.

TABLE OF CONTENTS

PREFACE ..... **i**

ABSTRACT ..... **ii**

TABLE OF CONTENTS ..... **iii**

LIST OF FIGURES ..... **iv**

LIST OF TABLES ..... **vi**

EXECUTIVE SUMMARY **1**

Introduction 1

Project Purpose 1

Project Results 2

Benefits to California 5

CHAPTER 1: Introduction **7**

CHAPTER 2: Empirical Data **11**

2.1 Data Collection Methods 11

2.1.1 Study Area 11

2.1.2 Measurement of Currents 12

2.2 Data Analysis 12

CHAPTER 3: Nearshore Circulation **15**

3.1 Summary of Nearshore Flow off Huntington Beach 15

3.2 Summary of Nearshore Circulation in General 21

3.3 Idealized Cross-shore Flow Structure in the Coastal Boundary Layer 23

CHAPTER 4: Particle Dispersion Model **25**

4.1 Inner-shelf Boundary Layer 26

4.2 Intake Entrainment 26

CHAPTER 5: Modeled Patterns of Larval Dispersal **27**

5.1 Larval Dispersal Results and Discussion 30

5.1.1 Non-Advection Scenarios 30

5.1.2 Unidirectional Advection Scenarios 31

5.1.3 Nearshore Countercurrent Scenarios 32

CHAPTER 6: Effects of Entrainment on Benthic Populations 45

6.1 Metapopulation Model Framework 45

6.2 Quantifying Effects of Entrainment on Metapopulation Dynamics 46

6.3 Parameterization of Metapopulation Model 48

6.4 Metapopulation Model Results 49

6.4.1 Unexploited Population 49

6.4.2 Overexploited Population 49

6.4.3 Cumulative Effects of Multiple CWIS 50

6.4.4 Disturbance 50

6.4.5 Relative Settlement 51

6.5 Metapopulation Model Discussion 51

CHAPTER 7: Assessment Protocols 64

7.1 Adult Equivalent Loss (AEL) 64

7.2 Fecundity Hindcasting (FH) 65

7.3 Empirical Transport Model (ETM) 65

7.4 Assessment Protocol Results and Discussion 66

CHAPTER 8: Future Directions 70

CHAPTER 9: Conclusion and Summary 74

REFERENCES 76

LIST OF FIGURES

Figure 1: Bathymetry of Huntington Beach Study Area 14
Figure 2: Times of Deployment for ADCP Instruments for each Mooring Station at Huntington Beach 14
Figure 3: Summary of Flow Patterns Measured by ADCP at Huntington Beach 16
Figure 4: Vectors of Mean Current Velocity at Surface (red) and Bottom (blue) for Huntington Beach ADCP Moorings 17
Figure 5: One-Week Depth-Averaged Time Series of Current Velocity from the Cross-Shore Transect of ADCP Moorings at Huntington Beach between July 19 and July 26, 2001 18
Figure 6: One-Month Depth-Averaged Time Series of Current Velocity from the Cross-Shore Transect of ADCP Moorings at Huntington Beach between July 19 and August 14, 2001 19

Figure 7: Cross-Shore Profile of Mean Alongshore Velocity (cm s^{-1}), Aggregated over a 1-week Time Scale at Huntington Beach, CA 19
Figure 8: Cross-Shore Profile of Mean Alongshore velocity (cm s^{-1}), Aggregated over a 1-month Time Scale at Huntington Beach, CA 20
Figure 9: Cross-Shore Profile of the Standard Deviation of Alongshore Velocity (cm s^{-1}), Aggregated over a 1-Month Time Scale at Huntington Beach, CA 20
Each point represents data from a different ADCP mooring station in the cross-shore transect. 20
Figure 10: Cross-Shore Profile of the Standard Deviation of Alongshore Velocity (cm s^{-1}), Aggregated over a 1-Week Time Scale at Huntington Beach, CA 21
Each point represents data from a different ADCP mooring station in the cross-shore transect. 21
Figure 11: Idealized Tri-Linear Profile used to represent the Cross-Shore Structure in Flow Parameters 24
Figure 12: Dispersal Kernels Calculated using Particle Dispersion Model for Diffusion-Only Scenario 33
Figure 13: Mean Particle Trajectories Calculated using Particle Dispersion Model for Diffusion-Only Scenario 34
Figure 14: Dispersal Kernels Calculated using Particle Dispersion Model for Scenarios with No Alongshore Advection but Varying Strengths of Alongshore Diffusivity (K_y) and Cross-Shore Diffusivity (K_x) 35
Figure 15: Mean Particle Trajectories Calculated using Particle Dispersion Model for Scenarios with No alongshore Advection but Varying Strengths of Alongshore Diffusivity (K_y) and Cross-Shore Diffusivity (K_x) 36
Figure 16: Time Series of Particle Entrainment for Scenarios with No Alongshore Advection but Varying Strengths of alongshore Diffusivity (K_y) and Cross-Shore Diffusivity (K_x) 37
Figure 17: Dispersal Kernels Calculated using Particle Dispersion Model for Scenarios with either Moderate (V_{max} = 0.1 m s^{-1}, left panels) or High (V_{max} = 0.3 m s^{-1}, right panels) Mean Alongshore Advection 38
Figure 18: Dispersal Kernels Calculated using particle Dispersion Model for Scenarios with either Moderate (V_{max} = 0.1 m s^{-1}, left panels) or High (V_{max} = 0.3 m s^{-1}, right panels) Mean Alongshore Advection and either relatively Weak (top panels) or Strong (bottom panels) Alongshore and Cross-Shore Diffusivities (K_y, K_x) 39
Figure 19: Time Series of Particle Entrainment for Scenarios with either Moderate (V_{max} = 0.1 m s^{-1}, left panels) or High (V_{max} = 0.3 m s^{-1}, right panels) Mean Alongshore Advection and either relatively Weak (top panels) or Strong (bottom panels) Alongshore and Cross-Shore Diffusivities (K_y, K_x) 40
Figure 20: Dispersal Kernels Calculated using Particle Dispersion Model for Scenarios in which Nearshore and Offshore Flows are in Opposite Directions 41
Figure 21: Dispersal Kernels Calculated using Particle Dispersion Model for Scenarios in which Nearshore and Offshore Flows are in Opposite Directions and with Varying Strengths of Alongshore Diffusivity (K_y) and Cross-Shore Diffusivity (K_x) 42
Figure 22: Mean Particle Trajectories Calculated using Particle Dispersion Model for sCenarios in which Nearshore and Offshore Flows are in Opposite Directions and with Varying Strengths of Alongshore Diffusivity (K_y) and Cross-Shore Diffusivity (K_x) 43

Figure 23: Time Series of Particle Entrainment for Scenarios in which Nearshore and Offshore Flows are in Opposite Directions and with Varying Strengths of Alongshore Diffusivity (K_y) and Cross-Shore Diffusivity (K_x) 44
Figure 24: Results of Metapopulation Model Showing the Distribution of Adult Density (individuals m^{-2}; top panel) and the Deletion Index (a dimensionless measure of conservation value; bottom panel) at each Alongshore Location 55
Figure 25: Results of Metapopulation Model Showing the Distribution of Adult Density (individuals m^{-2}; top panel) and the Deletion Index (a dimensionless measure of conservation value; bottom panel) at each Alongshore Location 56
Figure 26: Results of Metapopulation Model Showing the Distribution of Adult Density (individuals m^{-2}; top panel) and the Deletion Index (a dimensionless measure of conservation value; bottom panel) at each Alongshore Location 57
Figure 27: Results of Metapopulation Model Showing the Distribution of Adult Density (individuals m^{-2}; top panel) and the Deletion Index (a dimensionless measure of conservation value; bottom panel) at each Alongshore Location 58
Figure 28: Results of Metapopulation Model Showing the Distribution of Adult Density (individuals m^{-2}; top panel) and the Deletion Index (a dimensionless measure of conservation value; bottom panel) at each Alongshore Location for the Scenario with Two CWIS Intakes 59
Figure 29: Results of Metapopulation Model Showing the Distribution of Adult Density (individuals m^{-2}; top panel) at each Alongshore Location during the Recovery from a Localized Disturbance 60
Figure 30: Results of Metapopulation Model Showing the Distribution of Adult Density (individuals m^{-2}; top panel) at each Alongshore Location During the Recovery from a Localized Disturbance 61
Figure 31: Results of Metapopulation Model Showing the Distribution of Adult Density (individuals m^{-2}; top panel) at each Alongshore Location during the Recovery from a Localized Disturbance 62
Figure 32: Results of Metapopulation Showing *Relative Settlement* Calcuated from Model Runs with and without CWIS Entrainment 63
Figure 33: Results of Metapopulation Showing *Relative Settlement* Calcuated from Model Runs with and without CWIS Entrainment 63

LIST OF TABLES

Table 1: Details of Station Locations for Mooring Deployments at Huntington Beach in Summer 2001 13
Table 2: Summary of Cross-Shore and Along-Shore Components of Velocity for Cross-Shore Transect of Moorings at Huntington Beach in 2001 17
Table 3: Parameter Values Used in Partical Dispersion Model Runs 29
Table 5: Effect of Cooling Water Intake Entrainment on Population Persistence 52
Table 6: Comparison of Traditional ("trad") CWIS Impact Statistics with Equivalent Values ("actual") Derived from the Spatially Explicit Population Model 68
Table 7: Comparison of Traditional ("trad") CWIS Impact Statistics with Equivalent Values ("actual") Derived from the Spatially Explicit Population Model 69

EXECUTIVE SUMMARY

Introduction

Many power plants along California's coast use once-through cooling technology. Once-through cooling withdraws millions of gallons of water from a water body, passes the water by the plant's condenser once to remove waste heat, and then discharges it to a water body. Some organisms are carried along in the cooling water flow as water is diverted into the power plant. The larger of these organisms may be trapped against the water intake screens, while the smaller organisms that can pass through the screens are carried into the power plant's cooling system (known as entrainment) and subjected to thermal, physical, or chemical stresses. Entrainment of these smaller organisms, including fish eggs and juvenile (larval) stages, may be contributing to the population declines documented for many of the species found along California's coast and in its estuaries.

Most marine organisms have two distinct life stages, a relatively sedentary adult stage living near the bottom of the water body and a more mobile larval stage drifting with the currents. Water currents can disperse larvae over large distances, and the persistence of marine populations depends on connectivity and replenishment of adult populations through the larval stage. While most activities that affect marine species such as fishing threaten the adult stage, withdrawing significant amounts of water directly threatens the larval stage through entrainment into the power plant and may impair the persistence of marine populations by disrupting larval connectivity.

However, considerable challenges exist in quantifying the population-level effects of cooling water intake systems. First, natural rates of larval mortality are extremely high, so most entrained larvae would not have survived to enter the population anyway. Second, the origins and eventual destinations of entrained larvae are difficult to ascertain, so the challenge is determining how effects of cooling water withdrawal on larvae are distributed in near-shore waters. There are several methods in widespread use that attempt to quantify impacts of cooling water withdrawal on populations, but all rely on several simplifying assumptions about water circulation and population dynamics. It is unlikely that these methods yield appropriate results for coastal populations with complex patterns of larval movement and demography. Specifically, the existing methods do not recognize the dispersive nature of coastal flows or the importance of a "coastal boundary layer" (a near-shore area of slower moving water), that dominates larval transport outcomes. Further, these models do not account for spatial structure in a population or changes in mortality rate in response to variations in population density after larval settlement.

Project Purpose

The goals of this project were to use recent oceanographic observations over the inner shelf to develop models of near-shore circulation and population dynamics that reflect the key features of larval transport and post-settlement demography affecting population persistence. The authors used this modeling framework for demonstrating the importance of these features,

obtaining better estimates of the effects of cooling water intake systems entrainment, developing recommendations for placement of cooling water intake structures, and exploring alternative metrics for quantifying the effects of withdrawing large amounts of cooling water.

For exclusively coastal species, all larvae must begin their life in the inner-shelf region, and all those larvae that leave the inner-shelf must return in order to settle successfully. Thus all larvae must pass through this region at least once or twice. To describe larval transport, researchers needed a proper description of inner-shelf, near-shore circulation. Unfortunately, circulation in this region is difficult to characterize using remote sensing (satellites or high-frequency coastal radar), and placing sensitive oceanographic instruments in shallow nearshore waters is also challenging. , The researchers deployed acoustic Doppler current profilers in a cross-shelf transect off of Huntington Beach, California in 2001 to characterize inner-shelf circulation. They analyzed these data for this project and also conducted a preliminary analysis of similar deployments off Santa Barbara, Santa Cruz, Mission Beach and Moss Landing. Currents tend to be faster in the along-shore dimension than perpendicular to shore. They are also slower and steadier nearer the shore. These results, along with other data being collected in related projects at Bodega Marine Laboratory, supported the existence of a coastal boundary layer, a region of slow-moving water over the inner shelf with weaker mixing, resulting in slower along-shore transport than in faster-moving offshore waters. This type of boundary layer could temporarily retain larvae and decrease how far they can disperse.

The authors developed a particle-tracking model that tracked each individual particle to simulate larval transport along a coastline containing a power plant cooling water intake system. This model included a mathematical representation of a coastal boundary layer similar to that detected in the Huntington Beach data. Both cross-shore and along-shore mixing is weak near-shore (less than 1 kilometer), and increases with distance offshore, attaining a maximum over the shelf, away from the direct effect of the coast (less than 10 kilometers offshore). The model described the movement over time of individual particles released from a particular near-shore position as a result of advection (movement by water flow) and random diffusion. This allowed the authors to describe the dispersal of larvae within a coastal population and also explicitly describe the entrainment of those larvae through a cooling water intake system. The particle-tracking model was run with flow parameters representative of two different timescales: a typical pelagic or open ocean larval dispersal event covering from days to weeks, and population dynamics covering from months to years and representing circulation averaged over multiple spawning seasons within the generation time of a population. The shorter time scale has stronger directional advection with average flow and weaker random diffusivities, generating a larger ratio of advection to diffusion.

Project Results

Initial runs using the particle-tracking model parameterized for the shorter pelagic larval duration timescale revealed the general effects of inner shelf circulation on dispersal and entrainment. In general, dispersal patterns were not sensitive to how advection was described. This was encouraging because it suggested that the researchers' imperfect knowledge of the

nature of cross-shelf boundary layer profiles did not strongly affect model results, so long as this calmer near-shore water zone was recognized.

Conversely, the values chosen for the random diffusive component of circulation did strongly affect larval transport. Higher along-shore diffusivities produced broader spatial distributions of larval settlers and rapidly removed larvae released near a cooling water intake site, so that most entrainment happened immediately after spawning. Higher cross-shore diffusivities carried more larvae offshore, which also increased along-shore dispersion, but few larvae returned to near-shore to settle. This reduced the total number of larval settlers and also reduced the overall entrainment of larvae after the first several days post-spawning. This result reinforced the need to be precise about the scale under consideration – using high-advection short-time-scale patterns to predict population-time-scale results (which aggregate over longer-term variations) would lead to errors. Furthermore, these model runs strongly suggested that larvae are more commonly entrained very soon after spawning rather than later in their life. The entrainment rate of late-stage larvae never exceeded that of early-stage larvae, a pattern that would be amplified by a constant rate of larval mortality (not included in these models) that would result in many fewer larvae available for entrainment later in the larval period. However, each late-stage larva has a much higher chance of survival and thus much greater value to the persistence of the population.

The authors ran the particle-tracking model with the long-time-scale parameter set to estimate the probability of dispersal for a population occupying a 100 kilometer coastline with a cooling water intake system in the center in order to examine the effects of entrainment on population dynamics. The authors then simulated population dynamics for two types of populations: one that was unexploited and healthy, with a relatively long average post-settlement lifespan; and one that was overexploited and on the verge of collapse, with an average post-settlement lifespan that was relatively short and therefore spawned fewer eggs over their lifetime. In no case did cooling water intake systems affect the dynamics of a healthy population, regardless of intake rate (even intake rates 10 times the maximum observed in cooling water intakes for California power plants) or distance offshore. This was not true for populations near collapse, however. For these populations, the addition of cooling water intake systems often led to population collapse for intake rates similar to the maximum observed in California. This was always the case for cooling water intake systems in the near-shore (just 50 meters offshore; very close to where larvae were spawned), while cooling water intake systems sited further offshore led to collapse in some simulations, but not others. When two cooling water intakes were placed 10 kilometers apart, their cumulative effects exceeded that of a single cooling water intake system and only rarely did near-collapse populations persist in simulations. Even when entrainment from cooling water intake systems did not cause near-collapse populations to go extinct, it drastically increased the time it took for a population to recover from a catastrophic localized disturbance to pre-disturbance population densities.

The results of the population dynamics model led the authors to examine more closely the traditional measures used to gauge cooling water intake system impacts on populations: Adult Equivalent Loss, Fecundity Hindcasting, and the Empirical Transport Model. All three entrainment impact estimation models were flawed to varying degrees. The circulation model

was used to simulate realistic conditions and then applied to the calculation of Adult Equivalent Loss and Fecundity Hindcasting in our model population and also calculated the "actual" value the statistics are intended to estimate. In all cases examined, the two sets of values were off by large margins, often orders of magnitude. Moreover, the sampled values of those two statistics and Empirical Transport Model-derived Proportional Mortality (which is the proportion of larvae killed from entrainment to the larvae in the source population) had no apparent relationship to the actual effect of entrainment on the population. These errors appeared to derive from several systemic problems with the traditional statistics, including the lack of appreciation for the role of compensatory density-dependent mortality, variability in the eventual destination of entrained larvae, and the fact that healthy populations will spawn more larvae – and thus have more larvae entrained – than populations near collapse.

The aim of this study was to explore the general implications of near-coastal intake systems. Some of the future directions for improving assessment of the impact of cooling water intake systems on larval mortality (and thus coastal marine populations) would target specific sites. Actions could include:

- Using data obtained from the Coastal Ocean Observing System to conduct flow observations.
- Using transport models to assess larval loss through entrainment.
- Analyzing records of larvae entrained and of larvae in plankton surveys.
- Using population models for assessing the impact of enhanced larval mortality on population levels.
- Developing new assessment protocols for compliance.
- Developing ecosystem-based protocols for assessing the impact of cooling water intake in concert with other stressors and management actions in coastal waters.
- Considering operational changes in the management of intake systems.

The authors noted four general results obtained in this study. First, the actual extent of passive larval transport was likely to be substantially less than that predicted by traditional advection-diffusion approximations by incorporating a coastal boundary layer of reduced near-coastal flow into models of particle dispersal. Second, runs of the particle-dispersion model suggested that the majority of larval entrainment in nearshore cooling water intake systems occurs very soon after spawning, when larvae are at their highest concentrations. Third, incorporating model-estimated larval dispersal patterns into a population dynamics model revealed that entrainment has an insignificant effect on otherwise healthy populations. However, this small enhanced mortality can be detrimental to unhealthy, overexploited populations. Fourth, the importance of density-dependence to the population dynamics model explained why traditional statistics for quantifying effects of cooling water intake systems will often be highly inaccurate.

In this report the authors utilized idealized models that incorporated biological and physical features that have been observed empirically and are known to strongly influence marine population dynamics. These models captured the first-order essence of the problem and provided a reliable and general assessment of the potential consequences of cooling water intake systems entrainment for near-shore populations.

Benefits to California

In 2010, the State Water Resources Control Board of California adopted a *Policy on the Use of Coastal and Estuarine Waters for Power Plant Cooling*. The policy requires operators of power plants using once-through cooling technology to assess and reduce the harmful effects associated with cooling water intake structures on marine and estuarine life. This study provided robust scientific information that can improve the assessment of power plant entrainment effects on coastal organisms and can also help stakeholders make more informed decisions.

CHAPTER 1: Introduction

The conservation of marine resources in California waters is an issue of widespread public and scientific concern. There is ample evidence that human actions have led to declines in multiple marine species over the past several decades (Leet et al. 2001), and this has led to drastic changes in the administration of marine resources, including the closure of large areas to all harvest (CDFG 2008).

The implementation of effective marine conservation measures is complicated by the role of larval dispersal in marine population dynamics. Nearly all nearshore, benthic marine organisms possess a two-stage life history. Adults are relatively sedentary, remaining attached to one location or occupying a limited homerange for their entire lives. Adults reproduce by spawning eggs and larvae that spend days to months in the water column (Caley et al. 1996). Larvae have relatively limited swimming abilities, especially early in their development, and can be transported long distances by ocean currents (Gawarkiewicz et al. 2007). In order for the population at any coastal location to persist through time, adults that die (or are harvested) must be replaced over time by newly arriving larvae (Armsworth 2002, Hastings and Botsford 2006). Thus uncertainty about larval dispersal pathways necessarily leads to uncertainty about the persistence of adult populations.

Widespread dispersal during the larval phase may decouple reproductive output at a given location from subsequent larval settlement and demographic replacement at that location. As a consequence, the replacement and persistence of any one local population may depend on the persistence of populations elsewhere in the dispersal network (Hastings and Botsford 2006). Resolving dispersal pathways is thus a critical conservation goal (Cowen et al. 2007). Typically, marine conservation efforts involve scenarios in which dispersal pathways remain constant, but human activities reduce total larval production, either by harvesting large, fecund adults or by impairing the productivity of adult habitat (e.g., Kaplan et al. 2006). An entirely different conservation problem is posed when the dispersal pathways themselves are altered.

Power plants in California and elsewhere continuously withdraw seawater to recondense superheated steam used in their electricity-generating turbines. These once-through cooling water intake systems (CWIS) are a cost-effective cooling technique, but may have a large environmental impact (CEC 2005). In addition to the impingement of adult fishes on the mesh screens covering the intake and the thermal disturbance produced when heated seawater is returned to the ocean (two impacts that we do not address in this report), intakes entrain and kill potentially large numbers of planktonic larvae. Depending on the origin and erstwhile destination of those larvae, CWIS entrainment could have a substantial impact on larval dispersal pathways and thus the replacement and persistence of adult populations.

Quantifying the population-level effects of CWIS entrainment requires an understanding of water movement in the relatively shallow, nearshore regions where larvae are spawned and return to settle and where most cooling water intakes are placed. Perhaps surprisingly, flows in

this region of the ocean are relatively poorly known, because the effectiveness of remote sensing instruments (satellites, high frequency radar) is impaired by the coastal margin, the logistics required for very nearshore *in situ* measurements are challenging, and because analytical descriptions of fluid dynamics are complicated by the proximity of boundaries (the coastline and the seafloor).

In general, the movement of particles such as larvae can be described as follows. If the alongshore position of a particle at time t is given by xt, then the position at time t+1 is

$$xt+1 = xt + (V + v)\Delta t \qquad \text{(Eq. 1)}$$

where V is the mean alongshore current velocity, and v is a random variable that describes the fluctuations in the alongshore velocity (an equivalent equation could be written for the cross-shore position of the particle; Siegel et al. 2003). Given this framework, it is straightforward to simulate the release of large numbers of larvae from a single location, track the movement of those larvae over the typical pelagic larval duration (PLD) of the species of interest, and then use the distribution of those larvae at the end of the PLD as a probabilistic description of where larvae spawned at that location are likely to travel. This probability distribution is termed a dispersal kernel. When performing these simulations, V is held constant but a unique value of v is randomly sampled from a specified distribution for each larva at each time step. In general, V×PLD will describe the mean alongshore advection of the larvae (mode of the kernel), and the distribution of v×PLD will describe the variance in larval destinations (the width of the kernel). Typically the effect of transport due to mean flow V is referred to as "advection" and the transport due to flow variability v is referred to as (eddy) diffusion. We use these terms here and represent the diffusive effect by an (eddy) diffusivity K, as outlined in the description of the model (section 4).

Within this framework, it is important to note that both V and the distribution of v are intended to represent a particular temporal scale of interest (Largier 2003). For example, in order to describe the movement of particles over the span of several days, V describes the average current velocity in that time period and v describes both the variability in velocity within that time scale as well as the influence of turbulence and smaller-scale coherent motions that are typically described by an eddy diffusivity parameter. By contrast, to obtain a kernel that describes the distribution of larvae spawned over the duration of an entire spawning season, both parameters must be aggregated over a longer time scale. Thus V describes a seasonal mean and is typically smaller in magnitude than the shorter time estimate while v tends to increase as it includes larger-scale flow variability.

In a uniform flow field, it would be straightforward to describe the dispersal kernel using Eq. 1. It would also be relatively simple to estimate the effects of a CWIS intake by calculating the proportion of larvae released from a given location that move past the intake. However, flows are decidedly non-uniform near the coastal boundary. The general features of nearshore flow are poorly described, but clearly reflect reduced mean and variance in velocity (Csanady 1972a,b, Pettigrew and Murray 1981, Lentz and Winant 1986, Lentz et al. 1999, Noble and Xu 2004, Carrillo et al, unpublished manuscript). Previous modeling frameworks assume that the

nearshore is uniform, or completely exclude the nearshore. This limitation is not trivial; for many nearshore populations, all larvae begin their lives within this zone and must return to the nearshore to settle in adult habitat. The ultimate fate of coastal larvae, nutrients, sediment, and pollutants depends on the transport mechanisms occurring in the inner shelf, nearshore and in their transition zone (Largier 2002). Moreover, growing empirical evidence suggests that many larvae never leave the inner shelf during their time in the plankton (Morgan et al, in revision).

We refer to the reduced nearshore flow as a coastal boundary layer (CBL; Largier 2003). The CBL, operating at 100s to 1000s of meters, is an analogue to the small scale (mm to cm) boundary layers observed at the interface of a fluid and a surface described by fluid mechanics (Kundu and Cohen 2004). As coastal currents flow over the shelf into shallower nearshore areas, they "feel" the effect of the shallow bottom and of the proximity of the coastal boundary. The shoreline acts as a wall, so when water approaches the coast, its motions must adjust to the presence of the coast (Csanady 1972a,b; Pettigrew and Murray, 1981). Thus, coastal currents tend to be mainly along-shore polarized, with relatively weak cross-shore component (Csanady 1972a,b; Kundu and Allen, 1976; Pettigrew and Murray, 1981; Lentz, 1994). The mean and variability in those along- and cross-shore flows is reduced toward the coast, and the coastal boundary restricts the extent of cross-shore diffusive motions (Largier 2003). As a result, the innermost CBL can be described as a region of "sticky water" (Wolanski 1994) exhibiting limited exchange with offshore waters. Including this nearshore flow structure is important when modeling this important and complex region.

The complexity of nearshore oceanography and the details of spatial replacement and persistence of nearshore populations stand in contrast to the relatively simple quantitative methods currently used to assess CWIS entrainment impacts. The assessment methods currently in use fall into two categories (Steinbeck et al. 2007). The Adult Equivalent Loss (AEL) and Fecundity Hindcasting (FH) methods attempt to estimate the amount of adult mortality that would be equivalent to the larval mortality produced by entrainment (AEL) or estimate how many adults' total reproductive output is represented by the number of entrained larvae. These methods rely on highly restrictive and unrealistic assumptions regarding population dynamics and larval dispersal pathways. The Empirical Transport Model (ETM) attempts to obtain a more accurate estimate of the fraction of all larvae that are entrained (within some total volume of "source water") by accounting for the heterogeneous distribution of larvae within the source water. This approach, however, does not put the estimate of larval mortality in the context of adult population dynamics, nor is it straightforward to define the source water for a CWIS along the open coast (as opposed to within a bay or estuary). Given these limitations, it is likely that the traditional approaches are insufficient to accurately project the population-level effects of CWIS entrainment.

The basic goal of this study was to advance our understand of CWIS entrainment effects on coastal ecosystems by using more realistic models of oceanographically-forced larval dispersal and spatially explicit benthic adult population dynamics. To that end, our work consisted of several components:

1) Development of a Lagrangian particle-tracking model to describe nearshore flows, including the CBL, for a generic coastline surrounding a CWIS;
2) Analysis of field data to support the parameterization of the particle-tracking model;
3) Use of the particle-tracking model to describe the influence of local oceanography (flow speed, details of the CBL) and anthropogenic factors (position and intake rate of the CWIS) on larval entrainment;
4) Couple the particle-tracking model to a spatially explicit population model to determine the long-term demographic effects of entrainment and the cumulative effects of entrainment and other factors (such as overharvesting or multiple CWIS);
5) Contrast the results of the coupled bio-oceanographic model to existing protocols for assessing CWIS impacts;
6) Develop guidelines to shape future CWIS planning and assessments.

CHAPTER 2:
Empirical Data

Our present understanding of nearshore circulation posits that flows increase in magnitude and variability along a gradient from the coastal margin (beach) to offshore waters. The precise nature of this gradient is a matter of some dispute, and several different analytical predictions have been suggested (Largier 2003).

A key element of the larval dispersal and entrainment problem is obtaining an accurate characterization of nearshore circulation. Yet we focus here on a general representation and one that captures the essence of the CBL for all open-coast scenarios, as well as not requiring extensive data collection. As mentioned earlier, extremely nearshore flow regimes are difficult to characterize using remote sensing technologies. At present, the only viable option is rather labor intensive and requires the placement of *in situ* instrumentation in a nearshore region of interest. To resolve nearshore circulation, it is critical that studies be heavily instrumented.

A project aimed to gain more insight about the persistent high levels of indicator bacteria in the surf zone off Huntington Beach, California and their possible link to an offshore sewage outfall was carried out in summer 2001 (Noble et al. 2003). As part of this extensive survey, data on water currents and temperature were obtained from bottom mounted Acoustic Doppler Current Profilers (ADCPs) and thermistor strings deployed both nearshore (water depths of 5-10 m) and offshore (water depths of 15-60 m). The study area and instrument array are displayed in Figure 1. Given the dominant pattern of increased flow offshore, the array was comprised of a line extending offshore. This data set is used here to describe the changes in the velocity field from shelf to nearshore. There are no data from the wave-driven surfzone, so this is excluded. This location is typical of coastal regions in California and is particularly relevant to CWIS investigations because of its proximity to the AES Huntington Beach Generating Station.

2.1 Data Collection Methods

2.1.1 Study Area

The study area is located on the San Pedro shelf off the coast of Huntington Beach, California. It is a relatively narrow shelf (~10 km width). Given the scale of the observations, the coastline can be seen as a straight line aligned in a Northwest/Southeast orientation (approximately 301º from the North). There is minimal alongshore variation in topography, isobaths are parallel to the coast. However, there is a submarine canyon (Newport Canyon) located immediately southward of this region. As part of the Southern California Bight, the large-scale circulation of the San Pedro shelf is dominated by the California Current system (Hickey 1992).

Over the shelf, the circulation of coastal regions in the Southern California Bight is known to be complex (Hamilton et al., 2006). The shelf off Huntington Beach can be referred to as a narrow shelf. Wind-driven currents in the Southern California Bight do not account for a large portion of the current variance (Lentz and Winant 1986, Winant et al. 1987, Hickey 1992, 1998) as occurs in other west coast shelf regions, such as off central and northern California. This area

experiences mild prevailing winds out of the northwest in the summer, although on occasion sea breezes may attain strengths of 40 km/hour (25 miles per hour). However, strong summer winds far south, off the coast of Baja California, lead to coastal trapped waves propagating up the coast and driving significant alongshore currents in this region (Pringle and Riser 2002, Hamilton et al. 2006). In addition to wind-driven currents, and a weak southward mean current, tides drive strong alongshore flows over the shelf and nearshore. Cross-shore currents observed nearshore are primarily related to internal tides and internal motions driven by the diurnal sea breeze winds (Lerczack 2000, Lerczak et al. 2001).

2.1.2 Measurement of Currents

The data are part of the Huntington Beach Phase III (HB PIII) project conducted in the summer of 2001 off Huntington Beach, CA. This study was developed and carried out by the Orange County Sanitation District (OCSD) along with scientific teams including Science Applications International Incorporated (SAIC), U.S. Geological Survey (USGS), the Naval Postgraduate School (NPS), and Scripps Institution of Oceanography (SIO). A supplemental study was conducted by MEC Analytical Systems Incorporated (MEC) for the AES power plant. Surveys included hydrographic data collection, microbiological samples (bacteria), and direct current observations at the outer shelf, shelf and nearshore area. Here, the direct observations of coastal currents obtained from bottom mounted RD Instruments WorkHorse Acoustic Doppler Current Profilers (ADCP) in the inner-shelf area will be used. These instruments use sonar to measure water velocity throughout the water column.

This study included six moorings deployed at sites along the cross-shelf from the shelf area (60 m depth and ~ 7.9 km distance from the coast) to nearshore (5 m depth and ~ 0.3 km distance from the coast), two more moorings along the 10-m isobath, and one additional mooring nearshore at 6.5 m depth. Location of the moorings, and deployment details are shown in Table 1 and Figure 1.

2.2 Data Analysis

The operational periods of the ADCP's (Fig. 2) were variable, ranging from 139 days (station MO7) to 8 days (station ADCP1). Besides ADCP1, all the instruments recorded for almost the entire time. The sampling intervals for the different instruments varied from 1 minute to 3 minutes (Table 1). In order to keep a uniform time interval and to preserve temporal resolution of the data, 3 minutes was selected as the minimum sampling interval. The time series with a sampling interval of 1 minute were sub-sampled to obtain regular times series with data every 3 minutes. Data were edited for outliers; spikes were removed and short gaps in the time series were filled by linear interpolation. Velocity records from stations MO6 and AES2 with gaps of approximately 1 and 11 days respectively were separated into two time series. Conventionally, the first good bin above the ADCP head will be referred as the near-bottom measurement and the last good bin from the ADCP head as the near-surface measurement.

When analyzing cross-shore velocity profiles for the purposes of this entrainment study, velocity data were used from instruments in a cross-shore transect including stations ADCP1, AES3, MO3, MO5, and MO6. Data were depth-averaged, and means and standard deviations

were computed for week-long and month-long time scales. For the month-long computations, ADCP1 was dropped from analysis because the time series was only 8 days long.

Table 1: Details of Station Locations for Mooring Deployments at Huntington Beach in Summer 2001

Mooring ID	Location		Water Depth (m)	Instrument Type	Sampling Rate	Bin Size (m)	Deployment Time
	Latitude	Longitude					
M07	33°34.652'N	118°01.137' W	55	300 kHz ADCP	3 min	2	120 days
M06	33°35.667'N	118°00.423' W	35.2	300 kHz ADCP	1 min	2	60 days
M05	33°36.745'N	117°59.822' W	25.5	600 kHz ADCP	3 min	1	120 days
M03	33°37.598'N	117°59.227' W	15	1200 kHz ADCP	3 min	1	120 days
ADCP2	33°38.140'N	117°59.109' W	10	1200 kHz ADCP	1 min	1	91 days
ADCP3	33°38.657'N	118°00.221' W	10	1200 kHz ADCP	1 min	1	91 days
AES3	33°38.086'N	117°58.829' W	9.7	1200 kHz ADCP	3 min	1	30 days
AES2	33°38.367'N	117°58.957' W	6.3	1200 kHz ADCP	3 min	1	30 days
ADCP1	33°38.230'N	117°58.709' W	5	1200 kHz ADCP	1 min	0.5	8 days

Figure 1: Bathymetry of Huntington Beach Study Area

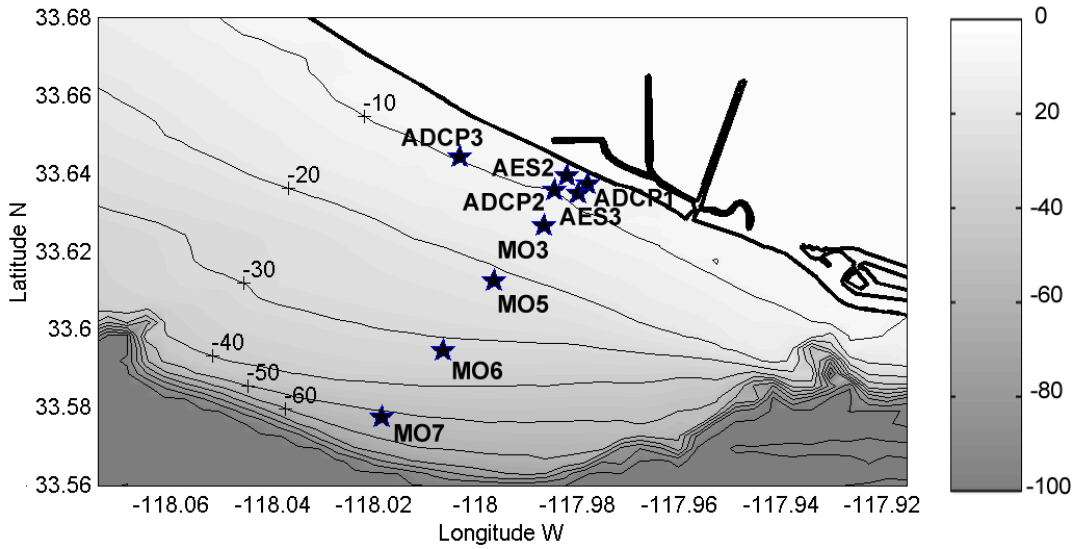

Shading and values on isobaths indicate depth in meters, stars denote the stations where ADCP instruments were moored.

Figure 2: Times of Deployment for ADCP Instruments for each Mooring Station at Huntington Beach

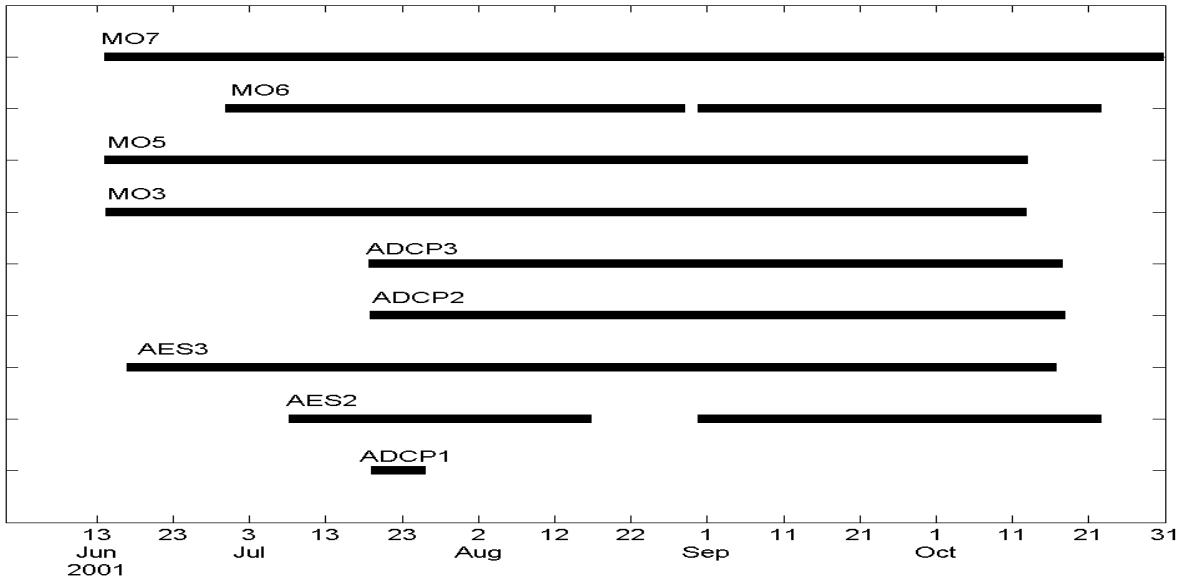

CHAPTER 3:
Nearshore Circulation

The data from Huntington Beach reveal details of nearshore circulation at Huntington Beach and clarify our general understanding of circulation on the inner shelf. Other studies off Santa Barbara, Elkhorn Slough, Santa Cruz and Mission Beach (San Diego) have recently been conducted and these nearshore data also show a clear coastal boundary layer (CBL). Further analysis of these data continues under an independent project related to larval dispersal (Nickols, in prep.).

3.1 Summary of Nearshore Flow off Huntington Beach

Principal axes were calculated for the Huntington Beach velocity time-series (see Table 1 for individual time series lengths). The results are shown together with scatter plots in Figure 3. Most of the variance is associated with the along-shore direction, but there is also non-zero variance in the cross-shore direction (Fig. 3). The elliptical shape of the current ellipses becomes more rectilinear towards the coast; i.e., the cross-shore component reduces its magnitude towards the coast with a slight increase of the along-shore component. This was numerically evident from the ratio between the semi-major and semi-minor axis (numbers in parentheses in Fig. 3), which clearly increases toward the coast (nearshore values were nearly double the offshore values). Thus, shore-parallel polarization in the current increases towards the shoreline, most notably near-surface. The near-bottom current ellipses exhibit weaker alongshore flow and consequently a shape less elongated than those near-surface, indicating the relative importance of the cross-shore flow at this depth. At some stations the near-bottom ellipse was nearly circular, such as at the nearshore stations MO3, AES3 and at the offshore station MO7. Also, whereas near-surface flows show an ellipse aligned to the coast, the near-bottom ellipses were more aligned to the bathymetric contours. Calculations of the ellipse orientation give us near-bottom differences up to 15° between the offshore stations and the nearshore, and for near-surface data only about 5° between offshore and nearshore stations. From these results, the selection of a coordinate system that is aligned with the shoreline is clearly justified. Thus, in order to obtain the velocity components oriented in the cross-shore and along-shore direction, the velocity records were rotated 301 degrees clockwise, which is approximately the direction of the coastline with respect to geographical North.

Figure 3: Summary of Flow Patterns Measured by ADCP at Huntington Beach

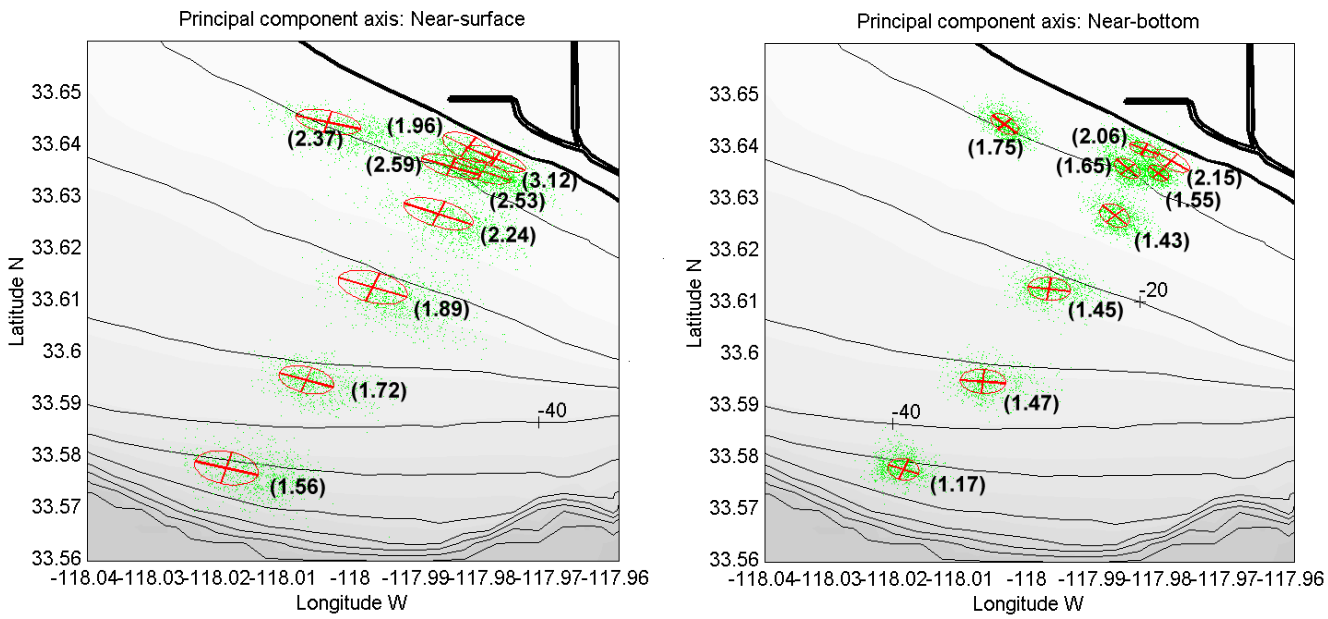

Red lines indicate semi-major and semi-minor axes of variability in near-surface (top panel) and near-bottom (bottom panel) velocity, calculated using principal components analysis. Green dots indicate individual velocity measurements with respect to the principal components axes. Numbers on parentheses represent the ratio between semi-major axis and semi-minor axis of the ellipses. Grey curves indicate 10 m isobaths, background shading indicates depth as in Fig. 1.

Mean and standard deviation (Table 2) were obtained for each velocity component (alongshore and cross-shore) for both near-bottom and near-surface currents. The common period of analysis is from July 20 to September 30 (except for station ADCP1, where the whole 1-week record was used). Surface mean currents (Fig. 4) are along-shore and down-coast (towards the southeast). The maximum mean velocities were near the surface with values up to 13 cm/s over the outer shelf. The mean alongshore near-surface current reduces toward the coast (Fig. 4 and Table 2), up to 1 order of magnitude and the mean cross-shore component is not clearly reduced. The near-surface cross-shore component is an order of magnitude smaller than the near-surface along-shore component (Table 2). However, near-bottom alongshore currents are weaker and of comparable strength to cross-shore currents (Fig. 4). The strong alongshore orientation observed near-surface, is not evident near-bottom. The variability of the velocity records (standard deviation) is much larger than the mean (Table 2), with the stronger variability occurring near the surface. The strength of variability in the cross-shore component did not show remarkable differences between surface and bottom in contrast to the alongshore variability (Table 2). However, variability of the cross-shore component reduced from offshore to nearshore whereas alongshore variability remained much the same.

Table 2: Summary of Cross-Shore and Along-Shore Components of Velocity for Cross-Shore Transect of Moorings at Huntington Beach in 2001

Mooring	Cross-shore		Along-shore	
	Near-Surface	Near-Bottom	Near-Surface	Near-Bottom
MO7	-3.21±9.87	-0.63±6.16	-12.48±14.37	1.48±7.15
MO6	-2.10±11.01	-2.11±7.86	-11.87±16.40	1.67±9.17
MO5	0.63±9.01	-1.26±7.17	-14.19±16.08	-1.55±9.21
MO3	1.93±7.78	-0.08±5.66	-9.82±16.47	-1.74±7.72
ADCP3	0.25±7.36	-0.15±4.47	-8.95±14.55	-1.19±7.37
ADCP2	-0.27±5.98	0.34±4.53	-7.56±14.08	0.22±6.88
AES3	-1.05±5.71	0.28±3.67	-5.87±13.76	0.95±5.46
AES2	4.70±6.30	-1.24±3.51	-0.001±10.80	0.62±7.66
ADCP1	0.04±4.94	-0.30±4.53	-2.35±14.86	2.32±9.54

Figure 4: Vectors of Mean Current Velocity at Surface (red) and Bottom (blue) for Huntington Beach ADCP Moorings

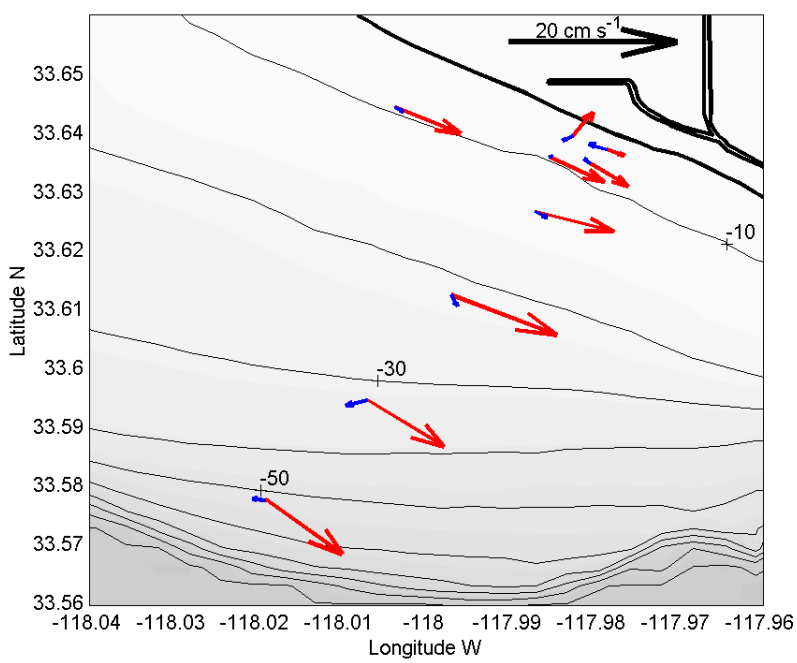

Vector length gives magnitude (scale indicated by black arrow at top), vector direction gives direction in the horizontal plane. Grey curves indicate 10 m isobaths, background shading indicates depth as in Fig. 1.

Depth-averaged time series of the cross-shore transect over periods of one week (Fig. 5) and one month (Fig. 6) including stations ADCP1, AES3, MO3, MO5, and MO6 show a variety of frequencies including significant tidal semi-diurnal and diurnal frequencies. These time series clearly show the polarization of currents, with alongshore velocity an order of magnitude larger than cross-shore velocity. In addition, the means of these time series decrease in shallower depths.

One way to examine the phenomenon of the coastal boundary layer (CBL) is to display the alongshore velocity data as it changes with distance from shore (analogous to small scale boundary layer graphs which display velocity as it changes with distance from a wall). Because we are interested in time scales associated with pelagic larval durations, we focus on means of 1 week and 1 month for short and mid-range dispersers. Mean alongshore velocity decreases toward shore for both one-week (Fig. 7) and one-month (Fig. 8) time periods. The relationship between distance from shore and velocity can be represented by a linear gradient nearshore and a uniform flow offshore, however it may also be approximated by a classical logarithmic profile (as in small-scale classical turbulent boundary layers). For one-month time scale, the flow variability decreases toward shore in a similar fashion (Fig. 9). However, this pattern is less strong over shorter time scales (Fig. 10).

These flow patterns indicate the presence of a coastal boundary layer at Huntington Beach, near the AES power plant (Noble and Xu 2004). Similar flow structure is seen also at other nearshore sites in California (K. Nickols, manuscript in preparation) and elsewhere (Lentz et al. 1999) and we use this coastal boundary layer structure as the foundation of an idealized nearshore flow model.

Figure 5: One-Week Depth-Averaged Time Series of Current Velocity from the Cross-Shore Transect of ADCP Moorings at Huntington Beach between July 19 and July 26, 2001

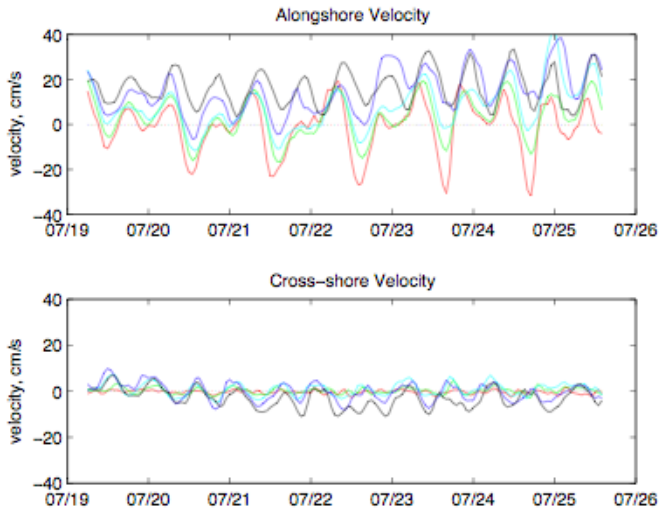

Velocity is decomposed into alongshore (top panel) and cross-shore (bottom panel) components. Each curve represents data from a single station. In order of increasing depth and distance offshore: Red = ADCP1 (5 m), Green = AES3 (10 m), Cyan = MO3 (15 m), Blue = MO5 (25 m), Black = MO6 (35 m).

Figure 6: One-Month Depth-Averaged Time Series of Current Velocity from the Cross-Shore Transect of ADCP Moorings at Huntington Beach between July 19 and August 14, 2001

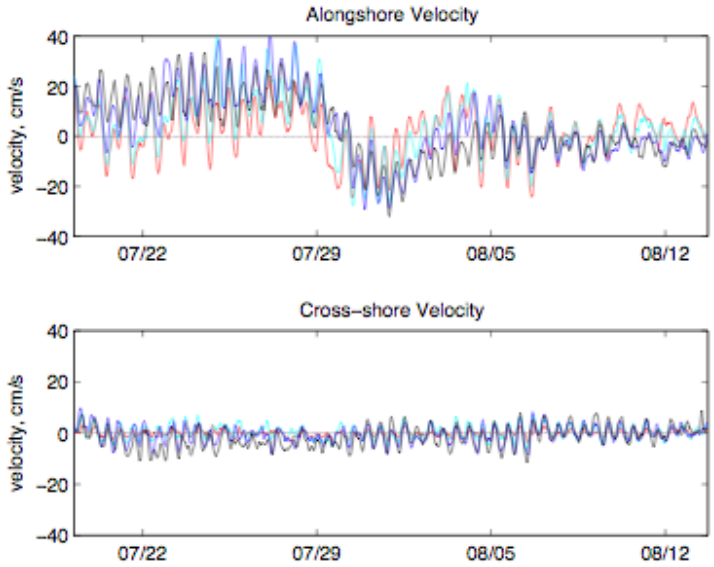

Velocity is decomposed into alongshore (top panel) and cross-shore (bottom panel) components. Each curve represents data from a single station. In order of increasing depth and distance offshore: Red = AES3 (10 m), Cyan = MO3 (15 m), Blue = MO5 (25 m), Black = MO6 (35 m).

Figure 7: Cross-Shore Profile of Mean Alongshore Velocity (cm s^{-1}), Aggregated over a 1-week Time Scale at Huntington Beach, CA

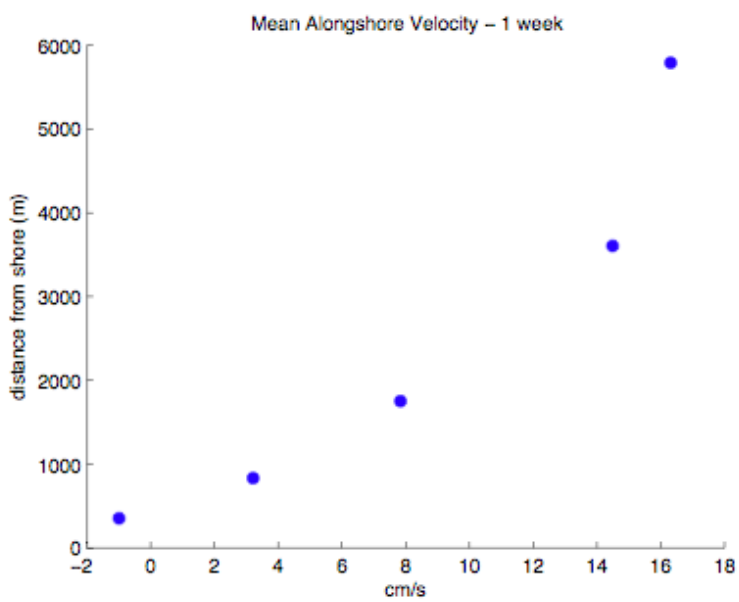

Each point represents data from a different ADCP mooring station in the cross-shore transect.

Figure 8: Cross-Shore Profile of Mean Alongshore velocity (cm s^{-1}), Aggregated over a 1-month Time Scale at Huntington Beach, CA

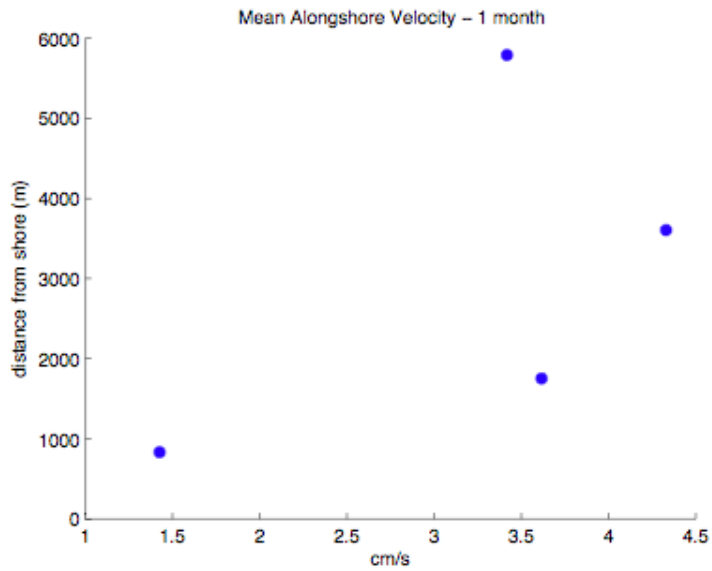

Each point represents data from a different ADCP mooring station in the cross-shore transect.

Figure 9: Cross-Shore Profile of the Standard Deviation of Alongshore Velocity (cm s^{-1}), Aggregated over a 1-Month Time Scale at Huntington Beach, CA

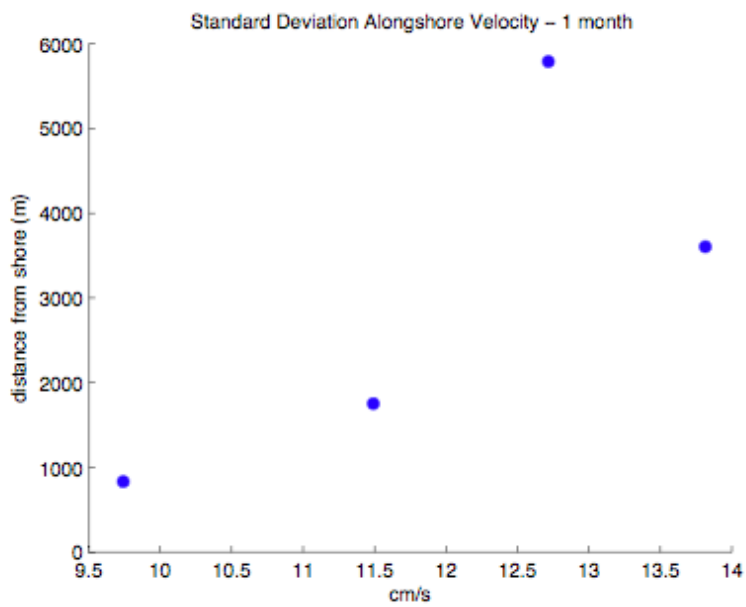

Each point represents data from a different ADCP mooring station in the cross-shore transect.

Figure 10: Cross-Shore Profile of the Standard Deviation of Alongshore Velocity (cm s^{-1}), Aggregated over a 1-Week Time Scale at Huntington Beach, CA

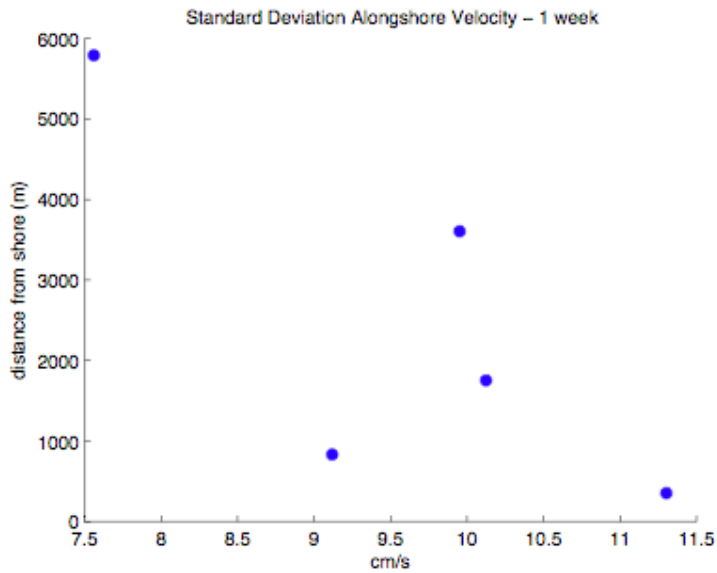

Each point represents data from a different ADCP mooring station in the cross-shore transect.

3.2 Summary of Nearshore Circulation in General

Nearshore circulation is notoriously complex, being affected by a range of processes. The importance of each one to larval dispersal, and how it is accounted for in dispersal modeling, depends on the time scale over which circulation features are aggregated.

Tidal circulation has strong diurnal and semidiurnal signals, which produce most of the variability in time series plots of current velocity (Figs. 5, 6). Because tidal forces are cyclic, they are responsible for considerable dispersion but do not produce any mean flow over time scales longer than a single tidal cycle. Although not apparent in the Huntington Beach data set, the amplitude of tidal oscillations often decreases very close to the shore within the coastal boundary layer (K. Nickols, unpublished data), which will likely decrease tidal mixing.

Wind forcing is especially notable in upwelling systems like those of coastal California. During the spring and summer, when the larvae of most coastal organisms are in the pelagic zone, coastal winds are predominantly from the northwest (i.e., alongshore). The surface layer of water moves in response to this wind stress, and due to the Coriolis effect the net transport of surface water is actually offshore. This leads to upwelling of deeper cold water near the coastal margin. Upwelling also sets up a pressure gradient that produces a geostrophically-forced alongshore jet in the southward (equatorward) direction that dominates alongshore flow over the mid-shelf several kilometers offshore. During the upwelling season, upwelling-favorable winds weaken periodically, leading to relaxation of pressure gradients and disruption of the alongshore jet, resulting in periods of northward (poleward) flow that are strongest over the inner shelf (e.g., Wing et al. 1995, Kaplan et al. 2005). Over the course of an entire spawning season, larvae that remain nearshore are likely to encounter multiple upwelling-relaxation

cycles, reducing the mean flow aggregated at this time scale. However, these flows that reverse on synoptic time scales are important in dispersion of larvae (i.e., in accounting for a diverse collection of outcomes for transport of individual larvae).

In southern California, the effects of local wind forcing are weaker and it is not uncommon that alongshore flow is driven more strongly by coastal trapped waves that were generated by upwelling winds far south, along the coast of Baja California (Pringle and Riser 2002, Hamilton et al. 2006). The effect on larval transport is similar, with a weak mean transport and significant variability in alongshore transport when aggregated over a spawning season that lasts several months.

These upwelling-related flows (whether due to local or remote wind forcing) are strongest over the mid-shelf and the core of the flow is often referred to as an upwelling jet. In general, the strength of this flow decreases towards the shore, and alongshore flow may stall completely very near to the shore where the roughness of the coastal topography obstructs the flow. Further, there are locations in the lee of large headlands where alongshore flow is blocked (as well as the prevailing winds). An example is northern Monterey Bay, where the alongshore flow then separates from the shore and a reversed alongshore flow is observed in the Bay (Graham and Largier 1997, Rosenfeld and Paduan 1997). Likewise, the alongshore flow off Santa Barbara tends to be "upcoast", i.e., towards the west.

Although wave-driven flow is not explicitly addressed in this study, the surf zone is an important, albeit narrow, region. Given the tendency for tidal and wind-driven currents to weaken towards the shore, and given the direct forcing of currents by waves breaking in the surf zone, the surf zone currents are predominantly wave-driven and independent of the coastal boundary layer, which is forced by offshore flows. However, waves and wave-driven currents change on synoptic time scales and it is often true that the mean alongshore flow in the surf zone is near to zero when averaged over a month or pertinent larval time scales, although, again, the variability and thus diffusive effects may be large. Little is known about the interface between the surf zone and offshore flows, and how exchange of constituents occurs. There are observations of rip-current exchange and internal-wave exchange (Smith and Largier 1995, Noble and Xu 2004). In general, however, one can recognize the shorter time scales within the surf zone and deduce that cross-shore exchange (as expressed by eddy diffusivity) must be weaker as in this very nearshore region.

From the perspective of a larva spawned in the nearshore region, the magnitude and direction of oceanographic transport is strongly affected by larval duration. Mean alongshore and cross-shore flows in the extreme nearshore are relatively weak, so transport is primarily diffusive. Diffusion will also be relatively weak in this region, both because the amplitudes of variability in alongshore and cross-shore flows are low and because the mixing length of small-scale turbulent flows are constrained by the proximity of the coastal boundary. These factors combine to limit the mixing experienced by larvae in their first hours or days post-spawning, so that they are initially retained in the nearshore. Over time, mixing is sufficient for larvae to reach faster-moving waters outsde of the surf zone and eventually beyond the coastal boundary layer, where they may be transported in strong alongshore flows (in the coastal jet). Advective

transport in this region scales with the product of mean flow and larval duration, while diffusion scales with the product of the standard deviation of the mean flow and the square root of the larval duration. Thus larvae with longer larval durations may be exposed to advective flows for a much longer proportion of their life and may also experience greater overall advection.

While we have been discussing larval transport as if larvae were passive particles, it is important to realize that larvae can significantly alter their dispersal trajectory by swimming (Largier 2003). The most common swimming behavior observed in temperate invertebrate and vertebrate larvae is vertical migration, which allows the larvae to maintain a relatively constant cross-shelf position by alternately entering seaward-flowing surface waters (e.g., the Ekman layer) and deeper shoreward-flowing waters (Morgan et al, in revision). Directed swimming in the horizontal direction would require some type of navigation on the part of the larvae (in order to be effective), and is not thought to be commonplace except in relatively late-stage fish larvae (Leis 2007; but see Gerlach et al. 2007).

3.3 Idealized Cross-shore Flow Structure in the Coastal Boundary Layer

As has been seen off Huntington Beach and elsewhere, there is a decrease in current speeds towards the shore. Consistent with fundamental hydrodynamic theory, the flow speed must go to zero at the shore (flow continuity precludes cross-shore flow and no-slip boundary condition precludes alongshore flow). Observations indicate that this shoreward decrease in flow strength extends at least a kilometer offshore and in some cases appears to extend multiple kilometers offshore. Given that the adult habitat and spawning of larvae of populations of interest typically occur within these nearshore waters, and given that power plant intakes are invariably also within this zone, it is critical that this flow structure is included in any model estimates of larval transport and dispersal and the associated potential for entrainment of these larvae by CWIS.

While the exact form of the cross-shore profile in currents in the coastal boundary layer varies from site to site (Largier 2003), there is a clear shoreward decrease and one that can be approximated by a linear relationship (current speed is related linearly to distance from the shore). This is combined with the recognition that (i) flows are likely to be more uniform offshore and (ii) one typical finds a very nearshore zone where alongshore flows are blocked by coastal topography or driven by waves independent of the coastal boundary layer. We thus use a "tri-linear" profile (Figure 11), with uniform conditions inshore of distance x_1 from the shore (the nearshore), uniform conditions beyond a distance x_2 from the shore (the offshore), and a linear relationship joining the two. This tri-linear profile is also a reasonable approximation of the theoretical law-of-the-wall logarithmic profile used to describe small-scale turbulent boundary layers (with x_1 related to the roughness length and x_2 related to the boundary layer thickness).

In the following modeling we express the cross-shore dependence of flow using four parameters, each with idealized tri-linear profiles. The model assumes alongshore

homogeneity. Symbol x is used for cross-shore location and y is used for alongshore location. The four parameters are as follows:

1) Alongshore advection – mean flow velocity $V(x)$.

2) Cross-shore advection – mean velocity $U(x)$.

3) Alongshore diffusion – eddy diffusivity due to zero-mean flow variability $K_y(x)$.

4) Cross-shore diffusion – eddy diffusivity due to zero-mean flow variability $K_x(x)$.

Further support for tri-linear idealized profiles arose from preliminary analyses in which it became clear that the relative magnitudes of advective and diffusive length scales (the Peclet number, $\mathrm{Pe} = L_{\mathrm{adv}}/L_{\mathrm{diff}} = (U_x T)/(K_x T)^{0.5}$, where T is the larval duration) are extremely sensitive to small differences in parameter values when the CBL is described using most combinations of the analytical, nonlinear functional forms mentioned above (e.g., the logarithmic law-of-the-wall profile). The nonlinear functional forms also tended to produce rapid changes in Pe across the breadth of the CBL as U and K_y changed at different relative rates. The Peclet number is a critical determinant of population persistence in advective environments, so we sought to minimize potentially unrealistic variability in this number by choosing a functional form that approximately fit empirical data but which had relatively constant first derivatives.

Figure 11: Idealized Tri-Linear Profile used to represent the Cross-Shore Structure in Flow Parameters

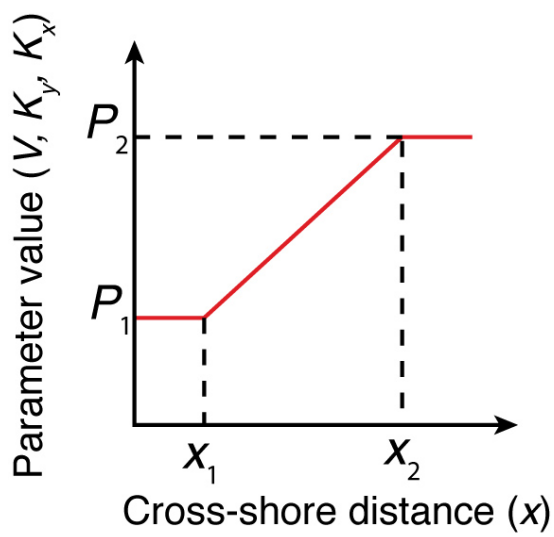

Alongshore velocity $V(x)$, alongshore diffusivity $K_y(x)$, and cross-shore diffusivity $K_x(x)$ are all assumed to vary as a function of cross-shore distance x. In the nearshore region (cross-shore distance $x < x_1$), flow is relatively uniform and slower because coastal topography blocks the influence of alongshore flows, and parameters take on value P_1. In the offshore region ($x > x_2$), free-stream flow is also assumed to be relatively uniform with parameter value P_2. Between points x_1 and x_2, the coastal boundary layer (CBL) produces a monotonic increase in flow parameter values.

CHAPTER 4:
Particle Dispersion Model

A Lagrangian random walk particle model was developed to simulate larval transport in a coastal environment like that described in section 3. The larval population is represented in the model by an array of particles. The position of individual particles, defined by a cross-shore coordinate, x and an alongshore coordinate, y, is updated each model time step with displacements resulting from diffusive and advective processes. The effects of a power plant CWIS on a larval population are simulated by designating a zone of entrainment within which particles are removed from the population.

The model assumes an infinite length of straight coastline with shoreline at $x = 0$ m and a zero-flux condition across the shoreline boundary. There is no offshore or alongshore boundary in the model. The model domain is defined by the extent of particle dispersion. Cross-shore current velocity, U, and alongshore current velocity, V, are defined by prescribed functions of cross-shore position.

Updates to particle position, Δx and Δy, are performed every time-step, Δt, (typically $\Delta t = 120$ seconds), as the sum of advective ($U\Delta t, V\Delta t$) and diffusive (L_x, L_y) displacements.

$$\Delta x = U\Delta t + L_x \qquad \text{(Eq. 2)}$$

$$L_x = \left.\frac{dK_x}{dx}\right|_{x(t)} \Delta t + [r]_{-1}^{1}\sqrt{6K_{x*}\Delta t} \qquad \text{(Eq. 3)}$$

$$x^* = x(t) + \frac{1}{2}\left.\frac{dK_x}{dx}\right|_{x(t)} \Delta t \qquad \text{(Eq. 4)}$$

$$\Delta y = V\Delta t + L_y \qquad \text{(Eq. 5)}$$

$$L_y = [r]_{-1}^{1}\sqrt{6K_y\Delta t} \qquad \text{(Eq. 6)}$$

where U and V are the cross-shore and alongshore advection velocities bilinearly interpolated at particle positions in the flow field and $[r]_{-1}^{1}$ is a random number in the interval [-1,1] (Sanchez-Arcilla et al., 1998).

Eq. (3) and Eq. (4) include the corrections necessary to account for the cross-shore gradient in Kx (dKx/dx) when calculating Lx (Hunter et al. 1993, Visser 1997). This correction term is missing from Eq. (6) because Ky is homogeneous in the alongshore dimension in all model runs.

4.1 Inner-shelf Boundary Layer

As discussed above in section 3.3, we represented the near-coastal reduction in flow speeds by making alongshore velocity V, alongshore diffusivity K_y, and cross-shore diffusivity K_x functions of the distance from shore x. Each parameter was represented by an idealized tri-linear function of x (Fig. 11), defined through 4 parameters: x_1 and x_2 defining the width of the nearshore ($x < x_1$) and the width of the coastal boundary layer ($x < x_2$), while P_1 is the parameter value in the nearshore and P_2 is the parameter value offshore (for $x > x_2$). Different values of x_1 and x_2 were chosen for different parameters to represent specific flow scenarios. The cross-shore velocity U was assumed to be zero everywhere for time scales of interest (a week or more). Only higher frequency cross-shore flows are found nearshore due to the presence of the shoreline boundary precluding any cross-shore flow at $x = 0$. While larvae may effect a mean transport in one or other direction due to direct swimming or vertical migrations which are correlated with reversing cross-shore flows, we do not investigate these effects in this report.

4.2 Intake Entrainment

The probability of particle entrainment by the cooling water intake is a function of radial distance from the intake location. Larvae that pass directly over the intake pipe will have a high likelihood of being entrained whereas larvae passing the intake at a distance have a lower likelihood, and beyond a certain distance there is no chance of entrainment. Given that the detailed flow structure in the withdrawal zone (near-field flow) is not a critical factor, we do not resolve this but rather represent the withdrawal zone by a cylindrical probability function. For a parcel of water located a radial distance, r, from the intake center, the probability of entrainment, $P(r)$ is defined as:

$$P(r) = b\left(1 - \frac{r}{r_0}\right) \qquad \text{(Eq. 7)}$$

where P(0) = b and P(r0) = 0.

During the interval ◎t = 120 seconds, the intake volume flux is Q0◎t and this must equal the volume entrained from the coastal flow passing the intake pipe:

$$Q_0 \Delta t = 2\pi h \int_{r_1}^{r_2} r P(r) dr \qquad \text{(Eq. 8)}$$

where Q0 is the intake flux (m3 s-1) and h is the mean water depth in the vicinity of the intake (h = 7 m in all model runs). For r1 = 0 and r2 = r0, Eq. (7) simplifies to:

$$r_0 = \sqrt{\frac{3\Delta t Q_0}{\pi b h}} \qquad \text{(Eq. 9)}$$

For all model runs, r0 = 24 m, but model results are not sensitive to the value of r0 for 10 ≥ ◎t ≤ 120 seconds.

CHAPTER 5:
Modeled Patterns of Larval Dispersal

A realistic representation of near-coastal flows and the consequent dispersal of larvae is necessary prior to assessing the impact of CWIS entrainment on larval populations. We used the particle dispersion model described in section 4 to estimate the extent to which planktonic larvae are dispersed by typical near-coastal ocean currents. We investigated larval dispersal for two time scales of interest, and then included the effects of CWIS entrainment.

The first time scale represents planktonic larval durations (PLD), on the order of days to weeks (within a season) and aggregating over alongshore distances of order 100 km. Alongshore flow is likely to be relatively consistent and thus the mean flow is quite strong. Modeling dispersal over this time scale represents the distribution of likely pathways of larvae released during a single spawning event. This time scale is addressed in this section.

The second, longer time scale represents population-scale processes. Reproduction in benthic populations typically lasts several months during the year, sometimes spanning multiple seasons and encompassing a wide range of flow conditions. For example, in coastal California, the spawning seasons for many benthic invertebrates span the "spring transition" (Shanks and Eckert 2005) – combining dispersal during winter conditions (variable winds) and spring upwelling conditions (persistent north winds). Given flow reversals, both seasonal and synoptic, the circulation at these longer time scales is best represented by smaller estimates for advective components of flow and larger estimates for the stochastic components of flow (Eq. 2). This is particularly true when one considers that the time scale relating to equilibrium population dynamics is actually the generation time of an organism, often on the order of several years (or decades) and potentially including the effect of anomalous years (e.g., El Nino events). In addition to temporal aggregation of circulation patterns, alongshore aggregation is needed, further increasing the stochastic flow component and reducing the advective component. This population time scale is addressed in section 6.

In this section we consider models of dispersal over the shorter PLD time scale. Parameter values are scale estimates based on a review of literature (e.g., Largier 2003; Carrillo et al, unpublished) combined with a synthesis of much unpublished data (drifters, dye, current meter, and HF radar data) in diverse locations throughout California and elsewhere. Nearshore, we expect weak alongshore flow due to the drag of the shoreline, the variable strength of wave-driven flows in the surfzone, and the presence of coves, points and stacks that obstruct the flow. The structure of the flow is complex and the default is to assume that the mean flow is uniform. We take $V = 0$ m s^{-1} as default, with speeds of -0.1 m s^{-1} and 0.1 m s^{-1} as alternatives (negative values indicate wave-driven flow counter to shelf flow). Depending on the roughness of the coastline the nature of the surfzone, the width of the nearshore zone varies and we take $x_1 = 100$ m as a default, but also consider cases where it is as little as 15 m (e.g., smooth shoreline and little waves) or as much as 500 m (e.g., in presence of headlands, kelp

forests, and macro-rip currents). In the CBL beyond the nearshore, we model a linear increase in alongshore flow. The default offshore (shelf) velocity is 0.1m s^{-1}, which is attained 3000 m offshore. The CBL width also is varied, and a width as small as 300 m is considered (for slow flow along a smooth coast and over a steeply sloping shelf). Also, monthly mean shelf flow may be stronger, and a value of 0.3 m s^{-1} is used to represent strongly wind-forced scenarios typical of central and northern California (e.g., Largier et al 1993).

Fluctuating alongshore currents (which account for alongshore eddy diffusivity K_y) are expected to have a structure similar to that of the alongshore mean flow, increasing linearly between a nearshore zone and an offshore (shelf) zone. We take 400 $m^2 s^{-1}$ as a scale that reasonably represents reversing flows associated either with tides or with synoptic variability (flows of order 0.1 m s^{-1} reversing on times scales of 10^5-10^6 s), but also consider weaker and stronger alongshore diffusivity by using 100 $m^2 s^{-1}$ and 1000 $m^2 s^{-1}$, respectively. Based on observations of strong alongshore tidal currents off Huntington Beach (Noble et al. 2003, Carrillo et al. unpublished), we model a narrower zone with x_2 value of 1000 m. This results in a band between 1000 and 3000 m offshore where the Peclet number has a minimum (i.e., diffusive effects are most important). However, typically alongshore mixing is dominated by shear dispersion due to mixing across the cross-shore shear in the alongshore flow; thus the exact value of K_y is less important than the values for K_x and $\Delta V/ \Delta x$. Nearshore, K_y is weak, but does not go to zero, owing to wave-driven flows and topographic eddy effects. We use a uniform value of 20 $m^2 s^{-1}$ nearshore. To ensure a continuous profile for $K_y(x)$, we choose x_1 such that the uniform nearshore value matches that of the CBL linear profile.

Cross-shore currents are assumed to have zero mean due to the shore boundary, and fluctuations that decrease to zero at the shore. Again, we expect a uniform nearshore zone due to wave-driven currents and use K_x = 10 $m^2 s^{-1}$ as a reasonable scale for surfzone mixing (Smith and Largier 1995; Clarke et al 2005). This extends offshore to where it matches the linear profile for $K_x(x)$. A maximum value of 100 $m^2 s^{-1}$ is reached at a distance of 1000 m offshore. We also explore the effects of stronger (K_x = 500 $m^2 s^{-1}$) and weaker (K_x = 20 $m^2 s^{-1}$)cross-shore mixing.

Given the four indices (x_1, x_2, P_1, P_2) that can be evaluated for each of three dispersion parameters represented by the tri-linear profile (V, K_x, K_y), as well as the need to specify the offshore position of the intake and the alongshore position of the intake relative to spawning locations, this is a high-dimension problem. While there are many variations that we modeled to develop our understanding, it is not realistic to conduct a systematic exploration of parameter space, nor a sensitivity analysis for each parameter value. Therefore, for reporting purposes, we have reduced the number of model runs and report on four different advective flow scenarios, ranging from zero mean flow to very rapid alongshore advection (Table 3). Within each advection scenario we explored the consequences of varying the width of the coastal boundary layer; that is, we varied the cross-shore position of break-points (x_1 and x_2) in the tri-linear CBL profile for both K_x and K_y. As a first cut we simply examined whether using a relatively wide CBL or a relatively narrow CBL for both diffusivities produced different results (Table 3). We also explored the effects of the magnitude of $K_{y\,max}$ and $K_{x\,max}$. Again, to capture a basic understanding of the effects of these parameters we considered four cases with $K_{y\,max}$ and $K_{x\,max}$ taking on strong/strong, weak/weak, strong/weak, and weak/strong values, respectively

(Table 3). This affords a general understanding of their relative importance without requiring a fully orthogonal exploration of parameter space.

Table 3: Parameter Values Used in Particle Dispersion Model Runs

Advection regime scenarios					
	Parameter	P_1	P_2	x_1	x_2
Diffusion only	V	0.0 m s^{-1}	0.0 m s^{-1}	100 m	3000 m
Moderate	V	0.0 m s^{-1}	0.1 m s^{-1}	100 m	3000 m
High	V	0.0 m s^{-1}	0.3 m s^{-1}	100 m	3000 m
Nearshore countercurrent	V	-0.1 m s^{-1}	0.1 m s^{-1}	100 m	3000 m
CBL width scenarios					
	Parameter	P_1	P_2	x_1	x_2
Wide CBL	K_y	20.0 m s^{-1}	400.0 m s^{-1}	50 m	1000 m
	K_x	10.0 m s^{-1}	100.0 m s^{-1}	100 m	1000 m
Narrow CBL	K_y	20.0 m s^{-1}	400.0 m s^{-1}	15 m	300 m
	K_x	10.0 m s^{-1}	100.0 m s^{-1}	15 m	300 m
Diffusivity strength scenarios					
	Parameter	P_1	P_2	x_1	x_2
Weak $K_{y\,max}$	K_y	20.0 m s^{-1}	100.0 m s^{-1}	200 m	1000 m
Weak $K_{x\,max}$	K_x	10.0 m s^{-1}	20.0 m s^{-1}	500 m	1000 m
Weak $K_{y\,max}$	K_y	20.0 m s^{-1}	100.0 m s^{-1}	200 m	1000 m
Strong $K_{x\,max}$	K_x	10.0 m s^{-1}	500.0 m s^{-1}	20 m	1000 m
Strong $K_{y\,max}$	K_y	20.0 m s^{-1}	1000.0 m s^{-1}	20 m	1000 m
Weak $K_{x\,max}$	K_x	10.0 m s^{-1}	20.0 m s^{-1}	500 m	1000 m
Strong $K_{y\,max}$	K_y	20.0 m s^{-1}	1000.0 m s^{-1}	20 m	1000 m
Strong $K_{x\,max}$	K_x	10.0 m s^{-1}	500.0 m s^{-1}	20 m	1000 m

For each model run, alongshore velocity V was defined using one of the advection regime scenarios, and diffusivities K_x and K_y were defined either by one of the coastal boundary layer (CBL) width scenarios or one of the diffusivity strength scenarios. For each parameter, a particular scenario was characterized by the shape of the tri-linear CBL profile (Fig. 11), which was defined in terms of the cross-shore positions x_1 and x_2 and the parameter values P_1 and P_2 associated with those positions. The shorthand names for each scenario are used in the figures to indicate which parameter set was used for a particular set of model results.

For each model run we released 10,000 particles (larvae) from a single location and examined the distribution of successful settlers. This distribution is an estimate of the probability of dispersal from the origin to each possible destination, i.e., the dispersal kernel. Settlers are defined as those particles within 500 m of the coastline after a specific time has elapsed (the species-specific PLD). It is assumed that larvae within 500 m of the shore will find habitat there, be mixed to the shore, or show some active behavior that would allow them to move to nearshore habitats. For each model run, we also show the mean trajectory of successful settlers and the time-dependent larval entrainment at the CWIS. In most of these runs, larvae were released 500 m offshore of position $y = 0$, and the CWIS was located 1 km downstream at $x = 500$ m, $y = 1000$ m.

5.1 Larval Dispersal Results and Discussion

5.1.1 Non-Advection Scenarios

Running the particle-tracking model with alongshore velocity V = 0, we examined the effects of the diffusivity parameters in isolation. First, we compared the dispersal kernels produced using a relatively wide coastal boundary layer (CBL), with the nearshore zone ending at 50 to 100 m (parameter x_1) and the offshore zone starting at 1000 m (parameter x_2) to the dispersal kernels produced with a relatively narrow CBL (x_1 = 15-30 m, x_2 = 300 m). These CBL dimensions applied to the cross-shore profile of both diffusivity parameters and values of $K_{y\,max}$ and $K_{x\,max}$ were not changed across these scenarios. These model runs reveal a basic result common to all advection-diffusion models: as particles spend more time in the plankton (longer PLD) they diffuse further in the alongshore dimension, producing more widespread distributions of successful settlers (Fig. 12). However, there was no apparent effect of CBL width on the shaped of the dispersal kernel for a range of PLDs (Fig. 12). An examination of the average trajectory of successful recruits for a range of PLDs reinforces this conclusion: there is no substantial difference between runs with wide and narrow CBLs (Fig. 13).

There was, however, a noticeable effect of the diffusivity parameters $K_{y\,max}$ and $K_{x\,max}$ on dispersal patterns. We examined four scenarios with different combinations of weak ($K_{y\,max}$ = 100 $m^2\,s^{-1}$, $K_{x\,max}$ = 20 $m^2\,s^{-1}$) and strong ($K_{y\,max}$ = 1000 $m^2\,s^{-1}$, $K_{x\,max}$ = 500 $m^2\,s^{-1}$) diffusivities. We interpret these scenarios as representing different intensities in the stochastic component of circulation over short time scales, but they also reveal the difference in patterns obtained when the same region is observed at relatively short (weak diffusivity) and long (strong diffusivity) time scales. In general, increasing $K_{y\,max}$ increased the width of the dispersal kernel for a given PLD, causing the same number of settlers to be spread over a much wider stretch of the coastline (compare horizontal axes in Figs. 14a and 14c). Increasing $K_{x\,max}$ had the effect of reducing overall settlement (the height of the kernel) without changing the alongshore distribution of successful settlers (compare Figs. 14a and 14b). Presumably this occurs because higher $K_{x\,max}$ values caused larvae to be mixed further offshore, from whence they were less likely to return to settle successfully. This explanation is supported by the mean particle tracks in each scenario, which reveal that when $K_{x\,max}$ is greater, even successful settlers make excursions much further offshore before returning to settle (Fig. 15).

Different diffusivity parameter values also produce strikingly different patterns of larval entrainment. When both diffusivities are relatively weak, cumulative larval entrainment increases relatively linearly over time; that is, there is an approximately constant rate of entrainment (Fig. 16a). Increasing $K_{x\,max}$ does not alter the shape of this curve substantially, but does reduce the overall rate of entrainment by a factor of four (Fig. 16b). By contrast, increasing $K_{y\,max}$ changes the shape of the cumulative entrainment curve, with a high proportion of total entrainment occurring in the first 5 days and entrainment tapering off thereafter (Fig. 16c). This occurs because larger values of $K_{y\,max}$ cause larvae to diffuse away from the CWIS more rapidly, so that most entrainment occurs soon after spawning when the larval cloud is relatively concentrated near the CWIS. It should be noted that these patterns depend on the relative position of the CWIS and would differ somewhat if larval mortality were taken into consideration. If larvae experience a temporally constant mortality rate during their time in the plankton, there will be a greater total number of larvae immediately after spawning and relatively few larvae remaining in the water column to be entrained after 10 or 20 d. Therefore most entrainment will occur soon after spawning, when there are more larvae to be entrained and they are more concentrated, and relatively less entrainment of older larvae (in absolute numbers, not in terms of proportional entrainment). However, as expanded on in the next section, older larvae are much more valuable because they have a much higher likelihood of surviving to settle. The cumulative entrainment curves are thus a better indication of proportional entrainment risk to larvae of different ages, rather than being an accurate indication of the total numbers of larvae entrained in a real system.

5.1.2 Unidirectional Advection Scenarios

Adding either moderate (V_{max} = 0.1 m s^{-1}) or high (V_{max} = 0.3 m s^{-1}) advection to the particle tracking model produced patterns generally similar to those described in the non-advective scenario. The primary difference, of course, is that dispersal kernels are displaced downstream, rather than being centered on the point of release. In a uniform flow field (i.e., no CBL shear) this displacement would have a mean of V × PLD, while the standard deviation in transport (due to diffusive effects) are estimated by $(K_y \times PLD)^{0.5}$. With V = 0.3 m s^{-1}, K_y = 400 m^2 s^{-1} and PLD = 4 d this would be a mean of approximately 105 km and standard deviation of approximately 40 km. When the CBL is included, introducing slower flows nearshore, the mean and standard deviation are smaller than those predicted by the uniform flow field approximation. For the 4-day PLD example, the actual kernel had a mean of approximately 75 km and a standard deviation of approximately 30 km (Fig. 17). Advection was thus considerable, but significantly less than that predicted by a model that did not account for the effects of the CBL.

The effects of varying $K_{x\,max}$ and $K_{y\,max}$ did not differ from the non-advective scenario: increasing $K_{y\,max}$ produced wider dispersal kernels, while increasing $K_{x\,max}$ depressed total settlement rates (Fig. 18). However, a noticeable difference from the non-advective results was in the cumulative entrainment curves. When there is advection in the system, all larvae are swept away from the CWIS relatively rapidly, so nearly all entrainment occurs in the first few days after spawning (Fig. 19).

5.1.3 Nearshore Countercurrent Scenarios

In addition to the relatively straightforward non-advective and advective scenarios, we also considered a case in which mean flow nearshore is in the opposite direction to that over the shelf. This represents significant and persistent wave-driven flow nearshore, e.g., during periods of south swell and north winds in southern California. To explore the effects of this pattern on dispersal and entrainment, we ran scenarios with $V = -0.1$ m s^{-1} in the nearshore (inshore of x_1) and an offshore "free-stream" velocity of $V = 0.1$ m s^{-1}.

The dispersal patterns produced by this flow scenario differed noticeably from the previous scenarios. For example, dispersal kernels revealed no net advection for PLDs less than 6-8 d, when successful larvae spend most of their time in the CBL, but strong advection for longer PLDs (Fig. 20). This pattern was strongly affected by the choice of diffusivity parameters: extremely strong cross-shore diffusivities ($K_{x\,max}$) produced kernels with high advection for all PLDs (Fig. 21b), apparently because more larvae were transported offshore more rapidly, where net advection is positive (Fig. 22b). By contrast, weaker cross-shore diffusivity produces weak or no net advection (Fig. 21c), as more larvae spend more time in the nearshore and CBL, thus experiencing net flow in both directions (Fig. 22c). In fact, the patterns of entrainment in the counter-current flow scenario were remarkably similar to those in the non-advection scenario (compare Figs. 16 and 23). Increasing along-shore diffusivity ($K_{y\,max}$) did not have a strong effect on advection, but did produce broader kernels (Fig. 21c,d).

While there are many other possible scenarios, this suite of model runs effectively communicates the importance of different parameters in controlling dispersal outcomes. Larvae that are mixed cross-shore by K_x sample a variety of alongshore flow speeds in the sheared coastal boundary layer, thus increasing the distribution of alongshore displacements across the larval population. This is a classical transport phenomenon known as shear dispersion and in the CBL model shear dispersion typically exceeds the effect due to fluctuations in the alongshore flow (represented by diffusivity K_y) – for example, see Clarke et al (2005). However, our concern is the impact of entrainment within the CBL, which is through reduced recruitment to adult populations and consequent population reduction. To explore this, we link the above-described dispersal results to a population model.

Figure 12: Dispersal Kernels Calculated using Particle Dispersion Model for Diffusion-Only Scenario

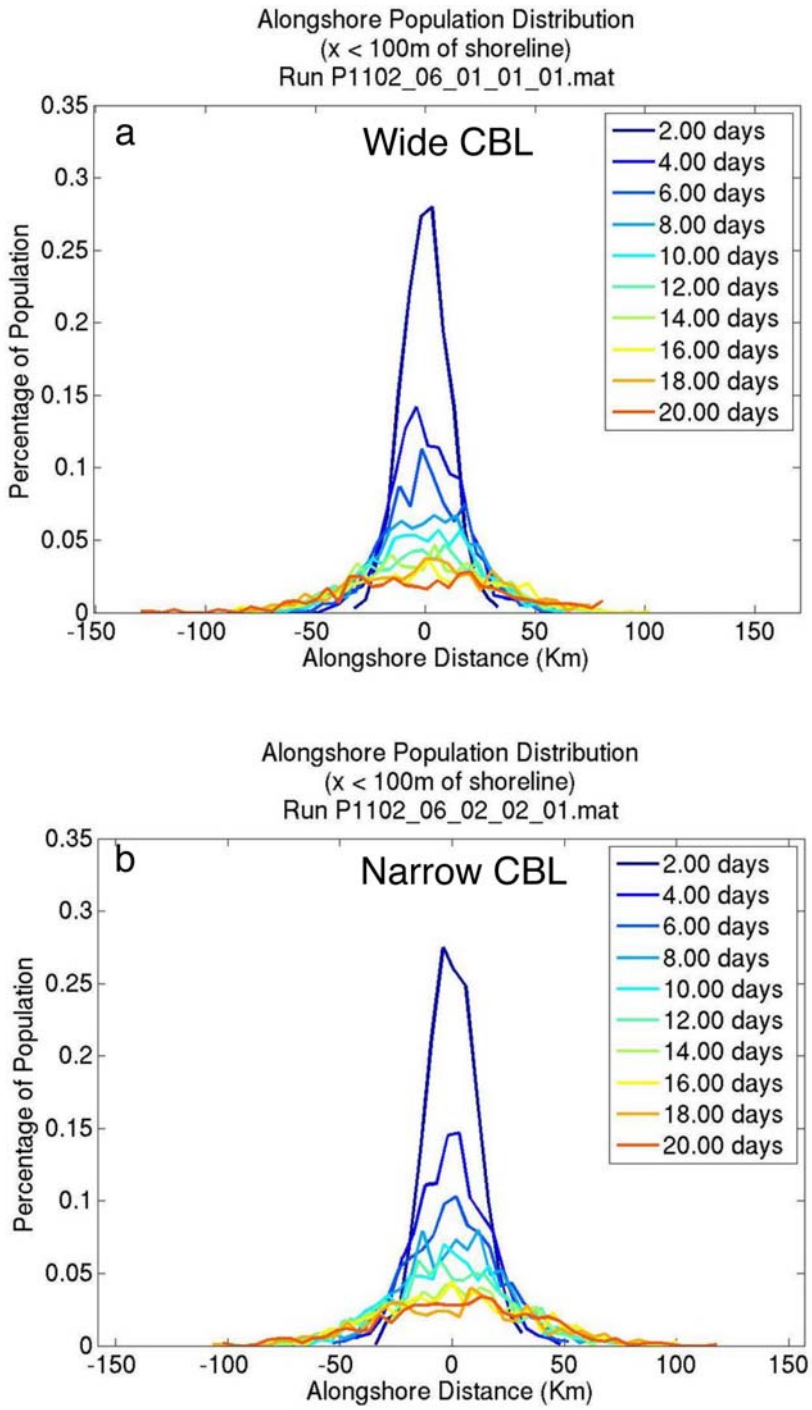

Curves show the percentage of larvae < 100 m from shore (i.e., potential settlers) at each alongshore location for a range of pelagic larval durations (indicated by curve color). Results are shown for model runs performed using a relatively wide (top panel) and relatively narrow (bottom panel) coastal boundary layer (CBL). Larvae were released near alongshore position $y = 0$.

Figure 13: Mean Particle Trajectories Calculated using Particle Dispersion Model for Diffusion-Only Scenario

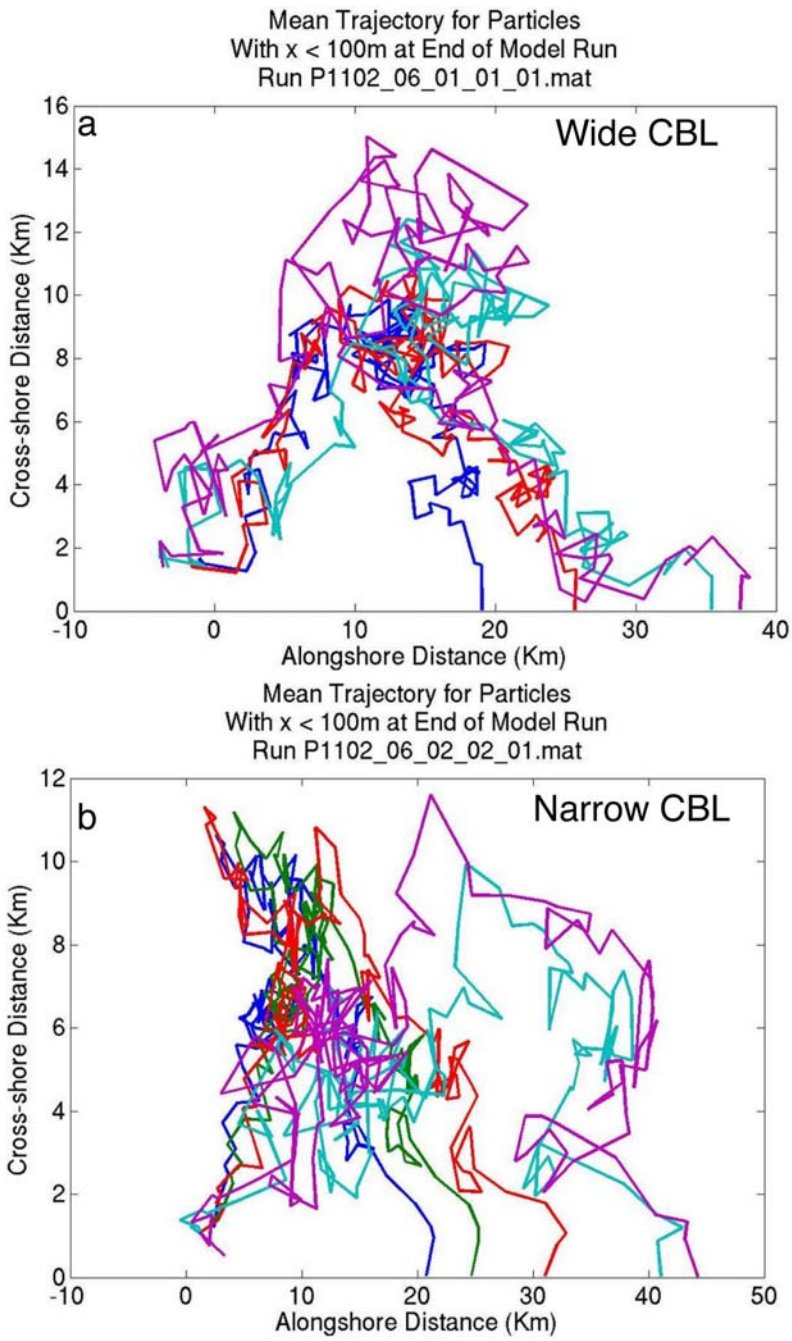

Curves show the average path of larvae that successfully returned to within < 100 m from shore (i.e., potential settlers) at each alongshore location for a range of pelagic larval durations (indicated by curve color; blue = 4 d, red = 8 d, green = 12 d, cyan = 16 d, magenta = 20 d). Results are shown for model runs performed using a relatively wide (top panel) and relatively narrow (bottom panel) coastal boundary layer (CBL). Larvae were released near alongshore position $y = 0$.

Figure 14: Dispersal Kernels Calculated using Particle Dispersion Model for Scenarios with No Alongshore Advection but Varying Strengths of Alongshore Diffusivity (K_y) and Cross-Shore Diffusivity (K_x)

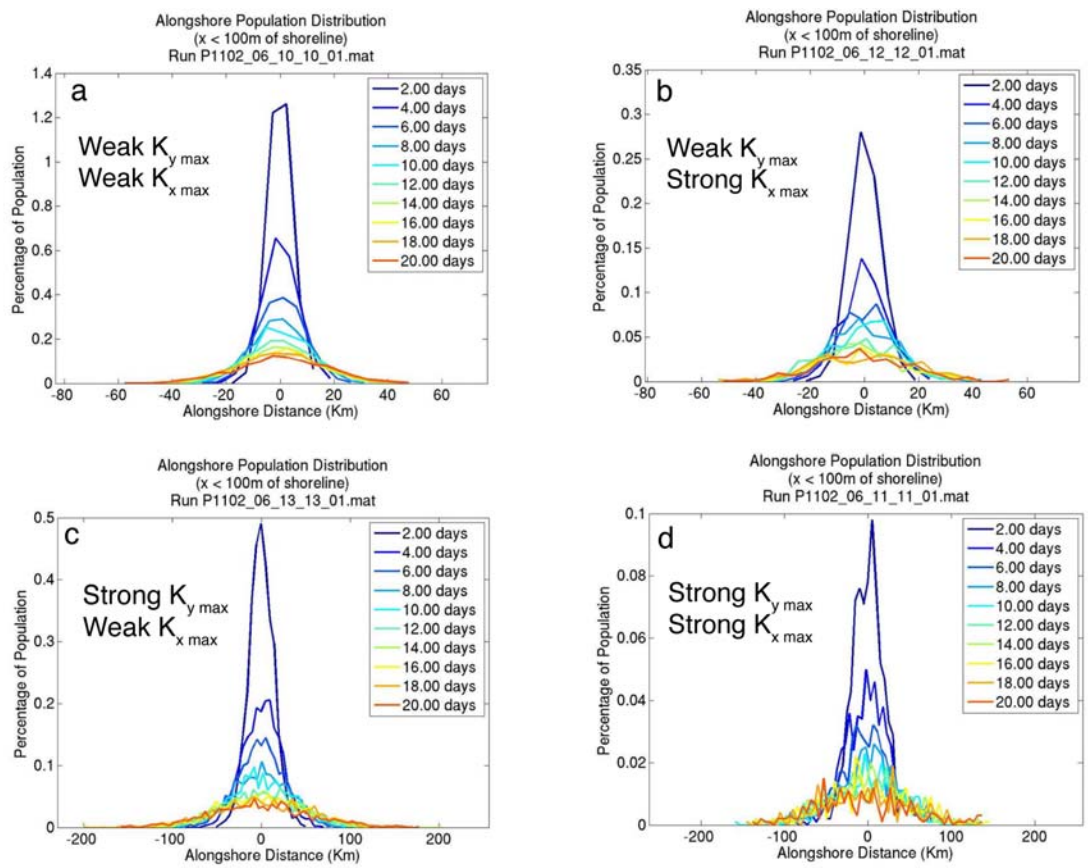

Curves show the percentage of larvae < 100 m from shore (i.e., potential settlers) at each alongshore location for a range of pelagic larval durations (indicated by curve color). The cross-shore profile of the coastal boundary layer (positions x_1 and x_2 in Fig. 11) was identical among all four panels. Larvae were released near alongshore position $y = 0$.

Figure 15: Mean Particle Trajectories Calculated using Particle Dispersion Model for Scenarios with No alongshore Advection but Varying Strengths of Alongshore Diffusivity (K_y) and Cross-Shore Diffusivity (K_x)

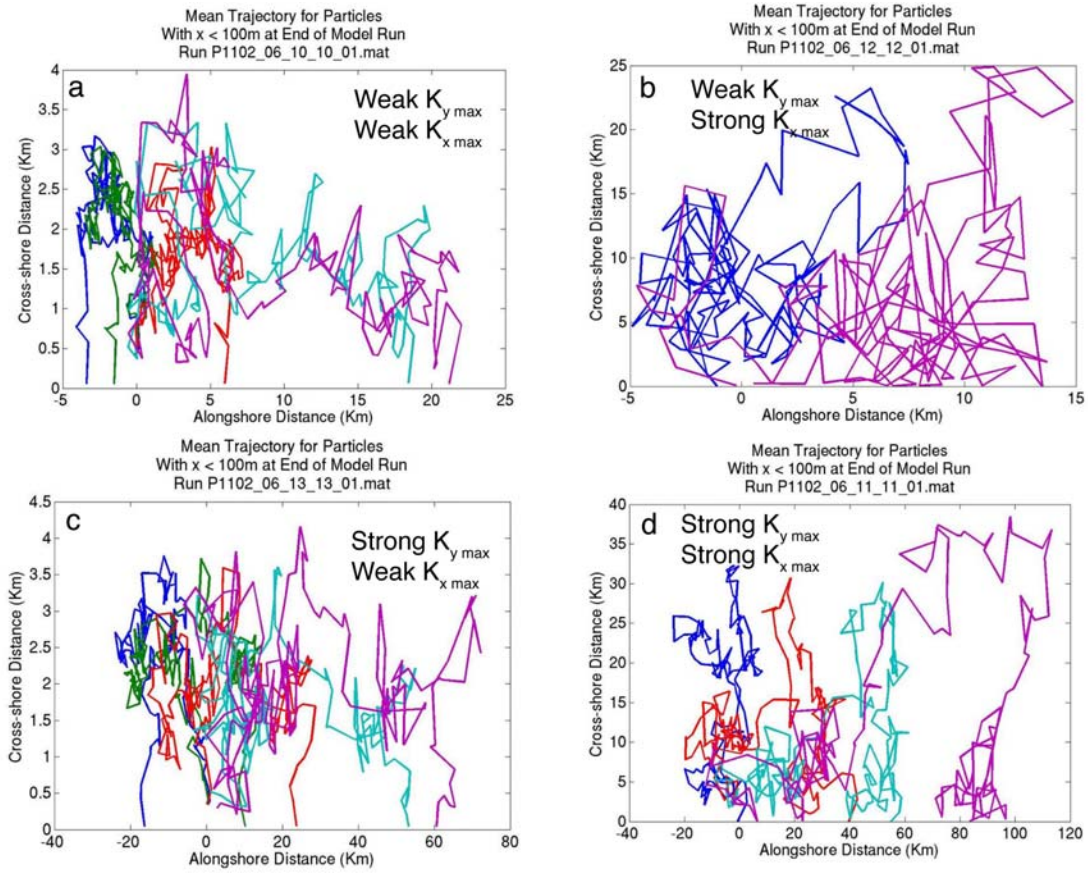

Curves show the average path of larvae that successfully returned to within < 100 m from shore (i.e., potential settlers) at each alongshore location for a range of pelagic larval durations (indicated by curve color; blue = 4 d, red = 8 d, green = 12 d, cyan = 16 d, magenta = 20 d). The cross-shore profile of the coastal boundary layer (positions x_1 and x_2 in Fig. 11) was identical among all four panels. Larvae were released near alongshore position $y = 0$. Notice that scales of x and y axes vary among panels.

Figure 16: Time Series of Particle Entrainment for Scenarios with No Alongshore Advection but Varying Strengths of alongshore Diffusivity (K_y) and Cross-Shore Diffusivity (K_x)

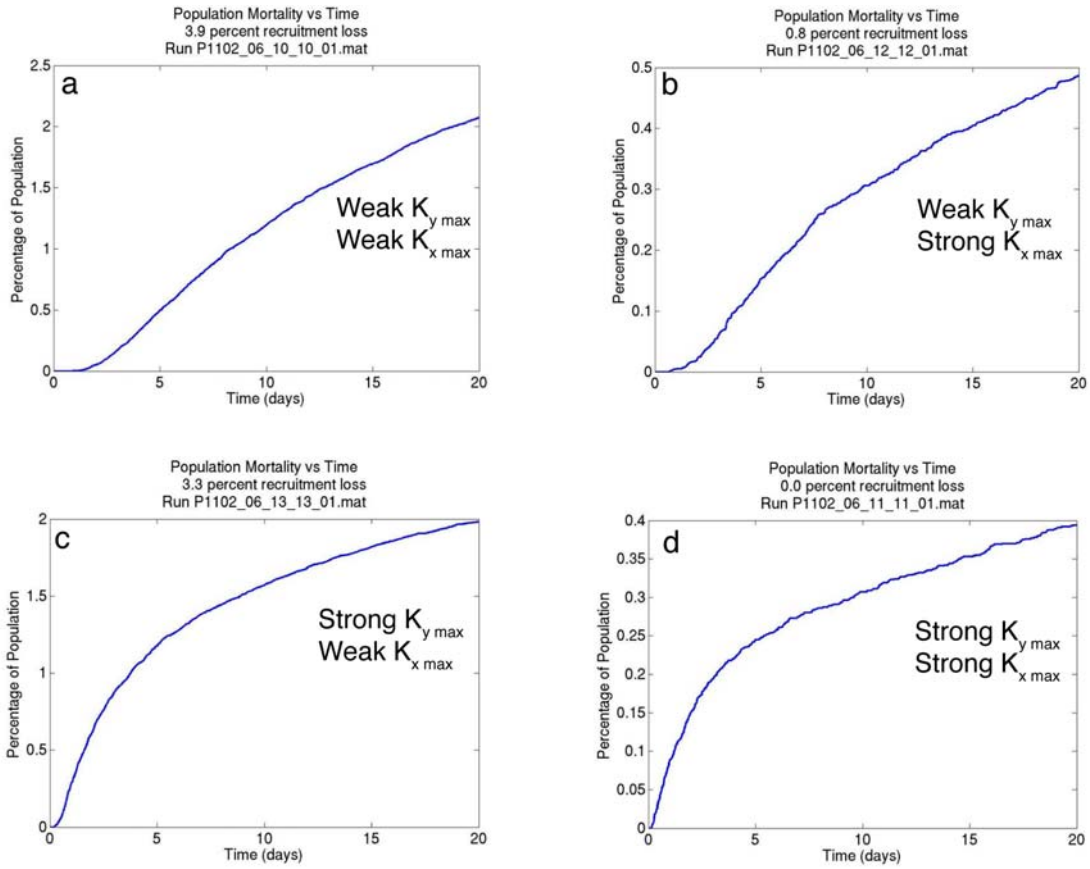

Curves show the cumulative percentage of larvae entrained in the CWIS over time. The cross-shore profile of the coastal boundary layer (positions x_1 and x_2 in Fig. 11) was identical among all four panels. Larvae were released near alongshore position $y = 0$. Notice that the scale of the vertical axis varies among panels.

Figure 17: Dispersal Kernels Calculated using Particle Dispersion Model for Scenarios with either Moderate (V_{max} = 0.1 m s^{-1}, left panels) or High (V_{max} = 0.3 m s^{-1}, right panels) Mean Alongshore Advection

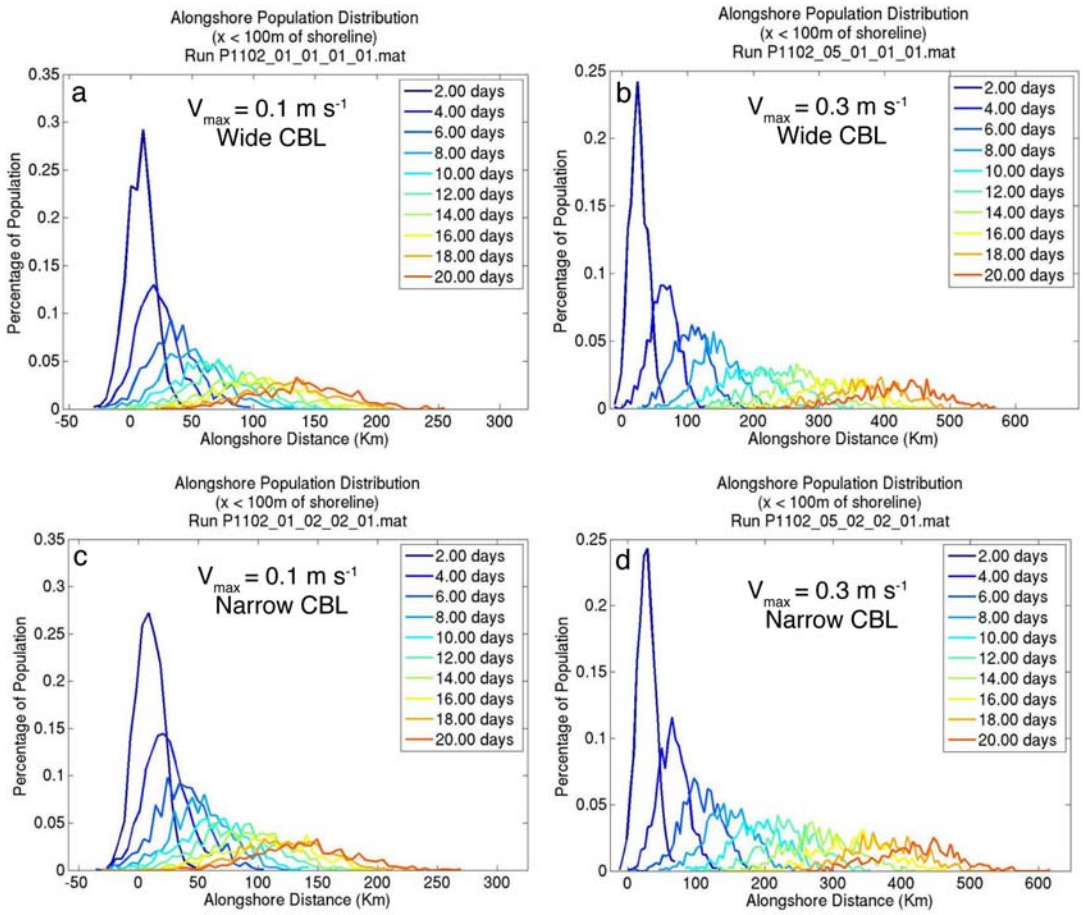

Curves show the percentage of larvae < 100 m from shore (i.e., potential settlers) at each alongshore location for a range of pelagic larval durations (indicated by curve color). Results are shown for model runs performed using a relatively wide (top panels) and relatively narrow (bottom panels) coastal boundary layer (CBL). Larvae were released near alongshore position y = 0.

Figure 18: Dispersal Kernels Calculated using particle Dispersion Model for Scenarios with either Moderate (V_{max} = 0.1 m s^{-1}, left panels) or High (V_{max} = 0.3 m s^{-1}, right panels) Mean Alongshore Advection and either relatively Weak (top panels) or Strong (bottom panels) Alongshore and Cross-Shore Diffusivities (K_y, K_x)

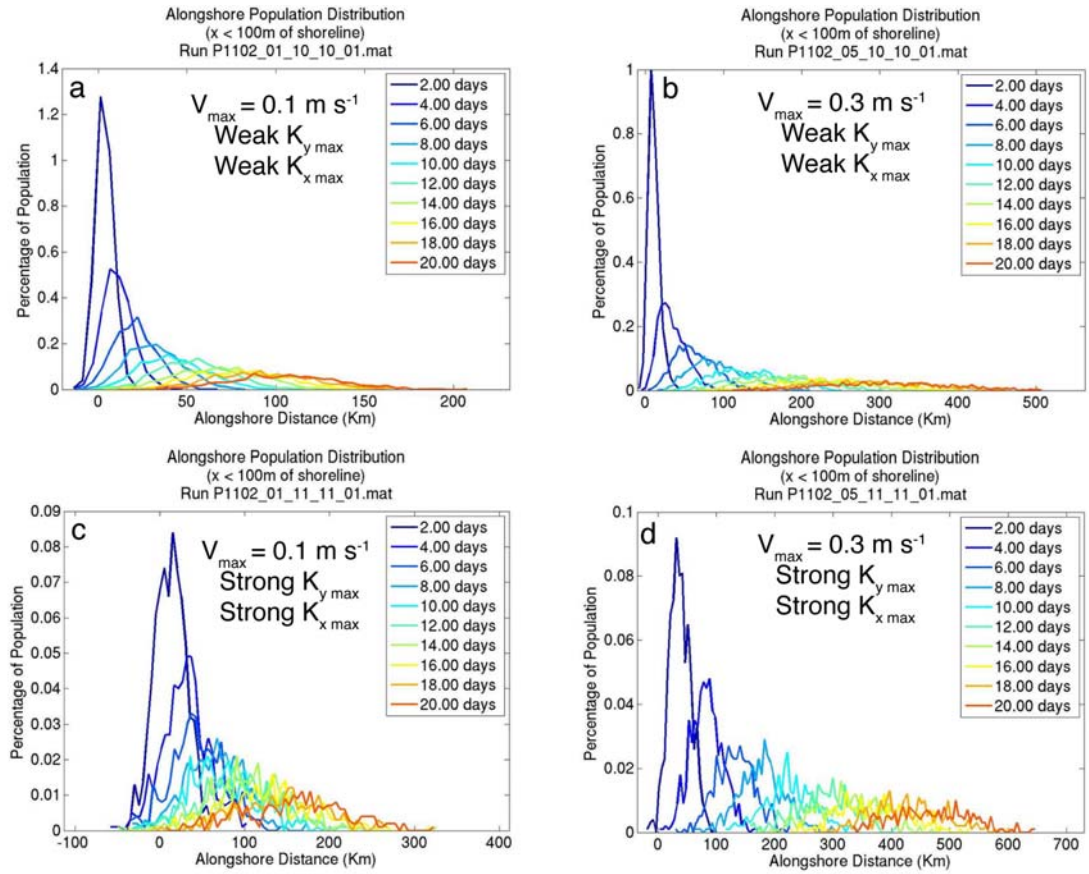

Curves show the percentage of larvae < 100 m from shore (i.e., potential settlers) at each alongshore location for a range of pelagic larval durations (indicated by curve color). The cross-shore profile of the coastal boundary layer (positions x_1 and x_2 in Fig. 11) was identical among all four panels. Larvae were released near alongshore position y = 0.

Figure 19: Time Series of Particle Entrainment for Scenarios with either Moderate (V_{max} = 0.1 m s^{-1}, left panels) or High (V_{max} = 0.3 m s^{-1}, right panels) Mean Alongshore Advection and either relatively Weak (top panels) or Strong (bottom panels) Alongshore and Cross-Shore Diffusivities (K_y, K_x)

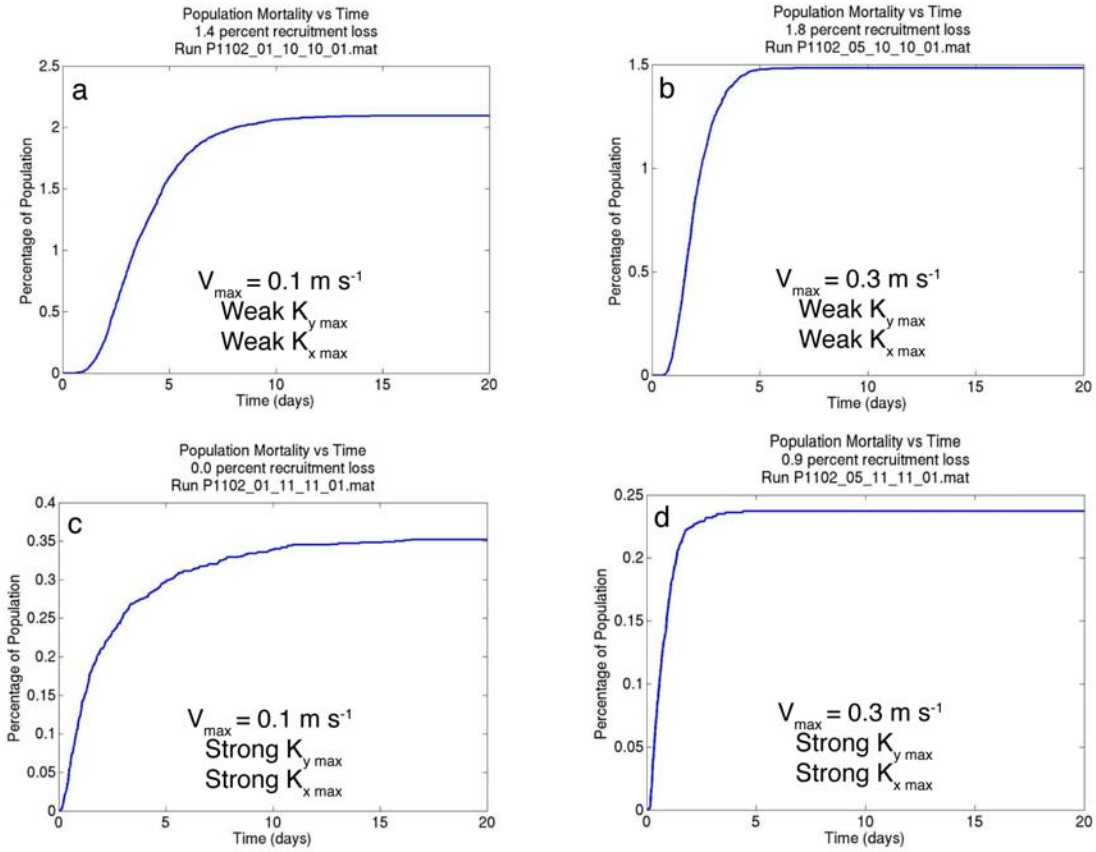

Curves show the cumulative percentage of larvae entrained in the CWIS over time. The cross-shore profile of the coastal boundary layer (positions x_1 and x_2 in Fig. 11) was identical among all four panels. Larvae were released near alongshore position y = 0. Notice that the scale of the vertical axis varies among panels.

Figure 20: Dispersal Kernels Calculated using Particle Dispersion Model for Scenarios in which Nearshore and Offshore Flows are in Opposite Directions

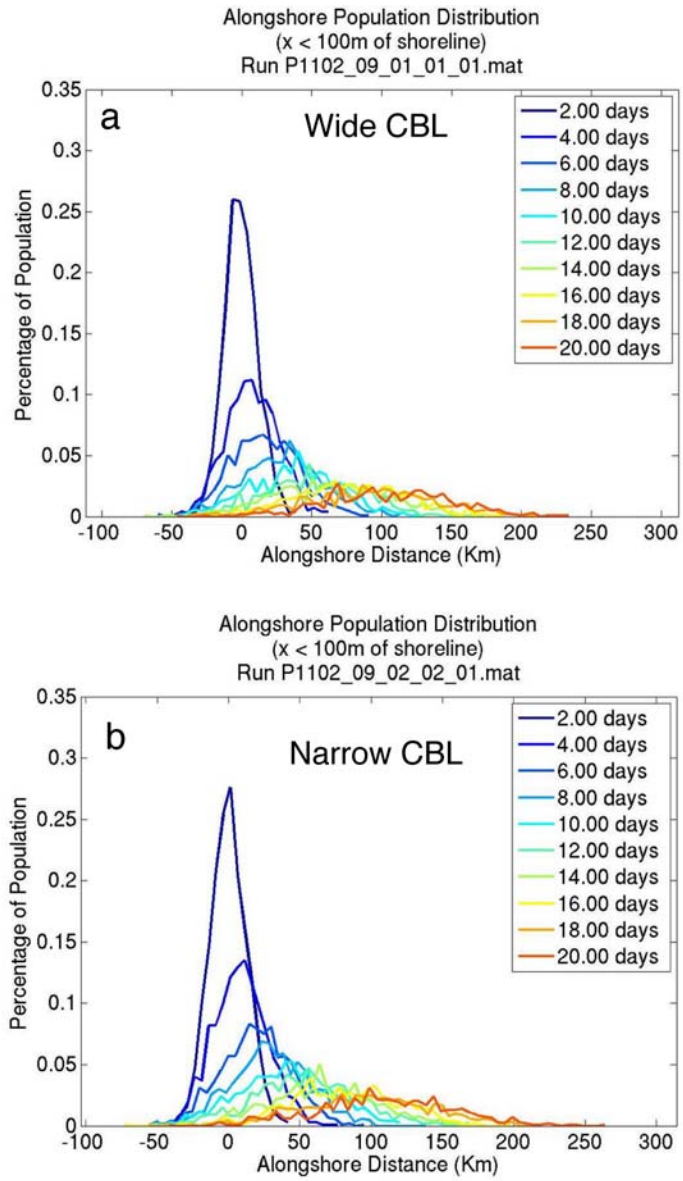

Curves show the percentage of larvae < 100 m from shore (i.e., potential settlers) at each alongshore location for a range of pelagic larval durations (indicated by curve color). Results are shown for model runs performed using a relatively wide (top panel) and relatively narrow (bottom panel) coastal boundary layer (CBL). Larvae were released near alongshore position y = 0.

Figure 21: Dispersal Kernels Calculated using Particle Dispersion Model for Scenarios in which Nearshore and Offshore Flows are in Opposite Directions and with Varying Strengths of Alongshore Diffusivity (K_y) and Cross-Shore Diffusivity (K_x)

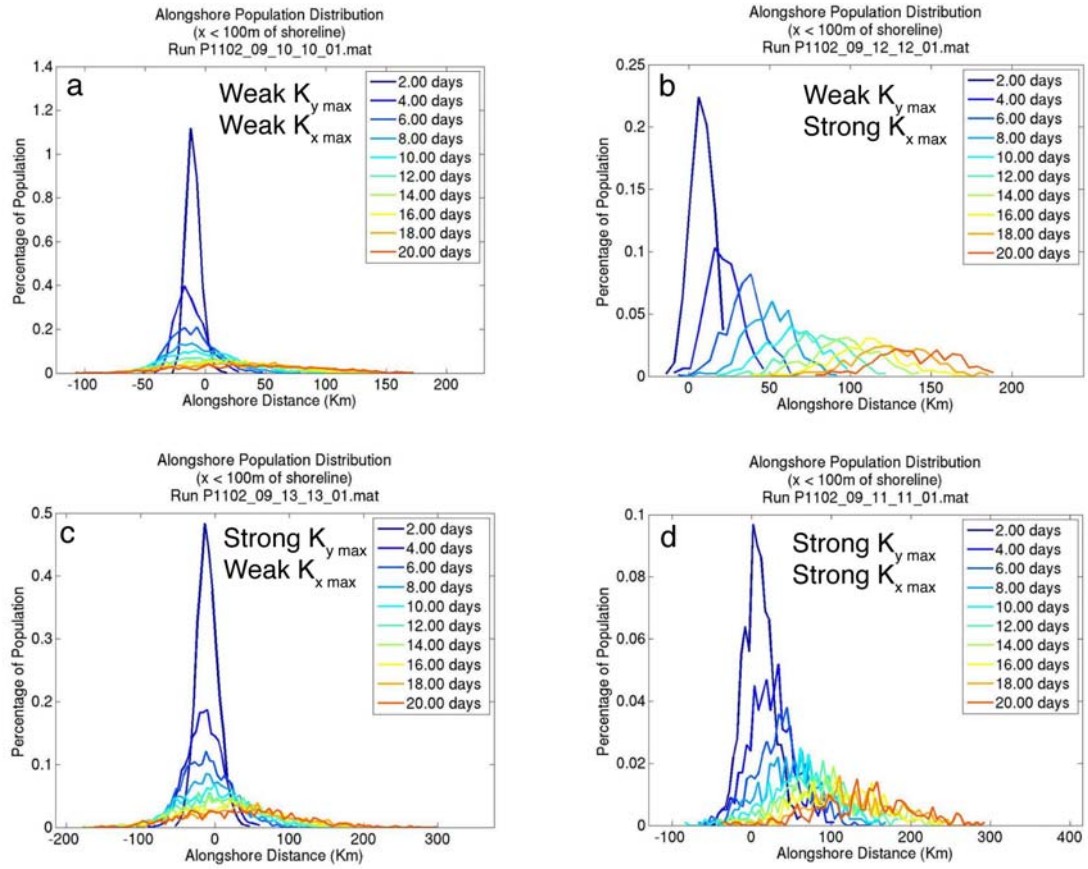

Curves show the percentage of larvae < 100 m from shore (i.e., potential settlers) at each alongshore location for a range of pelagic larval durations (indicated by curve color). The cross-shore profile of the coastal boundary layer (positions x_1 and x_2 in Fig. 11) was identical among all four panels. Larvae were released near alongshore position $y = 0$.

Figure 22: Mean Particle Trajectories Calculated using Particle Dispersion Model for sCenarios in which Nearshore and Offshore Flows are in Opposite Directions and with Varying Strengths of Alongshore Diffusivity (K_y) and Cross-Shore Diffusivity (K_x)

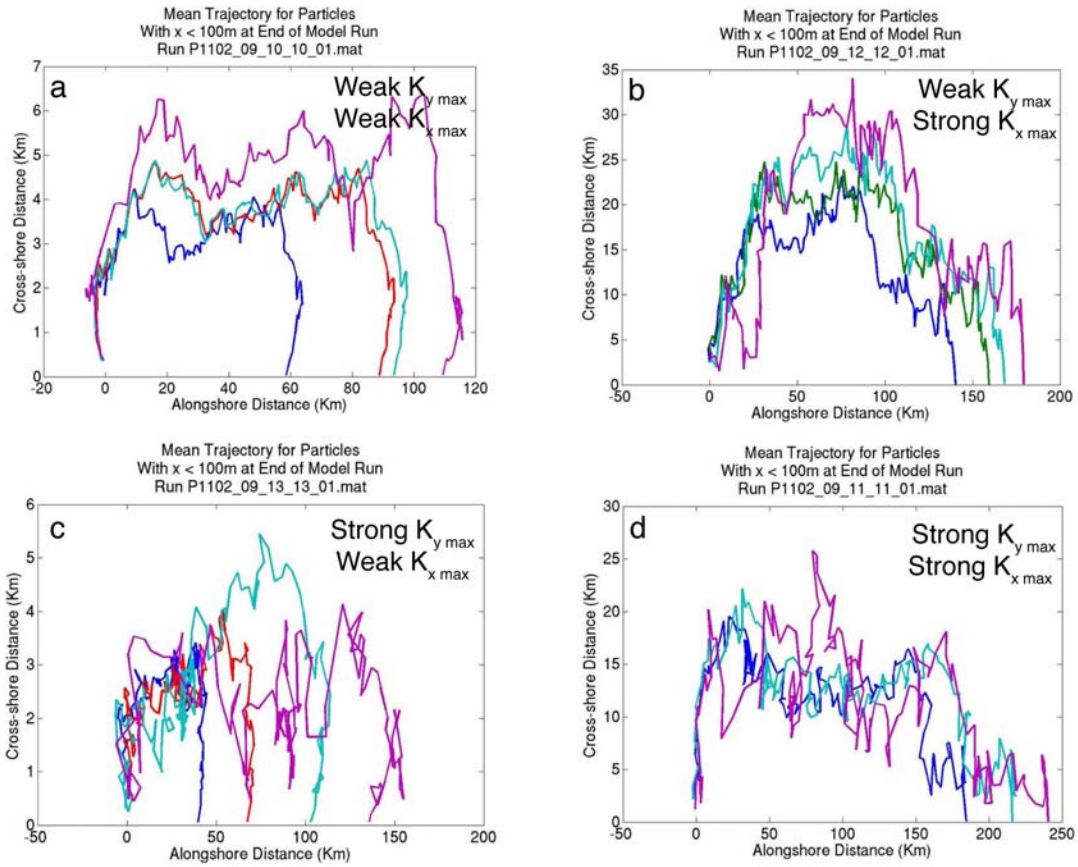

Curves show the average path of larvae that successfully returned to within < 100 m from shore (i.e., potential settlers) at each alongshore location for a range of pelagic larval durations (indicated by curve color; blue = 4 d, red = 8 d, green = 12 d, cyan = 16 d, magenta = 20 d) The cross-shore profile of the coastal boundary layer (positions x_1 and x_2 in Fig. 11) was identical among all four panels. Larvae were released near alongshore position y = 0.

Figure 23: Time Series of Particle Entrainment for Scenarios in which Nearshore and Offshore Flows are in Opposite Directions and with Varying Strengths of Alongshore Diffusivity (K_y) and Cross-Shore Diffusivity (K_x)

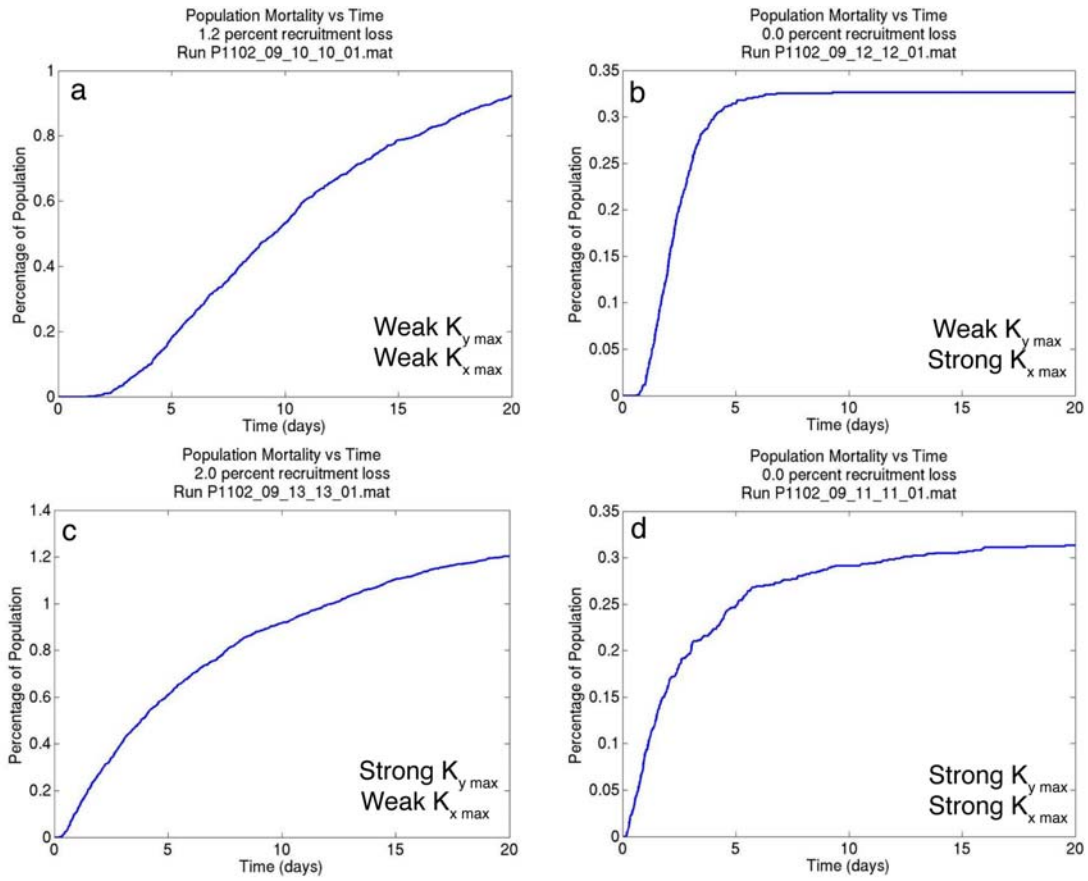

Curves show the cumulative percentage of larvae entrained in the CWIS over time. The cross-shore profile of the coastal boundary layer (positions x_1 and x_2 in Fig. 11) was identical among all four panels. Larvae were released near alongshore position $y = 0$. Note that vertical axis scales vary among panels.

CHAPTER 6:
Effects of Entrainment on Benthic Populations

Having explored the dispersal parameters affecting transport over short time scales, we then considered the demographic effects of different dispersal and entrainment scenarios. To do so, we parameterized the particle tracking model to reflect the aggregation of flow statistics over longer, population time scales that are representative of spawning over an entire season, or multiple seasons. To understand implications of entrainment for populations, we use the output from the particle-tracking model as input for a dynamic metapopulation model.

6.1 Metapopulation Model Framework

We model a metapopulation occupying a 100 km stretch of coastline with uniform habitat and a dispersal kernel generated from the random-walk, particle-tracking model. We limit ourselves to considering organisms that have limited movement as adults and remain in the shallow subtidal. Thus, we use a one-dimensional spatial domain and a resolution of 1 km, below which we assume individuals are well mixed.

The model time step is one year, and within each year there is a single, synchronous spawning event. Larval dispersal probabilities between each of the one hundred 1 km patches is represented by a dispersal matrix that is homogeneous alongshore and calculated once using the particle dispersion model and then used as a deterministic description of larval movement during each timestep of the metapopulation model. To generate the dispersal matrix, we released 1000 larvae into the water offshore of each 1-km patch, initially in a uniformly distributed pattern between land (x = 0 m) and 10 m offshore. Larvae were then dispersed by the random walk model for a particular pelagic larval duration (PLD). If larvae returned to within 500 m of the shoreline during a fixed competency window towards the end of the PLD, they were assumed to settle. If they remained offshore during the competency window or were entrained by the water intake at any time during the PLD, they were lost from the system. The number of larvae dispersing to each other location j from location i was divided by the number of larvae released from i (10^3) to obtain a probability D_{ji} that forms an element of the dispersal matrix D. In each timestep, the spatial distribution of new settlers was calculated as

$$S_t = DN_t\phi\xi, \qquad \text{(Eq. 10)}$$

where S and N are n×1 vectors giving the density of settlers and adults, respectively, in each of the n patches; ϕ is the per-capita annual adult fecundity and ξ is larval survivorship, both of which are assumed to be constant over space and time.

After dispersal, we assumed typical population dynamics (e.g., Armsworth 2002, James et al. 2002). In the first year, settlers in each patch i experience density-dependent mortality, which we modeled with a Beverton-Holt function:

$$R_{t+1,i} = \frac{\alpha S_{t,i}}{1 + S_{t,i}/\beta} \qquad \text{(Eq. 11)}$$

where α is a density-independent survivorship and β is the asymptotic maximum density of recruits, R. Surviving recruits enter the adult population, where they experience a constant, density-independent mortality rate μ:

$$N_{t+1,i} = (R_{t,i} + N_{t,i})e^{(-\mu)}. \qquad \text{(Eq. 12)}$$

6.2 Quantifying Effects of Entrainment on Metapopulation Dynamics

We used the metapopulation model to address two basic sets of questions about the ecological effects of larval entrainment. First, how does entrainment affect the persistence of the entire metapopulation? Second, how does entrainment affect the spatial distribution of individuals?

For long-term persistence of a population each adult must replace itself with at least one successful recruit within its lifetime (Caswell 2001, Hastings and Botsford 2006). This criterion can be expressed by defining a connectivity matrix

$$\mathrm{C} = \mathrm{D}\phi\xi\alpha L \qquad \text{(Eq. 13)}$$

where L is the mean lifespan of an adult,

$$L = 1/(1-e^{(-\mu)})-1 \qquad \text{(Eq. 14)}$$

and the other symbols are the population parameters described above. Essentially, **C** describes the spatial distribution and survival of settlers produced by a single individual during its lifetime in a metapopulation that has been reduced to near extinction (so density-dependent effects can be ignored). In this near-extinction scenario, the population dynamics are represented simply by $\mathbf{N}_{t+1} = \mathbf{C}\mathbf{N}_t$. Within this framework, the replacement criterion for metapopulation persistence is that the dominant eigenvalue of **C** must be > 1 (Hastings and Botsford 2006). This is equivalent to the rule that the lifetime reproductive rate R_0 must be > 1 in linear population models (Caswell 2001).

If we assume that all of the population parameters are constant over space and time, the criterion can also be expressed as

$$l_{max} > 1/\phi\xi\alpha L, \qquad \text{(Eq. 15)}$$

where l_{max} is the dominant eigenvalue of **D**. For a particular combination of biological parameters, this criterion reveals whether entrainment affects larval dispersal sufficiently to disrupt the persistence of the entire metapopulation. Conversely, for a particular flow and entrainment scenario, this criterion can be used to examine the effect of multiple stressors on the metapopulation. For example, harvesting adults at instantaneous rate η will increase the mortality rate to $\mu + \eta$, reducing the expected lifespan L and thus increasing the minimum value of l_{max} necessary for persistence. For each dispersal scenario, we calculated the minimum lifespan L_{min} for which the metapopulation was still persistent in the absence of entrainment and used a value of $1.01L_{min}$ to represent a population that has been heavily affected by anthropogenic stressors and is marginally above collapse. By then adding entrainment to these

"exploited" scenarios, we determined whether entrainment was sufficient to disrupt a population that was already bearing the cumulative effects of other stressors. We also examined the dynamics of a healthy population far from collapse. Collapse due to overharvesting occurs when lifetime egg production (LEP) falls below some critical fraction of its natural maximum (typically due to a reduction in the average reproductive lifespan of an individual). This critical threshold likely varies over space and time and among species, but meta-analyses of temperate fishery stocks suggest that a common value is approximately 35% of the natural maximum (Mace and Sissenwine 1993). Thus as a first approximation, we assumed that "unexploited" scenarios would have approximately $L = L_{min}/0.35$, where L_{min} is the minimum life expectancy associated with persistence in the no-entrainment scenario.

To examine the effect of entrainment on spatial variation in the metapopulation, we focused on three types of response variables. First, we examined spatial variation in adult population densities at equilibrium: where and by how much does entrainment reduce adult densities?

Second, we examined metapopulation dynamics in a conservation context and asked which locations had the greatest "value" to the metapopulation (sensu Ovaskainen and Hanski 2003). This approach determines which parts of the metapopulation are most essential to population persistence (and which should perhaps be protected from additional disturbance) and which are less essential (and which could be further exploited or disturbed). We calculated patch value using a deletion index (James et al. 2002, White 2008). The deletion index estimates the metapopulation-level effect of completely removing a focal patch from the system. It is calculated by running the population model to a long-term equilibrium and calculating the mean population density across all patches, $\overline{N}_{\bullet}$. The model is then run again, this time causing all larvae that arrive in patch i to die immediately, and the equilibrium mean density across all patches except i, $\overline{N}_{\bullet-i}$, is calculated. The deletion index for patch i is then

$$d_i = 1 - \overline{N}_{\bullet-i} / \overline{N}_{\bullet}. \qquad \text{(Eq. 16)}$$

A patch that is essential to metapopulation persistence (a global source) will have $d_i = 1$, while a completely superfluous patch (a global sink) will have $d_i = 0$.

Thirdly, we augmented these direct measures of the overall effects of CWIS entrainment on metapopulation dynamics with a more ad-hoc assessment of the spatial patterns of larval mortality using a metric we term "*relative settlement*" (RS). To calculate this statistic, we assumed that the same number of larvae (10^3) were released from each location in the metapopulation, then recorded the distribution of successful settlers. By determining the arithmetic difference in settlement between a scenario with entrainment and a scenario without entrainment, we were able to gauge the spatial extent of CWIS impacts on larval supply. In other words, we determine where entrained larvae would have settled. If there is no effect then relative settlement RS = 0.0, but if there is a reduction in settlement then RS < 0.0. Note the important assumption that the same number of larvae is released at any point. In a dynamic metapopulation model, successively fewer numbers of larvae would be spawned in populations that are under-saturated because of CWIS entrainment in the previous generation. Thus in the dynamic model, settler densities are affected by the cumulative effects of entrainment in the

current year and in previous years, while relative settlement only assesses entrainment effects in a single year.

6.3 Parameterization of Metapopulation Model

The metapopulation model is intended to simulate the dynamics of a generic species that occupies nearshore subtidal habitats, experiences density-dependent mortality among recently settled individuals but density-independent adult mortality, and is highly fecund as an adult. As such we did not use parameter values derived from a particular marine species, but chose values that are biologically plausible in general (Table 4). It is important to note that the population persistence criterion in Eq. (15) depends on just two factors: the eigenvalue of the dispersal matrix (simulated by the particle tracking model) and the product of the parameters describing mean lifespan, fecundity, larval survivorship, and settler survivorship. Thus the independent value of any of the demographic parameters is relatively unimportant; rather it is important to consider whether their product describes a population on the verge of collapse or one quite far from the collapse threshold. The goal of this modeling effort was not to document the effects of CWIS entrainment in any particular location, but to explore the regions of parameter space in which CWIS effects should be most severe, allowing us to draw more general conclusions about the potential impacts of CWIS.

For population models, dispersal matrices are generated with particle-tracking model parameters values that represent aggregation over a seasonal time scale. Flow variability offshore is represented by diffusivities $K_x = 500$ m^2 s^{-1} and $K_y = 1000$ m^2 s^{-1}, while nearshore flow variability is represented by diffusivities $K_x = 1$ m^2 s^{-1} and $K_y = 20$ m^2 s^{-1}. We consider a CBL 3 km wide ($x_2 = 3000$ m). Values for both K_x and K_y are linearly interpolated between x_1 and x_2 and the nearshore width x_1 is chosen such that the value of K at x_1 is equal to what that value would have been if K declined linearly to zero from x_2 to $x = 0$. In other words, the central segment of the tri-linear profile had approximately the same slope as a line representing a linear decline to the coastline. The relatively large offshore diffusivity parameters were intended to reflect the large magnitude of stochastic variations in mean flow that are observed over time scales of several months (through the spawning season).

To explore the population-level effects of both oceanographic and CWIS factors, we systematically varied the mean alongshore velocity, intake rate, and cross-shore intake position. We considered alongshore velocities of 0 m s^{-1} (diffusion only) and 0.1 m s^{-1} (advection), intake rates of 0 (no intake), 125 m^3 s^{-1} (approximately the highest intake rate realized by CWIS in CA; CEC 2005), and 1250 m^3 s^{-1} (an order of magnitude higher than the highest actual rate; this unrealistically high value provides a hedge against potential underestimates of CWIS effects by showing the range of effects possible for very high intake rates). We considered cross-shore intake locations of 50, 500, 1000, and 5000 m offshore. Note that the 50-m location is in the nearshore, while the 5000-m location is offshore of the CBL, in the free-stream flow region.

The spatial domain for the simulations was a 100 km coastline (spatial coordinates $y = 0$ to $y =$ 100 km) in which each 1 km interval was treated as an independent patch in the metapopulation. The CWIS intake was located in the center of the domain (at $y = 49.5$ km). We

performed two realizations of each dispersal scenario to capture some of the variability associated with the stochastic particle-tracking model.

6.4 Metapopulation Model Results

The results of the metapopulation model under various flow scenarios are presented in Table 5 and discussed in detail below.

6.4.1 Unexploited Population

When the population is healthy and unexploited, there is a noticeable but extremely minimal effect of entrainment. For example, in the diffusion scenario (Fig. 24a), population densities are very slightly reduced at the intake location, and patch value is somewhat lower there as well. Adding advection to the system produced similar results (Fig. 25a). Note that the y-axis scale is very narrow in these figures relative to those in the overexploited scenarios; i.e., the changes in population density are very minor. Entrainment never caused a healthy population to collapse in any flow scenario.

In both diffusive and advective flows, the deletion index (Figs. 24b, 25b) indicates that entrainment does sometimes reduce the conservation value of certain coastal locations. In the diffusive scenario, patch value is reduced in the vicinity of the intake for all intake locations except 5000 m offshore. Evidently, placing the intake further offshore minimizes the effect of entrainment on patch contribution to the larger metapopulation even though population densities are reduced somewhat at the intake location.

6.4.2 Overexploited Population

When the population was on the verge of collapse due to other stressors (average lifespan = Lmin), introducing entrainment sometimes provided enough additional disturbance to cause the population to collapse. With moderate intake velocities (125 m3/s) and no advection, the population remained persistent when the intake was very nearshore (Fig. 26). For intakes further offshore, both persistent and collapse results were obtained (Fig. 26, Table 5).

When advection was present with the same moderate intake velocity, collapse occurred when the intake location was either very near shore (50 m), and both persistence and collapse occurred with the intake very far offshore (5000 m) but the population remained persistent for other intake locations (Fig. 27). In scenarios with high intake velocities (1250 m3/s), the population collapsed regardless of flow scenario (Table 5).

In both cases note that very nearshore intakes produced the least favorable outcomes, while placing the intake further offshore was less likely to cause a near-collapse population to fail. Furthermore, while there were metapopulation-wide effects of CWIS entrainment, there was no noticeable effect of entrainment on population density near the intake in either the diffusive or advective scenario.

In contrast to results for the unexploited population, entrainment did not cause a reduction in patch conservation value immediately adjacent to the CWIS intake. While there was considerable spatial variability in patch value in both diffusive and advective scenarios (Figs. 26, 27), there was no consistent spatial pattern. The spatial variability appears to reflect the

stochastic nature of dispersal in the particle-tracking model. Differences in the overall magnitude of deletion index values among scenarios (e.g., differences in the mean height of the curves in the lower panel of Fig. 27) are a product of differences in mean population density. Lower mean population densities generally produce higher deletion index values; for comparison note that deletion index values for the unexploited population have similar population densities and similar deletion index values for all intake locations.

6.4.3 Cumulative Effects of Multiple CWIS

To evaluate the consequences of placing two CWIS in close proximity, we added a second intake location at y = 59.5 km, 10 km downstream from the first. The additional intake location exacerbated the negative impacts of entrainment. Advective flow scenarios with moderate intake velocities were all non-persistent (Table 5), and diffusive scenarios with moderate intake velocity were also non-persistent for all cross-shelf intake locations except the location furthest offshore (5000 m) (Table 5, Fig. 28). However, there was no discernible difference in the spatial patterns of abundance produced by a single CWIS or two CWIS for either persistent or non-persistent populations (compare Figs. 27, 28).

6.4.4 Disturbance

The majority of model runs focused on scenarios with temporally consistent conditions and examined the equilibrium distribution of population density. However, it sometimes took many hundreds of model years for the system to reach this equilibrium. This leaves open the possibility that CWIS entrainment could affect the transient approach to that equilibrium. In other words, a population subject to entrainment may take longer to reach equilibrium than a non-entrained population, even if both populations have a stable, persistent equilibrium. To evaluate this possibility, we performed model runs in which the system reached equilibrium (approximately 1000 timesteps), but was then subject to a single, spatially discrete disturbance in which population density was set to zero for a 10 km-wide swath of the coastline. The model was then run for an additional 5000 timesteps to monitor the recovery from disturbance. Disturbance zones were located either 5 km upstream, 5 km downstream, or centered directly on the intake.

For scenarios with healthy, nonexploited populations, adding a disturbance had an instantaneous effect on population densities in the disturbed zone but not elsewhere. The disturbed zone recovered rapidly and returned to equilibrium densities with approximately 25 model years (Fig. 29). There was no discernible effect of disturbance location on the population response in either diffusive or advective flow scenarios.

For scenarios in which the population was near collapse (i.e., exploited) but still persisted in the presence of entrainment (e.g. some scenarios with diffusive flow and moderate intake velocity, and scenarios with advective flow and intakes further offshore than 50 m), adding an instantaneous disturbance did not cause the population to collapse, but it did depress population densities across the coastline for many years before the population returned to equilibrium (Table 5, Fig. 30). Note that unlike the unexploited case, in which the effects of disturbance were entirely localized to the disturbed zone, in an exploited population the disturbance was initially localized but within 10 years had affected coast-wide population

densities. There was no noticeable effect of the location of the disturbance relative to the intake location, even in the advective flow scenario (Table 5, Fig. 31).

6.4.5 Relative Settlement

Plots of relative settlement across space for the high-intake scenario reveal the spatial pattern of entrainment effects. In the diffusive scenario, relative settlement is quite low right at the intake location (Fig. 32). The effect is slightly less for the 50 m intake, because larvae are assumed to be able to settle directly to the substrate once they reach a position inshore of 500 m. Consequently, some settlers are able to avoid entrainment in an intake pipe very near to shore. This result is realistic if one considers the case of a species that is able to settle directly to the substrate once within 500 m of shore. However, if the 500 m settlement threshold is interpreted as the distance from which larvae can swim to the shore (or move shoreward through vertical migrations) to settle in the shallow subtidal, then this type of result is as an artifact of the model.

In the advective scenario, relative settlement is depressed at the intake location for all cross-shelf intake positions except for 50 m, just as in the diffusive scenario (Fig. 33). Settlement was also reduced for a broad region downstream of the intake position for all cross-shelf intake positions in the advective scenario (Fig. 33).

6.5 Metapopulation Model Discussion

In general, the effects of CWIS entrainment on healthy populations (far from the persistence threshold) are relatively minor. This is most likely a result of the compensatory effect of density-dependent mortality that occurs soon after settlement (Menge 2000, Hixon and Jones 2005, Almany and Webster 2006). Because of this compensation due to limits in the extent of adult habitat, the density of settling larvae must be reduced considerably before any corresponding reduction in the abundance of juveniles and adults is observed. In other words, entrainment may kill many larvae, but the majority of those larvae would have died soon after settlement anyway.

The same is not true for a population very close to the persistence threshold. In this situation, larval replenishment is barely sufficient to offset mortality in the adult stage, so any small reduction in settlement may be sufficient to disrupt replacement and thus persistence. We modeled a “near-collapse” population by drastically increasing the adult mortality rate, such as may occur during over-harvesting. However, the model results are robust and would be identical for any type of disturbance that reduces the effective lifetime egg production of adults, whether it is overharvesting of adults, impaired survival of juveniles due to habitat destruction, reduced fecundity due to pollution, or reduced larval survival due to the availability of food resources in the pelagic zone. The cumulative effects of any or all of these types of impacts are best expressed in terms of their effects on lifetime reproductive success, which can serve as a common currency for the evaluation of population persistence. Heimbuch et al. (2007) recently described how the effects of entrainment on lifetime reproductive success can be expressed within the framework of commonly-used, non-spatial fishery assessment models. We have extended that set of results by incorporating spatial variability in replacement, much as Kaplan et al. (2006) suggest for the management of fished populations within marine protected areas.

Table 5: Effect of Cooling Water Intake Entrainment on Population Persistence

Single intake, no disturbance, near collapse						
			Offshore position of intake (m)			
Advection (m/s)	**Intake rate (m^3/s)**	**#intakes**	**50**	**500**	**1000**	**5000**
0	0	0	P	P	P	P
0	125	1	P	*	*	*
0	1250	1	NP	NP	NP	NP
0.1	0	0	P	P	P	P
0.1	125	1	NP	P	P	*
0.1	1250	1	NP	NP	NP	NP

Two intakes (10 km apart), no disturbance, near collapse						
			Offshore position of intake (m)			
Advection (m/s)	**Intake rate (m^3/s)**	**#intakes**	**50**	**500**	**1000**	**5000**
0	0	0	P	P	P	P
0	125	2	NP	NP	NP	P
0	1250	2	NP	NP	NP	NP
0.1	0	0	P	P	P	P
0.1	125	2	NP	NP	NP	NP
0.1	1250	2	NP	NP	NP	NP

One intake, near collapse, disturbance upstream of intake						
			Offshore position of intake (m)			
Advection (m/s)	**Intake rate (m^3/s)**	**#intakes**	**50**	**500**	**1000**	**5000**
0	0	0	P	P	P	P
0	125	1	P	*	*	*
0	1250	1	NP	NP	NP	NP
0.1	0	0	P	P	P	P
0.1	125	1	NP	P	P	*
0.1	1250	1	NP	NP	NP	NP

One intake, near collapse, disturbance centered on intake						
			Offshore position of intake (m)			
Advection (m/s)	**Intake rate (m^3/s)**	**#intakes**	**50**	**500**	**1000**	**5000**
0	0	0	P	P	P	P
0	125	1	P	*	*	*
0	1250	1	NP	NP	NP	NP
0.1	0	0	P	P	P	P
0.1	125	1	NP	P	P	*
0.1	1250	1	NP	NP	NP	NP

One intake, near collapse, disturbance downstream of intake						
			Offshore position of intake (m)			
Advection (m/s)	**Intake rate (m^3/s)**	**#intakes**	**50**	**500**	**1000**	**5000**
0	0	0	P	P	P	P
0	125	1	P	*	*	*
0	1250	1	NP	NP	NP	NP
0.1	0	0	P	P	P	P
0.1	125	1	NP	P	P	*
0.1	1250	1	NP	NP	NP	NP

Scenarios with persistent populations indicated with *P*, scenarios with non-persistent (collapsed) populations indicated with *NP*, scenarios in which both types of behavior are observed indicated with *. Advection refers to mean alongshore velocity in the region offshore of the coastal boundary layer. Populations in these model runs were near collapse (i.e., mortality rate was 99% of the value that would lead to collapse).

The spatial aspect of CWIS effects on populations is especially important to consider in light of the recent focus on spatial management through marine protected areas (MPAs) in California. Designing MPAs generally requires identifying locations of especially high value to the population, i.e., those that contribute disproportionately to population persistence. Although there is no commonly agreed-upon approach to measuring population value, we have favored the deletion index approach, which has proven useful in other coastal metapopulation models (James et al. 2002, White 2008).

There was a notable difference in the spatial distribution of CWIS effects for healthy and near-collapse populations. In the former, population densities and patch value were reduced (albeit only slightly) in the immediate vicinity of the CWIS. This suggests that the CWIS entrained some larvae that would otherwise have settled in those locations, and that the combination of lower population densities (and thus lower spawning output) and entrainment of recently spawned larvae from those locations reduced their contribution to the metapopulation. However, the reduced spawning output from those populations did not noticeably affect population densities elsewhere. By contrast, the same type of disturbance in a near-collapse population depressed population densities coastwide, and had the potential to drive the entire population to extinction. This difference in the spatial extent of disturbance can be understood in terms of the two types of population persistence: self persistence and network persistence (Hastings and Botsford 2006). In the unexploited, healthy population, each location along the coast receives enough settlement of locally produced larvae that it is entirely self-persistent, that is, the population in that location can replace itself without outside input. As a result, disturbances that reduce the spawning output of neighboring populations have little effect because the focal population is entirely self-sustaining. Such a system would be highly resilient to any type of disturbance, not just CWIS. By contrast, in the near-collapse population, larval settlement is depressed overall so no location receives enough locally-spawned larvae to be self-sufficient. Such a system persists only by replacement over space through multiple generations: larvae spawned in location A travel to B, where they settle, mature, and spawn larvae, some of which return to A and replenish the adult population there (Hastings and Botsford 2006). This network effect can sustain a population indefinitely, unless some of the larval connectivity pathways are disrupted. Because each location is dependent on replenishment from a wide network of sources, the depletion of successful spawning output from a single location (as a result of CWIS or other source) quickly resonates throughout the entire coastal metapopulation. The presence of multiple CWIS simply multiplies this effect in a near-collapse population. Specifically, the spatial distribution of abundance was reduced across the entire coastline for near-collapse populations in the presence of either one or two CWIS (compare Figs. 27, 28). This suggests that adding additional CWIS has the overall effect of impairing the network effect across the entire metapopulation rather than in any particular location, so that the cumulative effects of multiple CWIS is not related to their spatial proximity.

The same disparity in the spatial distribution of CWIS effects was evident when unexploited and near-collapse populations were perturbed by a disturbance. In the unexploited case, the effects of disturbance were restricted to the actual disturbance area, because the remainder of the population was self-sufficient even without a larval contribution from the disturbed area. Export from these neighboring areas also helped the disturbed area recover to pre-disturbance densities relatively quickly. By contrast, a disturbance in the near-collapse population disrupted connectivity within the network and produced a coast-wide decline in population densities that does not recover (recovery in the model is extremely slow, taking more than 4500 model years).

There appears to be some effect of the cross-shelf position of the CWIS on the severity of entrainment effects. Extremely nearshore CWIS (x = 50 m offshore) always led to collapse of the

overexploited populations, while CWIS further offshore only disrupted connectivity enough to produce collapse in some model runs. At this time, computation times limit our ability to run large numbers of simulations in order to estimate the probability of collapse under different conditions, but in general it appears that a CWIS further offshore would have weaker effects. This is like due to the lower concentrations of larvae further offshore. Additionally, CWIS further offshore tend to sample larvae with a wider variety of origins and destinations, rather than decimating the larvae leaving or departing a particular onshore location. Larval concentrations are highest immediately after spawning, so total entrainment will be greatest in the vicinity of spawning locations, although it is important to note that due to mortality during the larval stage, larvae entrained soon after spawning have a relatively low probability of surviving until they reach competency and are thus less valuable to the metapopulation relative to older larvae.

Figure 24: Results of Metapopulation Model Showing the Distribution of Adult Density (individuals m^{-2}; top panel) and the Deletion Index (a dimensionless measure of conservation value; bottom panel) at each Alongshore Location

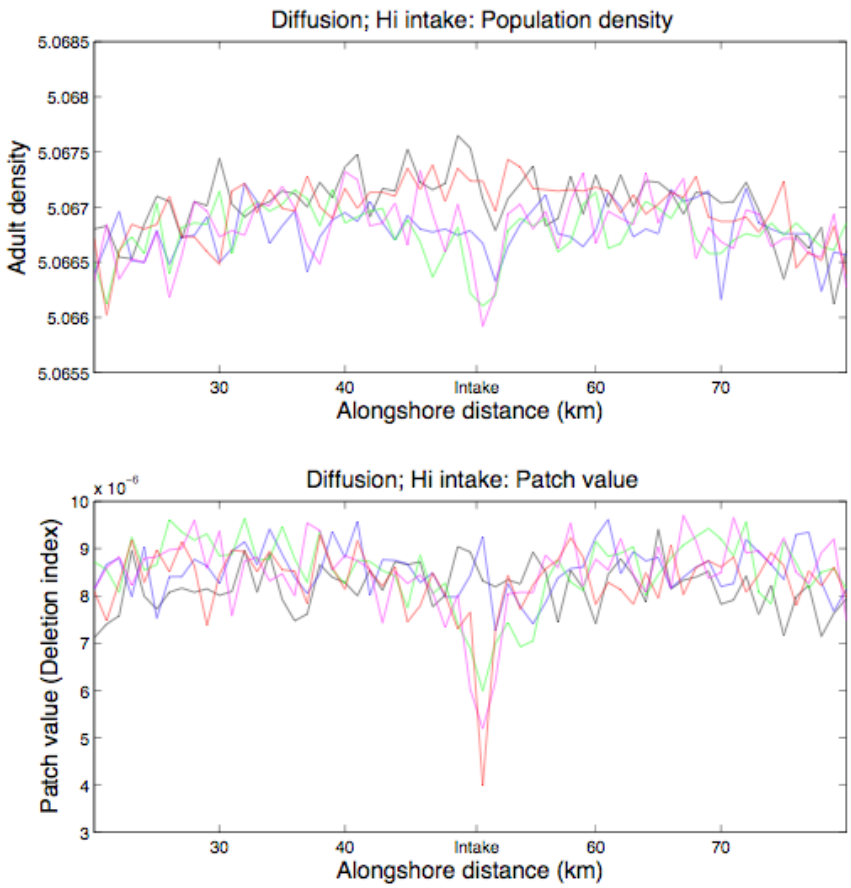

In these model runs the population was healthy (i.e., adult mortality rate was far from the collapse point) and there was no net alongshore advection (max alongshore current = 0 m s^{-1}). A single CWIS intake with high intake velocity (1250 m^3 s^{-1}) was located at alongshore position *y* = 50 km. Cross-shelf intake position: Black = no intake; Red = 50 m, Magenta = 500 m, Green = 1000 m, Blue = 5000 m. Note small range of vertical axis in top panel.

Figure 25: Results of Metapopulation Model Showing the Distribution of Adult Density (individuals m^{-2}; top panel) and the Deletion Index (a dimensionless measure of conservation value; bottom panel) at each Alongshore Location

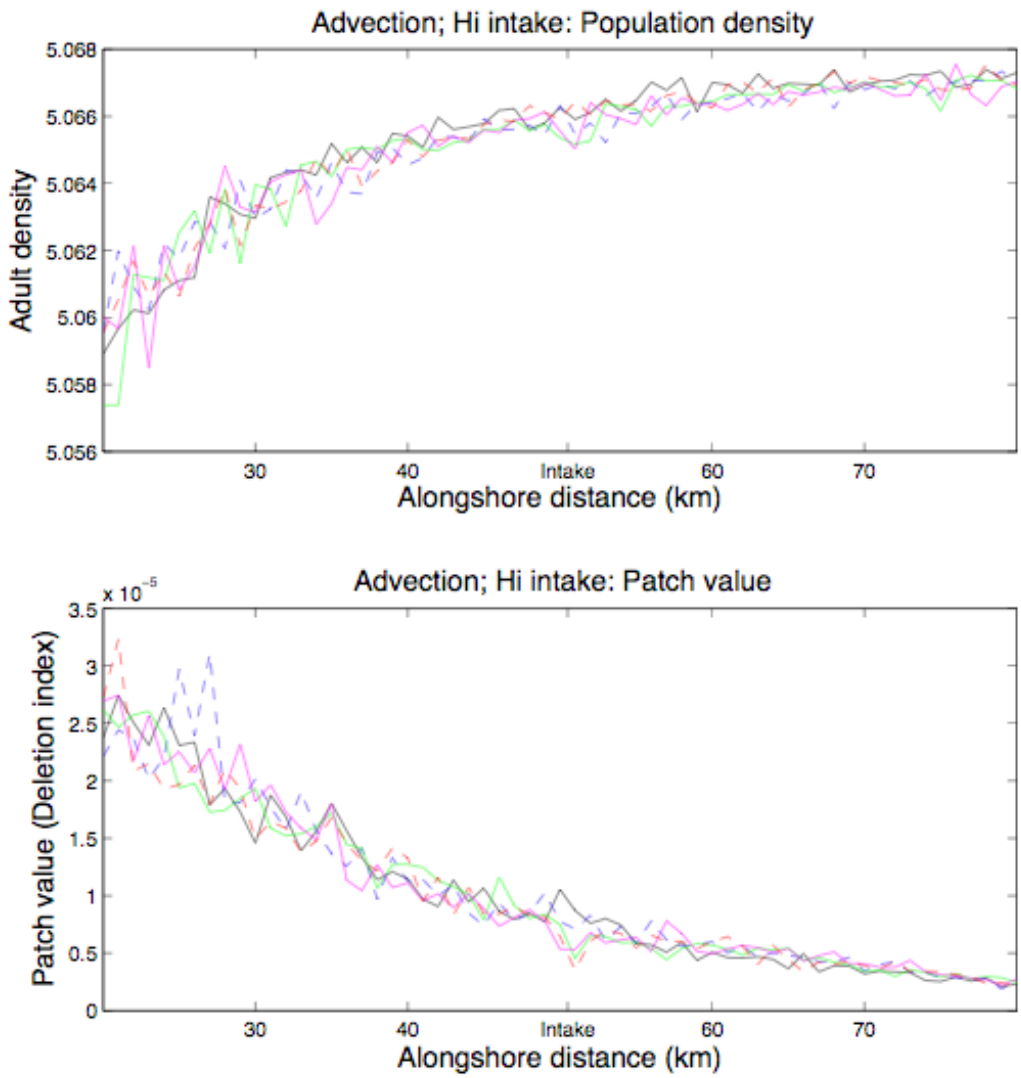

In these model runs the population was healthy (i.e., adult mortality rate was far from the collapse point) and there was net alongshore advection (max alongshore current = 0.1 m s^{-1}). A single CWIS intake with high intake velocity (1250 m^3 s^{-1}) was located at alongshore position *y* = 50 km. Cross-shelf intake position: Black = no intake; Red = 50 m, Magenta = 500 m, Green = 1000 m, Blue = 5000 m. Note small range of vertical axis in top panel.

Figure 26: Results of Metapopulation Model Showing the Distribution of Adult Density (individuals m^{-2}; top panel) and the Deletion Index (a dimensionless measure of conservation value; bottom panel) at each Alongshore Location

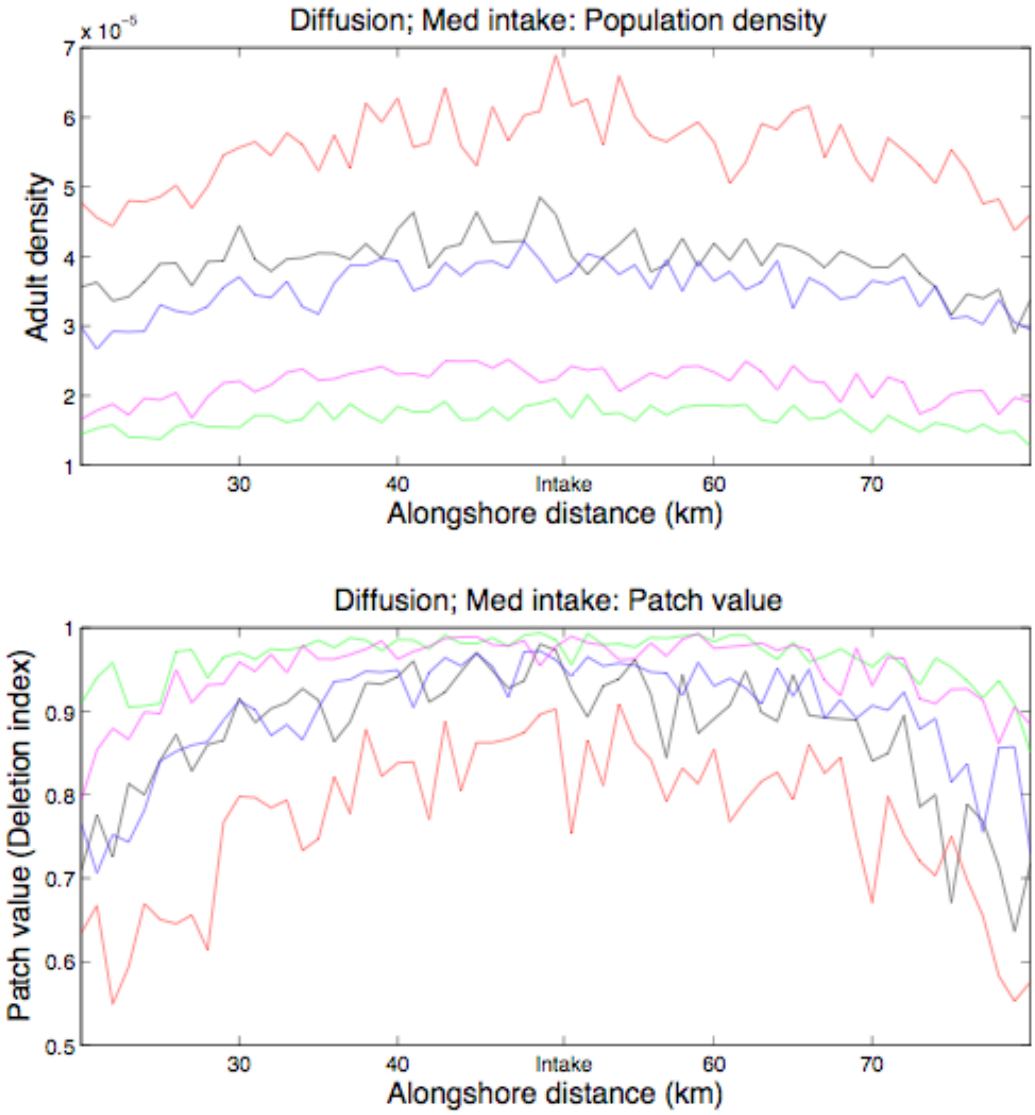

In these model runs the population was near collapse (i.e., the adult mortality rate was 99% of that needed to produce collapse) and there was no net alongshore advection (max alongshore current = 0 m s^{-1}). A single CWIS intake with moderate intake velocity (125 m^3 s^{-1}) was located at alongshore position *y* = 50 km. Cross-shelf intake position: Black = no intake; Red = 50 m, Magenta = 500 m, Green = 1000 m, Blue = 5000 m. Note that values on the vertical axis in the top panel are considerably less than those in Fig. 24.

Figure 27: Results of Metapopulation Model Showing the Distribution of Adult Density (individuals m^{-2}; top panel) and the Deletion Index (a dimensionless measure of conservation value; bottom panel) at each Alongshore Location

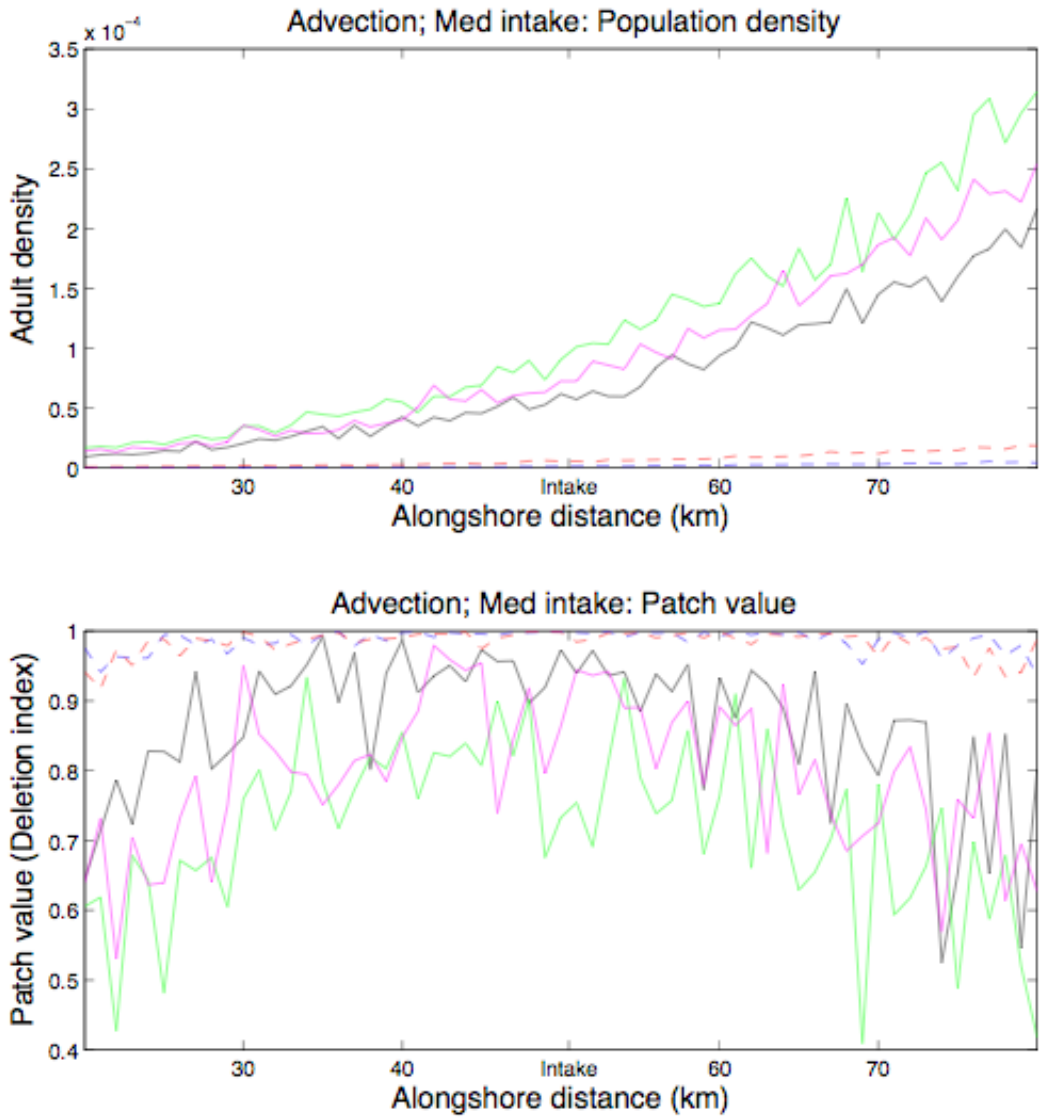

In these model runs the population was near collapse (i.e., the adult mortality rate was 99% of that needed to produce collapse) and there was net alongshore advection (max alongshore current = 0.1 m s^{-1}). A single CWIS intake with moderate intake velocity (125 m^3 s^{-1}) was located at alongshore position y = 50 km. Cross-shelf intake position: Black = no intake; Red = 50 m, Magenta = 500 m, Green = 1000 m, Blue = 5000 m. Dashed curves represent scenarios where the population is declining to eventual extinction.

Figure 28: Results of Metapopulation Model Showing the Distribution of Adult Density (individuals m^{-2}; top panel) and the Deletion Index (a dimensionless measure of conservation value; bottom panel) at each Alongshore Location for the Scenario with Two CWIS Intakes

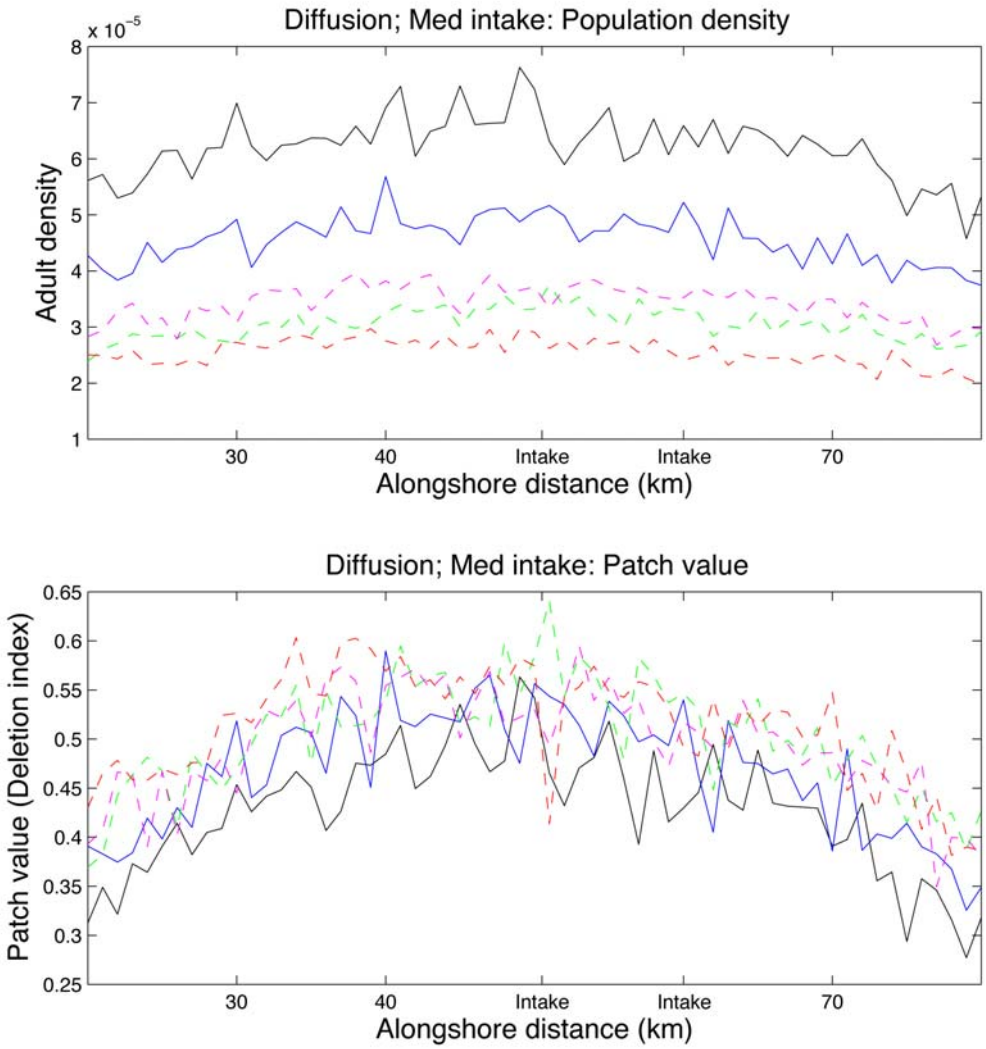

In these model runs the population was near collapse (i.e., the adult mortality rate was 99% of that needed to produce collapse) and there was no net alongshore advection (max alongshore current = 0 m s^{-1}). CWIS intakes with moderate intake velocity (125 m^3 s^{-1}) were located at alongshore positions y = 50 km and y = 60 km. Cross-shelf intake position: Black = no intake; Red = 50 m, Magenta = 500 m, Green = 1000 m, Blue = 5000 m. Dashed curves represent scenarios where the population is declining to eventual extinction.

Figure 29: Results of Metapopulation Model Showing the Distribution of Adult Density (individuals m^{-2}; top panel) at each Alongshore Location during the Recovery from a Localized Disturbance

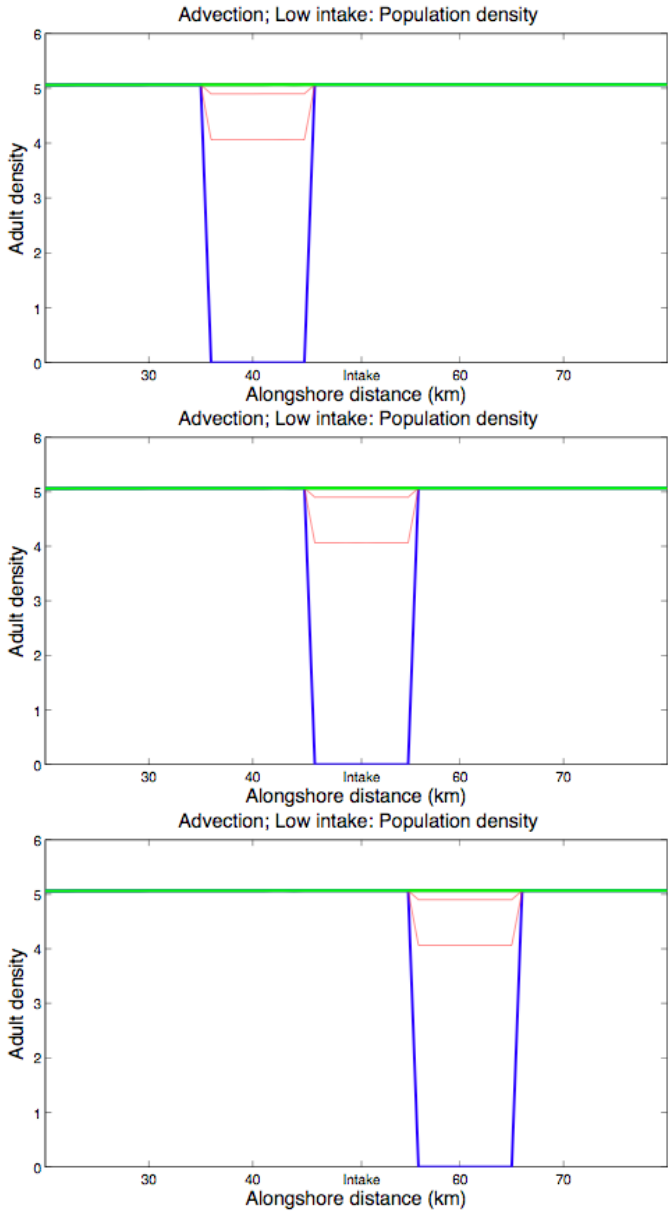

In these model runs the population was healthy (i.e., the adult mortality rate was far from that needed to produce collapse) and there was net alongshore advection (max alongshore current = 0.1 m s^{-1}). A single CWIS intake with moderate intake velocity (125 m^3 s^{-1}) was located at alongshore position y = 50 km and cross-shore position x = 500 m. Cross-shelf intake position: Black = no intake; Red = 50 m, Magenta = 500 m, Green = 1000 m, Blue = 5000 m. Dashed curves represent scenarios where the population is declining to eventual extinction. Black = initial population density; Blue = density immediately after disturbance, Red = 10, 20, 100, 200 years post-disturbance, Green = 4500 years post-disturbance (note that green obscures the later red curves). The location of the disturbance varies from top to bottom panel.

Figure 30: Results of Metapopulation Model Showing the Distribution of Adult Density (individuals m^{-2}; top panel) at each Alongshore Location During the Recovery from a Localized Disturbance

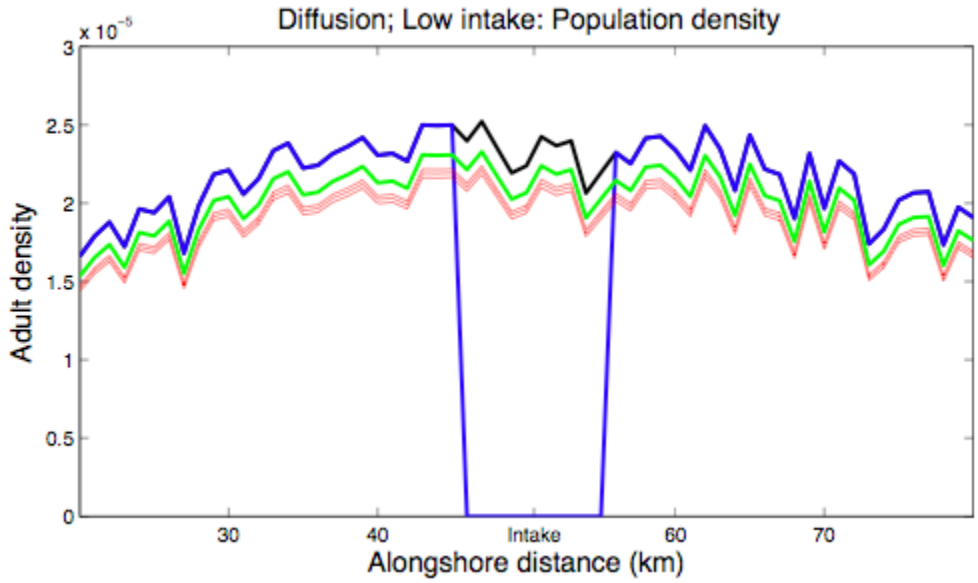

In these model runs the population was near collapse (i.e., the adult mortality rate was 99% of that needed to produce collapse) and there was no net alongshore advection (max alongshore current = 0 m s^{-1}). A single CWIS intake with moderate intake velocity (125 m^3 s^{-1}) was located at alongshore position *y* = 50 km and cross-shore position *x* = 500 m. Cross-shelf intake position: Black = no intake; Red = 50 m, Magenta = 500 m, Green = 1000 m, Blue = 5000 m. Dashed curves represent scenarios where the population is declining to eventual extinction. Black = initial population density; Blue = density immediately after disturbance, Red = 10, 20, 100, 200 years post-disturbance, Green = 4500 years post-disturbance (note that green obscures the later red curves).

Figure 31: Results of Metapopulation Model Showing the Distribution of Adult Density (individuals m^{-2}; top panel) at each Alongshore Location during the Recovery from a Localized Disturbance

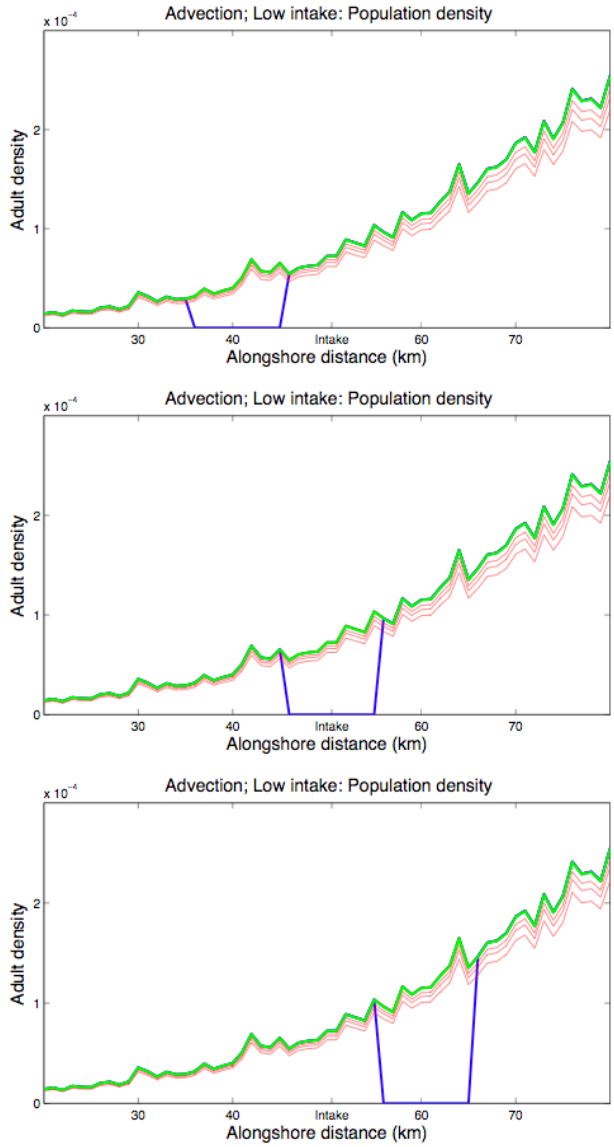

In these model runs the population was near collapse (i.e., the adult mortality rate was 99% of that needed to produce collapse) and there was net alongshore advection (max alongshore current = 0.1 m s^{-1}). A single CWIS intake with moderate intake velocity (125 m^3 s^{-1}) was located at alongshore position *y* = 50 km and cross-shore position *x* = 500 m. Cross-shelf intake position: Black = no intake; Red = 50 m, Magenta = 500 m, Green = 1000 m, Blue = 5000 m. Dashed curves represent scenarios where the population is declining to eventual extinction. Black = initial population density; Blue = density immediately after disturbance, Red = 10, 20, 100, 200 years post-disturbance, Green = 4500 years post-disturbance (note that green obscures the later red curves). The location of the disturbance varies from top to bottom panel.

Figure 32: Results of Metapopulation Showing *Relative Settlement* Calculated from Model Runs with and without CWIS Entrainment

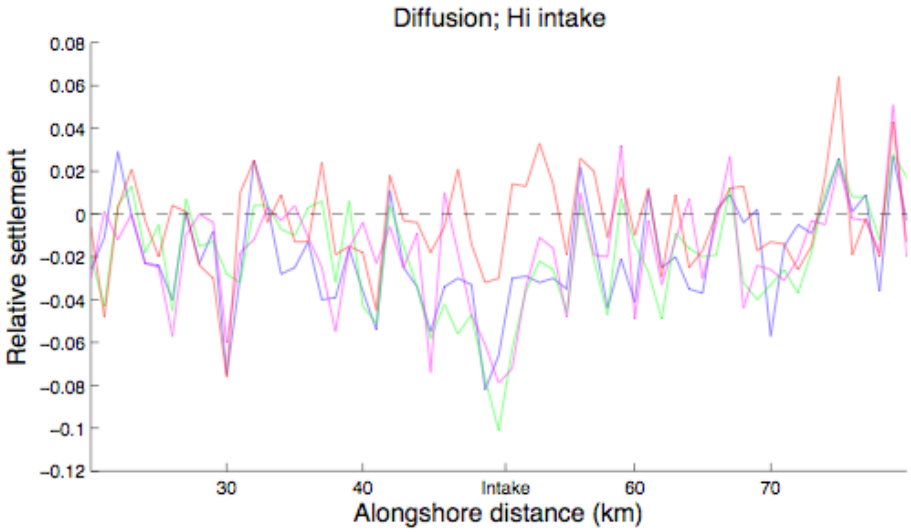

In these model runs, 100 larvae are released from each location and relative settlement gives the arithmetic difference in settlement between runs without and with CWIS entrainment (positive values indicate higher settlement without entrainment). In these runs, there was no net alongshore advection (max alongshore current = 0 m s^{-1}) and the model run with CWIS entrainment had a single intake at along-shore position *y* = 50 km with high intake velocity (1250 m^3 s^{-1}). Cross-shelf intake position: Black = no intake; Red = 50 m, Magenta = 500 m, Green = 1000 m, Blue = 5000 m.

Figure 33: Results of Metapopulation Showing *Relative Settlement* Calculated from Model Runs with and without CWIS Entrainment

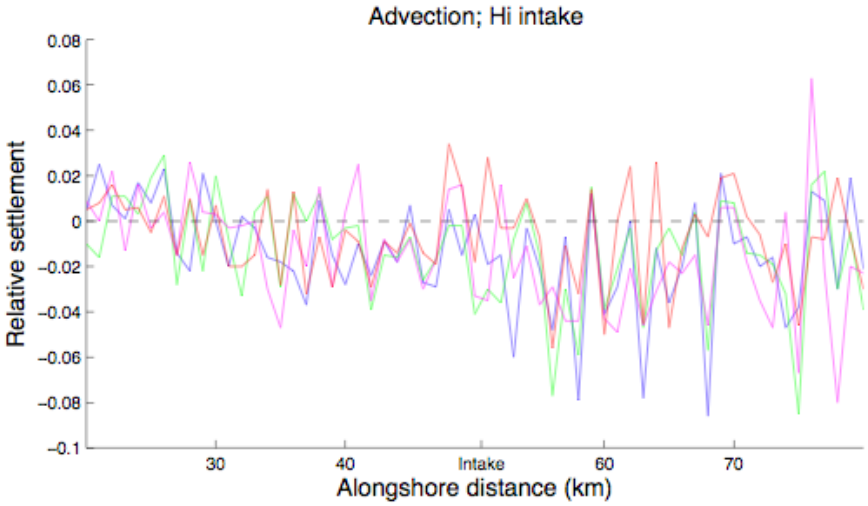

In these model runs, 100 larvae are released from each location and relative settlement gives the arithmetic difference in settlement between runs without and with CWIS entrainment (positive values indicate higher settlement without entrainment). In these runs, there was net alongshore advection (max alongshore current = 0.1 m s^{-1}) and the model run with CWIS entrainment had a single intake at along-shore position *y* = 50 km with high intake velocity (1250 m^3 s^{-1}). Cross-shelf intake position: Black = no intake; Red = 50 m, Magenta = 500 m, Green = 1000 m, Blue = 5000 m.

CHAPTER 7:
Assessment Protocols

There are three statistics traditionally computed to estimate the impacts of larval entrainment by cooling water intakes (Steinbeck et al. 2007). The first two (AEL, FH) essentially extrapolate the number of lost larvae to an estimated number of lost adults, assuming that all demographic rates are density independent. The third (ETM) is an attempt to account for spatial heterogeneity in the larval distribution as a means to better estimate larval mortality. However, unlike the first two it does not place the larval mortality in the context of the adult population. A potential problem with all three measures is that they do not account for 1) the compensatory nature of density-dependent population dynamics, and 2) the spatial structure of benthic populations.

We used the results of the coupled particle dispersion and metapopulation models to calculate these statistics using the usual formulae. For these calculations we used the known number of entrained larvae (simulating a situation in which sampling is perfectly accurate). We then used the model results to calculate alternative metrics that capture the intended definition of the traditional statistics (i.e., parallel to AEL we calculate the actual difference in the number of adults between entrainment and non-entrainment scenarios). These alternative statistics reflect the importance of post-settlement density dependence and the spatial distribution of settlement.

7.1 Adult Equivalent Loss (AEL)

This measure is intended to reflect the number of adults that would have been produced by the entrained larvae. It is calculated as

$$AEL = E_T S \qquad \text{(Eq. 17)}$$

where E_T is the total number of entrained larvae and S is the survivorship from the larval stage to adulthood. Typically this is calculated assuming that survivorship is purely density independent:

$$AEL_{traditional} = E_T\, \alpha e^{-\mu} \qquad \text{(Eq. 18)}$$

In this formulation, S has been replaced with terms for the survivorship through the settler and one-year-old stages (assuming "adults" are ≥ 1 year old) – see Eqs. (11, 12). For simplicity we assume that most larval mortality happens before entrainment, but we could make the opposite assumption and also include the term ξ for larval survivorship.

We then also calculated the value in a way that explicitly accounts for the spatial patterns of settlement and density dependence. This simply requires taking the distribution of adults at equilibrium in an entrainment scenario and calculating for each location i the number of one-year-olds at each location in the next generation that would be obtained if entrainment were halted, Anone , and the number obtained if entrainment continues, Aentrain:

$$AELactual = \sum_i \left(A_{none,i} - A_{entrain,i} \right) \qquad \text{(Eq. 19)}$$

7.2 Fecundity Hindcasting (FH)

This measure is intended to relate the number of larvae entrained to the number of adult females required to produce that number of larvae. The intent is to find the number of females that are effectively removed from the population by entrainment. Here a key value is the lifetime egg production (LEP) of one adult, which is the per-capita annual fecundity times the mean lifespan of an individual (LEP = $L\phi$) (we assume without loss of generality that all adults can produce eggs; this could either describe an hermaphroditic population or require that ϕ is scaled by ½). Given that value,

$$FH_{traditional} = E_T/(LEP\xi) \qquad \text{(Eq. 20)}$$

where E_T is the number of entrained larvae and ξ is larval survivorship. Note that this assumes that larval mortality takes place before entrainment, just as above in the AEL calculation. It does not actually matter whether we assume that larval mortality takes place before or after entrainment, so long as the same assumption is made for both statistics. In the future we plan to re-examine this question by keeping track of larval ages at entrainment, allowing us to explicitly account for the timing of natural larval mortality.

The conceptual weak link in this measure is that because of compensatory density-dependent mortality, one could actually remove quite a large number of reproductive females from the population before noticing an effect in the number of successful recruits. Therefore it may be more informative to consider the number of successful recruits removed from the population and calculate the equivalent number of females needed to produce that many recruits. The calculation then becomes

$$FH_{actual} = AEL_{actual}/(\ LEP\ \xi\alpha e^{-\mu}) \qquad \text{(Eq. 21)}$$

This calculation takes the number of adult equivalents lost from the population, removes the effects of post-settlement density-independent survivorship, and divides by LEP.

7.3 Empirical Transport Model (ETM)

This calculation is designed to extrapolate the total larval loss at the cooling water intake from several samples of the larval population within the source water. The formula is

$$P_M = 1 - \sum_{j=1}^{n} f_j \left(1 - P_S PE_j\right)^d \qquad \text{(Eq. 22)}$$

where P_M is proportional mortality, PE_j is the estimate of proportional larval entrainment during the jth survey, f_j is the number of larvae hatched during the jth survey, d is the number of days larvae are exposed to entrainment mortality, and P_S is the proportion of the entire source water population that was actually sampled. Quite a bit of effort goes into estimating P_S, especially for open coast populations. In theory it would be possible to run particle-tracking simulations that would also simulate plankton sampling in a way that would approximate empirical calculations of P_S and P_M. For simplicity, however, we used the difference between settlement in non-entrainment and entrainment scenarios to calculate the actual value of P_M.

Just as in the AEL calculation, this requires finding the distribution of population density at equilibrium, then calculating the number of settlers obtained in the next time step if entrainment continues ($S_{entrain}$), or if it is suddenly halted (S_{none}):

$$P_{M\ actual} = 1 - S_{entrain}/S_{none} \qquad \text{(Eq. 23)}$$

Given the value of $P_{M\ actual}$ in each scenario, it is straightfoward to see whether there is any relationship between that statistic and the actual effect of entrainment on the population.

7.4 Assessment Protocol Results and Discussion

The results of population simulations are compared to the AEL, FH, and P_M statistics for a population on the verge of collapse due to high adult mortality rates (e.g., from harvesting; Table 6) and for an unexploited, healthy population (Table 7). It is possible to draw several conclusions regarding the traditional entrainment statistics.

Firstly, AEL and FH are not reliable indicators of entrainment effects. Because the total concentration of larvae in the water column is greater when the population is healthy, both AEL and FH are higher for healthy populations than for populations near collapse, regardless of entrainment effects. Moreover, higher entrainment rates drive population densities down somewhat, so measures of AEL and FH taken at or near equilibrium (after the effects of entrainment have been felt in adult population densities), both values will be *lower* when entrainment has a greater population effect.

Secondly, the values of AEL and FH calculated assuming there is no density dependence are incorrect by several orders of magnitude when density dependence is strong (contrast $AEL_{traditional}$ and AEL_{actual} in Table 7). This is because many of the entrained larvae would have died anyway upon settlement. The bias is also slightly higher for intakes that are further offshore, because some of those larvae would not even return to settle. When the population is near collapse, however, population densities are much lower and density-dependent mortality is far less strong, so the traditional AEL and FH calculations are reasonably accurate. Fortunately, then, the statistics are most accurate for situations in which population persistence is most sensitive to entrainment effects. However, it is impossible to tell from AEL and FH alone whether the population is near the collapse point.

Regarding the estimates of P_M, these values are generally higher in scenarios with higher intake rates. However, there is no real relationship between P_M and population-level impacts. Values of P_M are quite similar for scenarios with a healthy population and a near-collapse population, yet larval mortality has a much greater potential effect on near-collapse populations (compare figures A and B). Thus P_M does not necessarily convey information about the effect of mortality on population persistence. More importantly, within the set of near-collapse scenarios, P_M is sometimes higher for cases in which the population is persistent than cases in which entrainment causes population collapse. Therefore, P_M itself is not diagnostic of population-level entrainment effects. This is because a point estimate of total larval mortality is not necessarily meaningful when the effects of that mortality (reduced larval settlement) are distributed in space.

So if these traditional estimates of entrainment effects are not useful, what would be a better approach? It will always be difficult to estimate entrainment effects from larval samples alone if those larvae would eventually experience density-dependent mortality in downstream settlement locations. This is because it is impossible to know where entrained larvae would have settled, and how many other settlers would have arrived at the same time to compete for resources. There are two approaches that might be more productive. The first option is to develop and parameterize a population model like this one to project entrainment effects. This would be the only viable solution if there is a lot of spatial heterogeneity in the benthic population that makes the "downstream" effects of entrainment difficult to estimate without modeling. For example, the presence of marine protected areas or substantial differences in habitat quality across the coastline would lead to nonrandom differences in settler survival and lifetime egg production. The persistence of metapopulations in the face of that sort of heterogeneity is difficult to estimate without a spatially explicit model (Kaplan et al. 2006).

The second option could still work in a spatially implicit framework. The general persistence criterion for a population is

$$\mathrm{LEP}\,\xi\alpha\rho > 1 \qquad \text{(Eq. 24)}$$

where LEP, ξ, and α are lifetime egg production, larval survivorship, and post-settlement survival, as defined earlier, and ρ is the probability that a spawned larva returns to settle at the coastline. The latter value is not trivial to estimate, but within a length of coastline with relative homogeneous flow, it could be roughly estimated by comparing total larval output to the total number of returning settlers. Alternatively it could be estimated with greater precision using genetic or natural tagging techniques (Hedgecock et al. 2007, Thorrold et al. 2007).

The criterion in Eq. (24) is equivalent to stating that each adult must spawn at least one offspring that successfully returns to recruit into the adult population (Caswell 2001, Hastings and Botsford 2006, Kaplan et al. 2006). In the models used here, LEP = $L\phi$. Entrainment will effectively reduce ρ by adding a new source of larval mortality.

Using Eq. (24), a rough estimate of the population effects of entrainment could be obtained by calculating $\rho' = \rho\,(1\text{-}P_M)$. That is, assume that the probability of returning to shore is reduced by the proportion of larve that are entrained in the CWIS. By comparing the new value of ρ' to field estimates of LEP, ξ, and α, it should be possible to tell whether the population is near collapse or not.

The weakness of this approach is that it assumes there is no spatial variability in P_M. So if the population has quite a large geographic extent, P_M will underestimate larval mortality for the part of the range near the intake, but overestimate larval mortality at points distant to the intake, and this will bias the predictions regarding population persistence. Clearly there are empirical challenges involved in estimating the parameters necessary to evaluate Eq. (24), but it does afford a demographically relevant estimate of CWIS effects on persistence without requiring the development of a full circulation model.

Table 6: Comparison of Traditional ("trad") CWIS Impact Statistics with Equivalent Values ("actual") Derived from the Spatially Explicit Population Model

Single intake, no disturbance, healthy population													
		Offshore position of intake (m)											
Advection (m/s)	Intake rate (m^3/s)	50						500					
		Persist	AEL		FH		P_M	Persist	AEL		FH		P_M
			trad	actual	trad	actual	actual		trad	actual	trad	actual	actual
0	0	P	0	0	0	0	0	P	0	0	0	0	0
0	125	P	2.92e3	0.0017	0.6885	4.04e-7	0.026	P	3.94e3	0.0023	0.93	5.35e-7	0.0352
0	1250	NP	4.19e3	0.0025	0.99	5.81e-7	0.0374	NP	7.11e3	0.004	1.68	9.51e-7	0.0634
0.1	0	P	0	0	0	0	0	P	0	0	0	0	0
0.1	125	NP	3.46e3	0.0063	0.8175	1.48e-6	0.0386	P	3.29e3	0.007	0.7767	1.82e-6	0.0367
0.1	1250	P	4.94e3	0.0073	1.1671	1.73e-6	0.0551	NP	6.68e3	0.0096	1.58	2.26e-6	0.0745

Single intake, no disturbance, healthy population													
		Offshore position of intake (m)											
Advection (m/s)	Intake rate (m^3/s)	1000						5000					
		Persist	AEL		FH		P_M	Persist	AEL		FH		P_M
			trad	actual	trad	actual	actual		trad	actual	trad	actual	actual
0	0	P	0	0	0	0	0	P	0	0	0	0	0
0	125	P	3.90e3	0.0022	0.92	5.29e-7	0.0348	P	3.39e3	0.0019	0.80	4.54e-7	0.0302
0	1250	NP	7.53e3	0.0043	1.78	1.01e-6	0.0672	NP	7.25e3	0.004	1.71	9.50e-7	0.0648
0.1	0	P	0	0	0	0	0	P	0	0	0	0	0
0.1	125	P	2.89e3	0.005	0.6828	1.17e-6	0.0322	NP	3.94e3	0.0076	0.9293	1.78e-6	0.0439
0.1	1250	NP	6.45e3	0.0086	1.5238	2.04e-6	0.072	NP	6.52e3	0.009	1.54	2.12e-6	0.0728

This table presents results for an unexploited, healthy population (adult mortality far less than that needed to produce collapse). Scenarios with persistent populations indicated with *P*, scenarios with non-persistent populations indicated with *NP.*

Table 7: Comparison of Traditional ("trad") CWIS Impact Statistics with Equivalent Values ("actual") Derived from the Spatially Explicit Population Model

SINGLE INTAKE, NO DISTURBANCE, NEAR COLLAPSE													
		OFFSHORE POSITION OF INTAKE (M)											
ADVECTION (M/S)	INTAKE RATE (M3/S)	50						500					
		PERSIST	AEL		FH		PM	PERSIST	AEL		FH		PM
			TRAD	ACTUAL	TRAD	ACTUAL	ACTUAL		TRAD	ACTUAL	TRAD	ACTUAL	ACTUAL
0	0	P	0	0	0	0	0	P					
0	125	P	1.38E-4	1.34E-4	0.0099	0.0097	0.0275	P	7.58E-5	7.50E-5	0.0054	0.0054	0.0382
0	1250	NP	9.12E-6	9.11E-6	6.55E-4	6.54E-4	0.0381	NP	7.66E-14	7.66E-14	5.50E-12	5.50E-12	0.0664
0.1	0	P	0	0	0	0	0	P	0	0	0	0	0
0.1	125	NP	4.83E-5	4.81E-5	6.37E-4	6.34E-4	0.0487	P	5.28E-4	5.01E-4	0.007	0.0066	0.039
0.1	1250	P	2.93E-7	2.93E-7	3.86E-6	3.86E-6	0.0561	NP	6.32E-17	6.32E-17	8.32E-16	8.32E-16	0.0683

SINGLE INTAKE, NO DISTURBANCE, NEAR COLLAPSE													
		OFFSHORE POSITION OF INTAKE (M)											
ADVECTION (M/S)	INTAKE RATE (M^3/S)	1000						5000					
		PERSIST	AEL		FH		P_M	PERSIST	AEL		FH		P_M
			TRAD	ACTUAL	TRAD	ACTUAL	ACTUAL		TRAD	ACTUAL	TRAD	ACTUAL	ACTUAL
0	0	P	0	0	0	0	0	P					
0	125	P	5.43E-5	5.38E-4	0.0039	0.0039	0.0357	P	1.02E-4	1.01E-4	0.0074	0.0072	0.0319
0	1250	NP	1.45E-15	1.45E-15	1.04E-13	1.04E-13	0.0687	NP	1.04E-14	1.04E-14	7.47E-13	7.47E-13	0.0675
0.1	0	P						P					
0.1	125	P	5.28E-4	4.98E-4	0.007	0.0066	0.32	NP	1.12E-5	1.12E-5	1.48E-4	1.48E-4	0.0438
0.1	1250	NP	5.02E-14	5.02E-14	6.62E-13	6.62E-13	0.0771	NP	1.54E-10	1.54E-10	2.03E-9	2.03E-9	0.0571

This table presents results for an exploited population near collapse (adult mortality is 99% of that needed to produce population collapse). Scenarios with persistent populations indicated with *P*, scenarios with non-persistent populations indicated with *NP.*

CHAPTER 8:
Future Directions

The models described in this report provide insight to the complexity of the larval dispersal process and the importance of reduced nearshore flow in determining dispersal outcomes. While making simplifying assumptions about a number of key biological and physical factors, this study demonstrates that existing protocols for assessing larval entrainment are inadequate and may be yielding misleading results. We have used the model to evaluate these assessment protocols and suggested some additional approaches. Below we identify seven themes for action that can be taken to improve assessment protocols and/or reduce entrainment impacts.

Some of the simplifying assumptions in this model study include:

(i) That larvae do not control position (swimming, buoyancy).

(ii) That larval distribution is vertically mixed.

(iii) Zero net cross-shore transport of larvae – see (i).

(iv) Fluctuations in currents can be represented as random – see (i), (ii), (iii).

(v) That near-field details of the withdrawal zone are secondary considerations in the large-scale problem.

(vi) That details of surfzone circulation and rip currents are secondary consideration in large-scale problem.

(vii) That cross-shore variations in currents are well represented by tri-linear coastal boundary layer profiles.

(viii) That alongshore flow structure is secondary.

(ix) That alongshore population and habitat structure is secondary.

(x) That non-intake larval mortality is spatially uniform and temporally constant (i.e., common) and thus can be excluded from model analyses.

That post-settlement density-dependent mortality is significant.

While future modeling could include some of these aspects, to do so will require implementation of the model for specific sites and thus generation of site-specific results. The aim in this study was to explore the general implications of near-coastal intake systems.

Some of the future directions for improving assessment of the impact of cooling water intake systems on larval mortality (and thus coastal marine populations) are outlined below.

(1) <u>Flow observations</u>: *Make use of data obtained from Coastal Ocean Observing Systems.*
Both the Southern California Coastal Ocean Observing System (SCCOOS) and the Northern and

Central California Ocean Observing System (CeNCOOS) are collecting routine data on surface currents throughout the state. These high-frequency radar data can provide empirical estimates of offshore surface currents that would allow particle tracking runs in more realistic flow scenarios than those used in this idealized and alongshore-homogeneous flow model. Thus, one can define a typical data-based flow field for any specific site. However, these HF-radar data are sparse very close to shore and it would be necessary to include representation of the coastal boundary layer as in this study. Where SCCOOS and CeNCOOS do not have existing nearshore current monitoring stations near CWIS sites, there is a need to establish ongoing current measurement stations. These data can then be used both in aggregate form to assess typical entrainment probabilities as well as in retrospective analysis of times of high entrainment of late-stage larvae (events which are expected to be of most concern in reduced recruitment). In associated studies, we are investigating optimum methods for monitoring and incorporating nearshore current data in large-scale data-based estimates of larval dispersal off California (e.g., K. Nickols, manuscript in preparation). In addition to ongoing current monitoring, local drifter studies would be an effective way of validating dispersion patterns obtained from models using SCCOOS and CeNCOOS data. These ongoing data would be equally valuable for assimilation in more complex models, if those come to be used.

(2) Transport models: *Make use of transport models to assess larval loss through entrainment.*

The use of transport models recognizes that larvae follow complex pathways and that the majority of larvae do not survive the planktonic period, making it difficult to estimate larval entrainment from rudimentary representations of coastal flow. Reduced complexity models, as used here, can be effective in scoping out the problem, yielding improved information for assessment of entrainment. With application of this model to a specific site, information on flow and habitat can be incorporated to increase the realism of the results. Useful data are described above in (1). While one could implement high-resolution circulation models, these models are more expensive to run and presently do not resolve the coastal boundary layer adequately. However, there is potential to combine this coastal boundary layer model with existing large-scale circulation models for southern California (some of which also assimilate the offshore HF radar on currents). Whatever the approach, the use of transport models allows quantification of the probability of being entrained and identification of the taxa that are more likely to be significantly impacted by entrainment.

(3) Larval observations: *Analyze records of larvae entrained and of larvae in plankton surveys.*

The very larvae that are entrained can be sampled and analyzed more effectively than it appears happens now. In particular, it is clear from transport modeling that the age of entrained larvae is a critical factor, given the much-increased likelihood of late-stage larvae recruiting to the adult population. Time series of daily entrainment will also point to days on which entrainment is highest and allow identification of oceanographic conditions when this occurs. It may be that the majority of larval mortality occurs on just a few days. In addition to analysis of entrained larvae, analysis of plankton surveys should be re-designed following analysis of transport patterns based on (1) and (2) above. What is the distribution and

concentration of larvae in the waters that are susceptible to entrainment? How are larvae distributed vertically under different ambient stratification conditions?

(4) Populations models: *Use of population models to assess impact of enhanced larval mortality on population levels.*

As in this report (and recognized in AEL and FH concepts), it is critical to assess larval mortality in terms of impact on the population. Marine populations have high fecundity and high larval mortality, so one needs to determine whether the increased mortality due CWIS has a significant impact on population levels or viability. Models to do this exist and they should be routinely used to express assessed larval mortality in terms of population consequences. Most marine populations experience post-settlement density-dependent mortality and this mitigates the consequences of changes in larval mortality. The general scenarios investigated here suggest that CWIS entrainment is unlikely to have a significant impact on populations, unless these populations are simultaneously under stress from other phenomena.

(5) Assessment protocols: *Development of new protocols for compliance.*

New data and the use of models provide much increased insight to larval entrainment and population impacts. However, this enhanced information can also be used to develop new indices and new protocols for assessment. Some preliminary suggestions have been made in this report. When conducting CWIS impact studies in the future, it would be best to move away from ecologically and oceanographically unrealistic statistics that are currently in use. Based on the above, it is possible to develop protocols such include site-specific coupled bio-oceanographic models and/or the LEP-based persistence criterion given in Eq. (23). These revised protocols should be implemented in new regulations.

(6) Ecosystem-based management: *Development of protocols that assess impact of cooling water intake in concert with other stressors and management actions in coastal waters.*

While going beyond single-agency responsibilities, it is clear that CWIS effects need to be considered in the context of larger-scale conservation and management plans, and it should be recognized that the conservation value of a location depends on the overall status of the location. In relatively healthy, unexploited populations, the areas near an intake have lower conservation value. However, in highly depleted populations close to collapse, there is no spatial pattern of conservation value. In other words, increasing LEP or $\circledcirc$ in any location would favorably affect the population. The State of California is heavily invested in the Marine Life Protection Act and the Marine Life Management Act and policy on entrainment by CWIS should be integrated with these parallel efforts.

(7) Operational management: *Consideration of changes in management of intake systems.*

Going beyond assessment of entrainment impact on populations, attention can be given to management actions that would reduce entrainment. While it may be costly to act on it, the results of this study suggest that placing intakes very nearshore in regions of slow flow is especially detrimental to populations. If water is pumped in from further offshore there is a lower impact on nearshore populations. However, it may be that there is as much benefit in

pumping from depth in a stratified water column, or from pumping from beneath the sand. These strategies were not evaluated in this work. There may also be opportunities to reduce impacts by temporarily reducing flow rates during brief events when larvae are highly concentrated at the CWIS location. The recommendations made above would provide the information needed to make assessments of the benefits of changes in management of CWIS versus continuing unchanged or shutting down entirely.

CHAPTER 9:
Conclusion and Summary

We have used a particle-tracking model for larval transport and coupled this with a metapopulation model to investigate the population impact of larval entrainment by power plant cooling-water intake systems. We highlight four general conclusions about the consequences of CWIS entrainment for nearshore populations.

First, by incorporating a semi-realistic description of reduced near-coastal flow (i.e., a coastal boundary layer, CBL) into models of particle dispersal, one sees that the actual extent of passive larval transport is likely to be substantially less than that predicted by traditional advection-diffusion approximations. While there are insufficient empirical data to support a detailed mechanistic representation of the CBL in a circulation model, the results of model runs using a simple tri-linear approximation of the cross-shore profile of flows within the CBL were relatively insensitive to the exact shape of that profile.

Second, runs of the particle-dispersion model suggest that the majority of larval entrainment in nearshore CWIS occurs very soon after particle release (i.e., spawning), when larvae are at their highest concentrations. However, if natural mortality were explicitly modeled, there would be far fewer late-stage larvae and the proportion of immediately-post-release larvae would be even higher. Nevertheless, the loss of relatively few late-stage larvae may be more important for population recruitment due to the high likelihood that these individuals would settle if they weren't entrained.

Third, incorporating model-estimated larval dispersal patterns into a metapopulation model reveals that entrainment has an insignificant effect on otherwise healthy populations. But, this small enhanced mortality can be detrimental to unhealthy, overexploited populations. This is a result of early-adult density-dependent mortality, which has a compensatory effect on population dynamics. In other words, for a healthy population, entrainment merely removes larvae that were likely to die after settlement anyway. However, the same is not true for a population that is near collapse as a result of other stressors, such as over-harvesting. In such cases, larval densities are already reduced, and the additional reduction due to entrainment can lead to population collapse. Furthermore, such population-level effects of entrainment may be observed not just near the CWIS but spread across the entire coastline, because near-collapse populations are more likely to persist via "network connectivity" than to consist of individual self-persistent units.

Fourth, the importance of compensatory density dependence to the metapopulation model explains why traditional statistics for quantifying CWIS effects (AEL, FH, and ETM) will often be highly inaccurate. These methods implicitly exclude compensatory density dependence. Thus they will tend to overestimate the demographic effects of entrainment in a healthy population. They are likely to be more accurate for near-collapse populations in which density dependence has a weaker influence, but it is impossible to tell from those traditional statistics

themselves whether a population is healthy or not. Indeed, a healthy population will produce more larvae and thus have higher entrainment rates – and higher values of AEL, FH, and ETM – than an unhealthy population.

In this report we have utilized idealized models that do not capture the full complexity of coastal circulation or population ecology in any particular location or species. Nonetheless, these models are strategic in the sense that they incorporate biological and physical features that have been observed empirically and which are known to strongly influence marine population dynamics. Furthermore, these models capture the first-order essence of the problem that is incomplete in existing protocols. Consequently, these models provide a reliable and general assessment of the potential consequences of CWIS entrainment for nearshore benthic populations.

REFERENCES

Almany, G. R., and M. S. Webster. 2006. The predation gauntlet: early post-settlement mortality in reef fishes. *Coral Reefs* 25: 19-22.

Armsworth, P. R. 2002. Recruitment limitation, population regulation, and larval connectivity in reef fish metapopulations. *Ecology* 83: 1092-1104.

Caley, M. J., M. H. Carr, M. A. Hixon, T. P. Hughes, G. P. Jones, and B. A. Menge. 1996. Recruitment and the local dynamics of open marine populations. *Annual Review of Ecology and Systematics* 27: 477-500.

California Department of Fish and Game (CDFG). 2008. California Marine Life Protection Act Master Plan for Marine Protected Areas. Available online at http://www.dfg.ca.gov/mlpa/masterplan.asp. Accessed 30 Nov 2008.

California Energy Commission (CEC). 2005. Issues and environmental impacts associated with once-through cooling at California's coastal power plants. Staff report in support of the 2005 Environmental Performance Report and 2005 Integrated Energy Policy Report (Docket 04-lep-1). Available online at http://www.energy.ca.gov/2005publications/CEC-700-2005-013/CEC-700-2005-013.PDF. Accessed 30 Nov 2008.

Carillo, L., J.L. Largier, M. Noble, L. Rosenfeld, and P. Hamilton, 2004 unpublished manuscript. Polarization of currents over the inner shelf off Huntington Beach, California.

Caswell, H. 2001. Matrix population models: construction, analysis, and interpretation. Sinauer, Chicago, IL.

Clarke, L.B., D. Ackerman, J. Largier. 2005. Dye dispersion in the surf zone: measurements and simple models. *Journal of Geophysical Research* 27: 650-669

Cowen, R.K., G. Gawarkiewicz, J. Pineda, S.R. Thorrold, and F.E. Werner. 2007. Population connectivity in marine systems: an overview. Oceanography 20: 14-21.

Csanady, G.T. 1972a. The Coastal Boundary Layer in Lake Ontario. Part I: The Spring Regime. *Journal of Physical Oceanography* 2: 41-53.

Csanady, G.T. 1972b. The Coastal Boundary Layer in Lake Ontario. Part II: The Summer-Fall Regime. *Journal of Physical Oceanography* 2: 168-176.

Gawarkiewicz, G., S. Monismith, and J. Largier. 2007. Observing larval transport processes affecting population connectivity: progress and challenges. *Oceanography* 20: 40-53.

Gerlach, G., J. Atema, M.J. Kingsford, K.P. Black, and V. Miller-Sims. 2007. Smelling home can prevent dispersal of reef fish larvae. *Proceedings of the National Academy of Science* (USA) 104: 858-863.

Graham, W. M., and J. L. Largier. 1997. Upwelling shadows as nearshore retention sites: the example of northern Monterey Bay. *Continental Shelf Research* 17: 509-532.

Hamilton, P., M.A. Noble, J. Largier, L.K. Rosenfeld, and G. Robertson. 2006. Cross-shelf subtidal variability in San Pedro Bay during summer 2001. *Continental Shelf Research*, 26: 681-702

Hastings, A., and L. W. Botsford. 2006. Persistence of spatial populations depends on returning home. Proceedings of the National Academy of Sciences 103: 6067-6072.

Hedgecock, D., P. H. Barber, and S. Edmands. 2007. Genetic approaches to measuring connectivity. *Oceanography* 20: 70-79.

Heimbuch, D.G., E. Lorda, D. Vaughan, L.W. Barnthouse, J. Uphoff, W. Van Winkle, A. Kahnle, B. Young, J. Young, and L. Kline. 2007. Assessing coastwide effects of power plant entrainment and impingement on fish populations: Atlantic menhaden example. *North American Journal of Fisheries Management* 27: 569-577.

Hickey, B.M. 1992. Circulation over the Santa Monica-San Pedro basin and shelf. *Progress in Oceanography* 30: 37–115.

Hickey, B.M. 1998. Coastal oceanography of western North America from the tip of Baja California to Vancouver Island. Pages 345–393 *in* Robinson, A.R., and K.H. Brink, Eds. *The Sea*, Vol. 11.

Hixon, M. A., and G. P. Jones. 2005. Competition, predation, and density-dependent mortality in demersal marine fishes. *Ecology* 86: 2847-2859.

Hunter, J. R., P. D. Craig, and H. E. Phillips. 1993. On the use of random walk models with spatially variable diffusivity. *Journal of Computational Physics*. 106: 366–376.

James, M. K., P. R. Armsworth, L. B. Mason, and L. Bode. 2002. The structure of reef fish metapopulations: modeling larval dispersal and retention patterns. *Proceedings of the Royal Society of London* (B) 269: 2079-2086.

Kaplan, D. M., J. Largier, and L. W. Botsford. 2005. HF radar observations of surface circulation off Bodega Bay (northern California, USA). *Journal of Geophysical Research* 110: C10020.

Kaplan, D. M., L. W. Botsford, and S. Jorgensen. 2006. Dispersal per recruit: an efficient method for assessing sustainability in marine reserve networks. *Ecological Applications* 16: 2248-2263.

Kundu, P.K., and I.M. Cohen. 2004. *Fluid mechanics, third edition*. Elsevier Academic Press, San Diego, CA.

Largier, J. L., B.A. Magnell, and C.D. Winant. 1993. Subtidal circulation over the northern California shelf. *Journal of Geophysical Research* 98: 18147-18179.

Largier, J. L., 2002. Linking oceanography and nearshore ecology: perspectives and challenges. Pages 207-239 in Castilla, J.C., and J.L. Largier, eds. *The Oceanography and*

Ecology of the Nearshore and Bays in Chile. Ediciones Universidad Católica de Chile, Santiago, Chile.

Largier, J. L. 2003. Considerations in estimating larval dispersal distances from oceanographic data. *Ecological Applications* 13: S71-S89.

Leet W.S., C.M. Dewees, R. Klingbeil, and E. Larson. 2001. *California's Living Marine Resources: A Status Report*. California Department of Fish and Game.

Leis, J. M. 2007. Behaviour as input for modeling dispersal of fish larvae: behavior, biogeography, hydrodynamics, ontogeny, physiology, and phylogeny meet hydrography. *Marine Ecology Progress Series* 347: 185-193.

Lentz, S.J. 1994. Current dynamics over the Northern California Inner Shelf. *Journal of Physical Oceanography* 24: 2461-2478.

Lentz, S.J., and C.D Winant. 1986. Subinertial currents on the Southern California shelf. *Journal of Physical Oceanography* 16: 1737–1750.

Lentz, S. J., R. T. Guza, S. Elgar, F. Feddersen, and T. H. C. Herbers. 1999. Momentum balances on the North Carolina inner shelf. *Journal of Geophysical Research* 104:18205–18226.

Lerczak, J. A. 2000. Internal waves on the southern California shelf, Ph.D. thesis, Univ. of Calif., San Diego, La Jolla, CA.

Lerczak, J. A., M.C. Hendershott, and C.D. Winant. 2001. Observations and modeling of coastal internal waves driven by a diurnal seabreeze. *Journal of Geophysical Research* 106: 19715.

Mace, P. M., and M. P. Sissenwine. 1993. How much spawning per recruit is enough? *Canadian Special Publication of Fisheries and Aquatic Sciences* 120: 101-118.

Morgan, S.G., J.L. Fisher, S.H. Miller, S.T. McAfee, and J.L. Largier. *in press*. Nearshore larval retention in a region of strong upwelling and recruitment limitation. *Ecology*.

Noble, M.A., H.F. Ryan, and P.L. Wiberg. 2002. The dynamics of subtidal poleward flows over a narrow continental shelf, Palos Verdes, CA. *Continental Shelf Research* 22: 923-944.

Noble, M., P. Hamilton, B. Jones, J. Largier, K. Orzech, L. Rosenfeld, and J. Xu. 2003. Executive summary, Huntington Beach Shoreline Contamination Investigation, Phase III, Draft Final report. Prepared for OCSD.

Noble, M. and J. Xu. 2004. Huntington Beach Shoreline Contamination Investigation, Phase III, Final Report: Coastal Circulation and Transport Patterns: The Likelihood of OCSD's Plume Impacting Huntington Beach Shoreline: *U.S. Geological Survey Open-File Report* 2004-1019. 28 pp. Available online at http://pubs.usgs.gov/of/2004/1019/.

Ovaskainen, O., and I. Hanski. 2003. How much does an individual habitat fragment contribute to population dynamics and persistence? *Theoretical Population Biology* 64: 481-495.

Pringle, J. M., and K. Riser. 2003. Remotely forced nearshore upwelling in Southern California. *Journal of Geophysical Research* 108: 3131.

Sanchez-Arcilla, A., A. Rodriguez, and M. Mestres. 1998. A three-dimensional simulation of pollutant dispersion for the near- and far-field in coastal waters. *Journal of Marine and Environmental Engineering* 4: 217–243.

Shanks, A. L., and G. L. Eckert. 2005. Population persistence of California Current fishes and benthic crustaceans: a marine drift paradox. *Ecological Monographs* 75: 505-524.

Siegel, D. A., B. P. Kinlan, B. Gaylord, and S. D. Gaines. 2003. Lagrangian descriptions of marine larval dispersion. *Marine Ecology Progress Series* 260: 83-96.

Smith, J.A., and J.L. Largier, 1995. Observations of nearshore circulation: rip currents. *Journal of Geophysical Research* 100:,10967-10975.

Steinbeck, J., J. Hedgepeth, P. Raimondi, G. Cailliet, and D. Mayer. 2007. Assessing power plant cooling water intake system entrainment impacts. Consultant report prepared for California Energy Commission. Available online at http://www.energy.ca.gov/2007publications/CEC-700-2007-010/CEC-700-2007-010.PDF. Accessed 30 Nov 2008.

Thorrold, S. R., D. C. Zacherl, and L. A. Levin. 2007. Population connectivity and larval dispersal: using geochemical signatures in calcified structures. *Oceanography* 20: 80-89.

Visser, A. W. 1997. Using random walk models to simulate the vertical distribution of particles in a turbulent water column, *Marine Ecology Progress Series* 158: 275–281.

White, J. W. 2008. Spatially coupled larval supply of marine predators and their prey alters the predictions of metapopulation models. *American Naturalist* 171: E179-E194.

Winant, C.D., R.C. Beardsley, and R.E. Davis. 1987. Moored wind, temperature, and current observations made during coastal ocean dynamics experiments 1 and 2 over the northern California continental shelf and upper slope. *Journal of Geophysical Research* 92:1569–1604.

Wing, S. R., L. W. Botsford, J. L. Largier, L. E. Morgan. 1995. Spatial structure of relaxation events and crab settlement in the northern California upwelling system. *Marine Ecology* Progress Series 128: 199–211.

Wolanski, E. 1994. Physical oceanographic processes of the Great Barrier Reef. CRC, Boca Raton, Florida, USA.